Award Number:
W81XWH-07-1-0215

TITLE:
Cellular Therapy to Obtain Rapid Endochondral Bone Formation

PRINCIPAL INVESTIGATOR:
Elizabeth A. Olmsted-Davis, Ph.D.,

CONTRACTING ORGANIZATION:
Baylor College of Medicine
Houston, TX 77030

REPORT DATE:
February 2010

TYPE OF REPORT:
Final Year 3

PREPARED FOR: U.S. Army Medical Research and Materiel Command
Fort Detrick, Maryland 21702-5012

REPORT DOCUMENTATION PAGE

Form Approved
OMB No. 0704-0188

1. REPORT DATE *(DD-MM-YYYY)*	2. REPORT TYPE	3. DATES COVERED *(From - To)*
28-02-2010	Final year 3	1 mar 2009-28 jan 2010

4. TITLE AND SUBTITLE

Cellular Therapy to Obtain Rapid Endochondral Bone Formation

5a. CONTRACT NUMBER

5b. GRANT NUMBER
W81XWH-07-1-0215

5c. PROGRAM ELEMENT NUMBER

5d. PROJECT NUMBER

5e. TASK NUMBER

5f. WORK UNIT NUMBER

6. AUTHOR(S)
Elizabeth A. Olmsted-Davis, Ph.D.

Email: edavis@bcm.tmc.edu

*

7. PERFORMING ORGANIZATION NAME(S) AND ADDRESS(ES)

Baylor College of Medicine
One Baylor Plaza, BCM505
Houston, Texas 77030

8. PERFORMING ORGANIZATION REPORT NUMBER

9. SPONSORING / MONITORING AGENCY NAME(S) AND ADDRESS(ES)

DEPARTMENT OF THE ARMY
US ARMY MEDICAL RESEARCH AND
MATERIEL COMMAND
504 SCOTT STREET
FORT DETRICK, MD 21702-5012

10. SPONSOR/MONITOR'S ACRONYM(S)

11. SPONSOR/MONITOR'S REPORT NUMBER(S)

12. DISTRIBUTION / AVAILABILITY STATEMENT

Distribution is unlimited.

13. SUPPLEMENTARY NOTES
N.A.

14. ABSTRACT The goal of this study is to provide a safe effective system for inducing bone formation for fracture healing in situations of significant trauma. This set of proposed experiments will provide significant knowledge to the field of bone tissue engineering. Proposed studies will provide essential biological information and involves the development of a novel biomaterial that can safely house the cells expressing the bone inductive factor to produce the new bone at which time the material is then selectively eliminated. Ultimately this system has significant applicability. Often bone graft must be surgically removed from the pelvis, to implant into the site of difficult fractures for proper healing. This additional surgery often results in significant pain, and long term healing. Further, this system would be applicable to orthopedic trauma situations that previously resulted in amputation. We propose in these studies to complete the development of this bone induction system and test it in a preclinical animal model. Validation of our hypothesis will provide a safe and efficacious material for the production of bone leading to reliable fracture healing, circumventing the need for bone grafts, or for direct administration of cells, viruses, or other materials that could lead to significant adverse reactions.

15. SUBJECT TERMS
BMP2, critical size defect, nonunion, Gene Therapy, Adenovirus.

16. SECURITY CLASSIFICATION OF:			17. LIMITATION OF ABSTRACT	18. NUMBER OF PAGES	19a. NAME OF RESPONSIBLE PERSON
a. REPORT	b. ABSTRACT	c. THIS PAGE			19b. TELEPHONE NUMBER *(include area code)*
U	U	U	U	116	

Standard Form 298 (Rev. 8-98)
Prescribed by ANSI Std. Z39.18

Table of Contents

Introduction: This project, on the use of cell-based gene therapy for the production of rapid endochondral bone formation, and fracture healing is a collaborative effort between a bio-engineering/biomaterials group at Rice University and Baylor College of Medicine. Although bone possesses the rare capacity to continually renew and repair itself, more than 500,000 bone repair surgical procedures are performed annually within the United States alone. The need to enhance or initiate bone formation in a controlled clinical manner has brought tissue engineering to the forefront of orthopedic research. Much recent effort has been directed to the identification of factors essential to normal bone formation, and the development of new osteoconductive materials that can temporarily fill areas of missing osteoid. Still lacking are effective osteoinductive components that could be seeded into the osteoconductive materials to generate normal bone which this study will explore. The central hypothesis of this application is that rapid bone formation can be successfully achieved with only minimally invasive percutaneous techniques and without a scaffold, by using cells transduced with adenovirus vectors to express an osteoinductive factor (BMP2), which have been encapsulated in hydrogel material and later photopolymerized at the desired site.

The goal of this study is to provide a safe effective system for inducing bone formation for fracture healing. This set of proposed experiments will provide significant knowledge to the field of bone tissue engineering. Proposed studies will provide essential biological information and involves the development of a novel biomaterial that can safely house the cells expressing the bone inductive factor to produce the new bone at which time the material is then selectively eliminated. Ultimately this system has significant applicability. Often bone graft must be surgically removed from the pelvis, to implant into the site of difficult fractures for proper healing.This additional surgery often results in significant pain, and long term healing. Further, this system would be applicable to orthopedic trauma situations that previously resulted in amputation. We propose in these studies to complete the development of this bone induction system and test it in a preclinical animal model. Validation of our hypothesis will provide a safe and efficacious material for the production of bone leading to reliable fracture healing, circumventing the need for bone grafts, or for direct administration of cells, viruses, or other materials that could lead to significant adverse reactions.

Body: The central hypothesis of this application is that rapid bone formation can be successfully achieved with only minimally invasive percutaneous techniques and without a scaffold, by using cells transduced with adenovirus vectors to express an osteoinductive factor (BMP2), which have been encapsulated in hydrogel material and later photopolymerized at the desired site.

Task 1: To produce high levels of BMP2 from human mesenchymal stem cells transduced Ad5F35BMP2 adenovirus in the presence of tetracycline carrying a red luciferase reporter gene.

a. *To determine if sustained expression of BMP2 is more efficient at inducing rapid bone formation than a pulse of expression using the tetracycline regulated vectors.* ***(Months 0-12)***

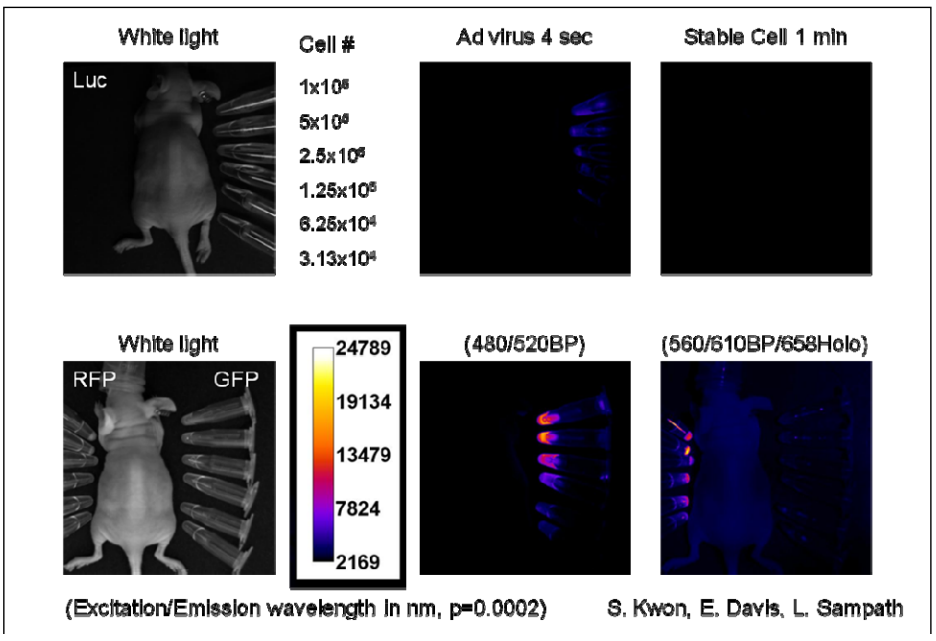

Figure 1: Detection of a red luciferase reporter in live animal imaging. Expression of a red shifted luciferase reporter was compared both in cells, and in live animals after subcutaneous intramuscular injection. Two types of cells were tested, one which was a cell line that had the reporter stably integrated, and the other cells which had been transduced with an AdCBRluc virus.

We have conducted a number of these experiments using the originally described methodology, and compared the red luciferase reporter gene expression to other red-shifted reporters to determine if we could

obtain something more sensitive which would allow us to image the expression of the transgene during bone formation. In original experiments using luciferase (figure 1) we were unable to readily detect the reporter after intramuscular injection of our transduced cells at the levels routinely used for induction of bone formation. However, as seen in figure 2, when this was compared to dsRED, a red fluorescent protein, we could readily detect dsRED. Therefore we initiated studies using dsRED in place of the red luciferase.

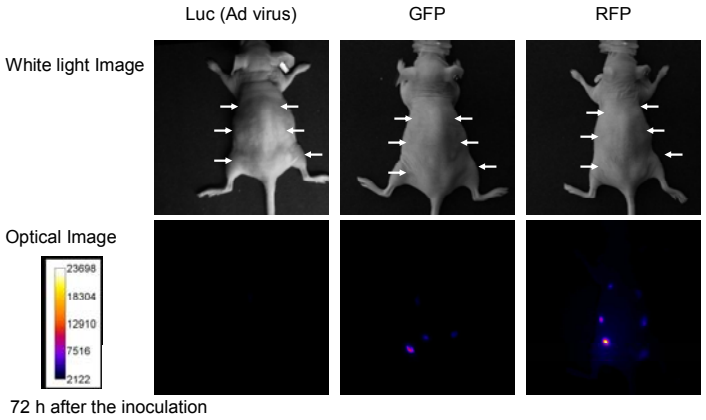

Figure 2: Comparison of reporter expression after intramuscular injection of dsRED, GFP, and CBRluc in live animals, through optical imaging.

We also generated adenoviruses that have tetracycline regulated transgenes (reporters, dsRED and green flourescent protein, GFP) so that in the presence of the antibiotic, doxycycline, will express the reporter, but in the absence do not express the transgene. Thus the reporter expression can be regulated in cells transduced with this vector, by delivery of doxycycline. Figure 3 shows the reporter expression in cells transduced with a vector using an AdGFP virus made using this similar tetracycline regulatory backbone in the presence and absence of doxcycline.

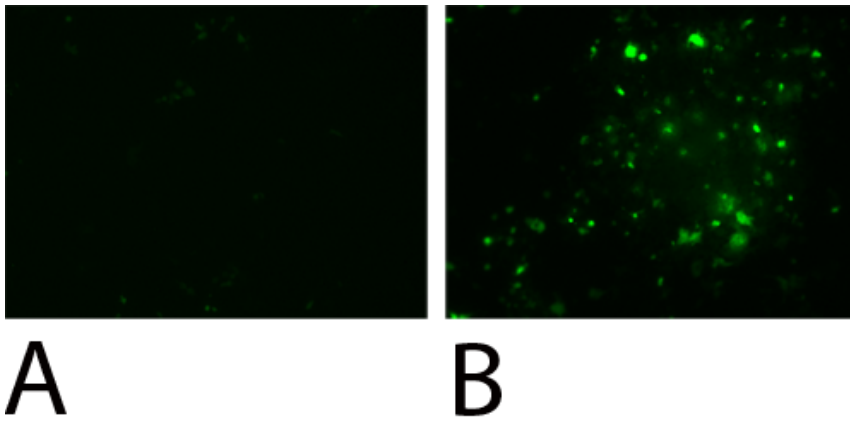

Figure 3: Fluorescent microscopy of A549 cells which have been transduced with Ad5tet-GFP in the absence (A) and presence (B) of tetracycline.

We have started to implement these in the live animal studies, and finding that sustained release of the BMP2 is much more effective than a short pulse, as predicted from the studies using recombinant protein. In studies where we reduce the length of BMP2 expression from less than 4 days which is the current length of time the majority of the transduced cells reside in the tissues, we totally ablate bone formation. In studies where we enhance the length of time BMP2 is expressed within the tissues, (see next section) we observe an increase in bone volume. Therefore we are requesting some changes be associated with the procedures, to focus on sustained expression of BMP2, at high levels, rather than termination of BMP2. We are also working on delivering a caspase gene to the delivery cells so that we can selectively destroy these cells in a targeted fashion. This would be a better approach for removing the gene therapy system than simply turning off the transgene itself.

b. *To determine if longer expression times of BMP2 from cells embedded in hydrogel and longer cellular viability lead to more rapid bone formation than the rapid but short burst of BMP2 release obtained from the cells directly injected.* ***(Months 9-12)***

We are highly focused on completing this aim, using the reporter dsRED in place of the click beetle red luciferase gene. We have observed a repressed effect of our cell based gene therapy system on bone formation with inclusion of a carrier as compared to in its absence. We have previously found that our BMP2 delivery cells are rapidly cleared (Fouletier-Dilling *et al* 2007) in the absence of a carrier, whereas inclusion of the cells in a collagen carrier (Gugala *et al,* 2007) or encapsulation of hydrogel (Bikram et al, 2007) greatly reduces the amount of BMP2 secreted to the local environment and ultimately bone. Interestingly, our preliminary data suggests that inclusion of a carrier such as hydrogel does however; lengthen the lifespan of the transduced cell within the tissues resulting in prolonged BMP2 expression. However these millimeter scale

beads employed in our previous study were a proof of concept and exceeded the 250 μm diffusion limit beyond which cell death is inevitable. As a result BMP-2 culture supernatant levels from cells encapsulated in bead structures was significantly reduced as compared to the same number of cells in a monolayer. The radii of the microspheres in this study were roughly in the 50 - 150 μm range, well under the diffusion limit. In order to ensure that the cells tolerated encapsulation and that BMP-2 could freely diffuse out of the material; cells were microencapsulated and then stained using a Live/Dead cytotoxicity assay to determine the number and extent of viable cells within the PEGDA hydrogel microspheres. With this method, live cells enzymatically convert non-fluorescent calcein acetoxymethyl (calcein AM) into fluorescent calcein, while an ethidium homodimer compound enters dead cells through damaged membranes and binds DNA to emit red fluoresence (Figure 4). As seen in Figure 4, cells that had been encapsulated within

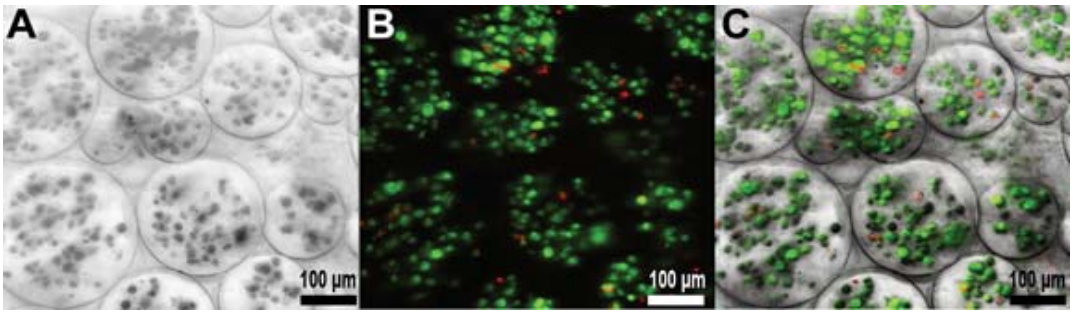

Figure 4. Viability of AdBMP2 transduced cells (2500 vp/cell) within microspheres was assessed at day 7 using a LIVE/DEAD® Viability/Cytotoxicity Kit for mammalian cells (Invitrogen, Molecular Probes, Eugene, OR). **A.** Live cells appear green, **B.** dead show red. **C.** Overlay of panels A and B. Living cells accounted for 95.08% ± 0.47% of total cells encapsulated.

PEGDA microspheres and placed in culture for seven days, showed high viability, 95.08% ± 0.47%, suggesting that microencapsulation process was not leading to cell death.

The level of BMP-2 in the culture supernatant was then measured to determine if the protein could adequately diffuse from the microspheres. Equivalent numbers of cells were transduced with AdBMP2 or AdEmpty cassette (2500 vp/cell) and either placed in culture directly, or after microencapsulation in PEGDA microspheres. Culture supernatant was removed 72 hours later, and BMP-2 and its activity within the supernatants were quantified (Figure 5). BMP-2 levels were quantified by ELISA and found to be approximately 17,500 pg/ml and 15,000 pg/ml of culture supernatant for directly plated and microencapsulated cells, respectively. No BMP-2 was detected in either culture supernatant from Adempty cassette transduced cells, or control cells which had no additions. In larger bead structures, we observed a significant drop in the level of BMP-2 as compared to equivalent numbers of cells either directly plated or in microspheres (data not shown). The data suggests that optimal BMP-2 production and secretion is achieved when cells are encapsulated into the smaller microsphere structures. Further, the data shows that the PEG-DA hydrogel material is not affecting the production, secretion or diffusion of BMP-2 within the microspheres (figure 5A). We next assayed BMP-2 activity in the culture supernatant to confirm that the protein that diffused through the PEGDA hydrogel possessed similar specific activity as BMP-2 in culture supernatant from cells directly plated. The release of proteins from hydrogels is related both to diffusion distances and the hydrogel mesh size, both of which change with swelling[24]. The hydrogels in the current study were formed with 10% 10 kDa PEGDA, which has been estimated to have a mesh size of 280 Å. Proteins having radii smaller than the hydrogel mesh size enjoy relatively free diffusion through the polymer[25]. Mature BMP-2 is a small protein (approximately 16 kDa) and it has been suggested that it dimerizes immediately after synthesis. The biologically active form of BMP-2 is a homodimer whose dimensions are 70 Å × 35 Å × 30 Å[26]. Thus, BMP should pass freely through the microspheres. To confirm this result and ensure that the PEG-DA hydrogel microspheres were not selecting for a less active form of BMP-2, culture supernatants were tested in a cell based functional assay. Culture supernatants were tested, using the murine bone marrow stromal cell line, W20-17 cells, which have previously been shown to respond to functional BMP-2 by undergoing osteogenesis with a rapid increase in alkaline phosphatase (AP). W20-17 cells were exposed for 72 hours to a portion of the culture supernatants used for BMP-2 quantification and then cells were lysed for quantification of alkaline phosphatase (AP) activity (figure 5B). Both the culture supernatants from cells directly plated and encapsulated in microspheres led to significant elevation in alkaline phosphatase over the cells with no additions, suggesting the BMP-2 is functionally active. Further, culture supernatant from cells which had been transduced with Adempty cassette did not elevate alkaline phosphatase significantly above the W20-17 cells with no additions (figure 5B). The

data collectively suggest that microencapsulation of the cells in PEG-DA hydrogel does not significantly reduce the level of functional BMP-2 produced after transduction of the cells with AdBMP2.

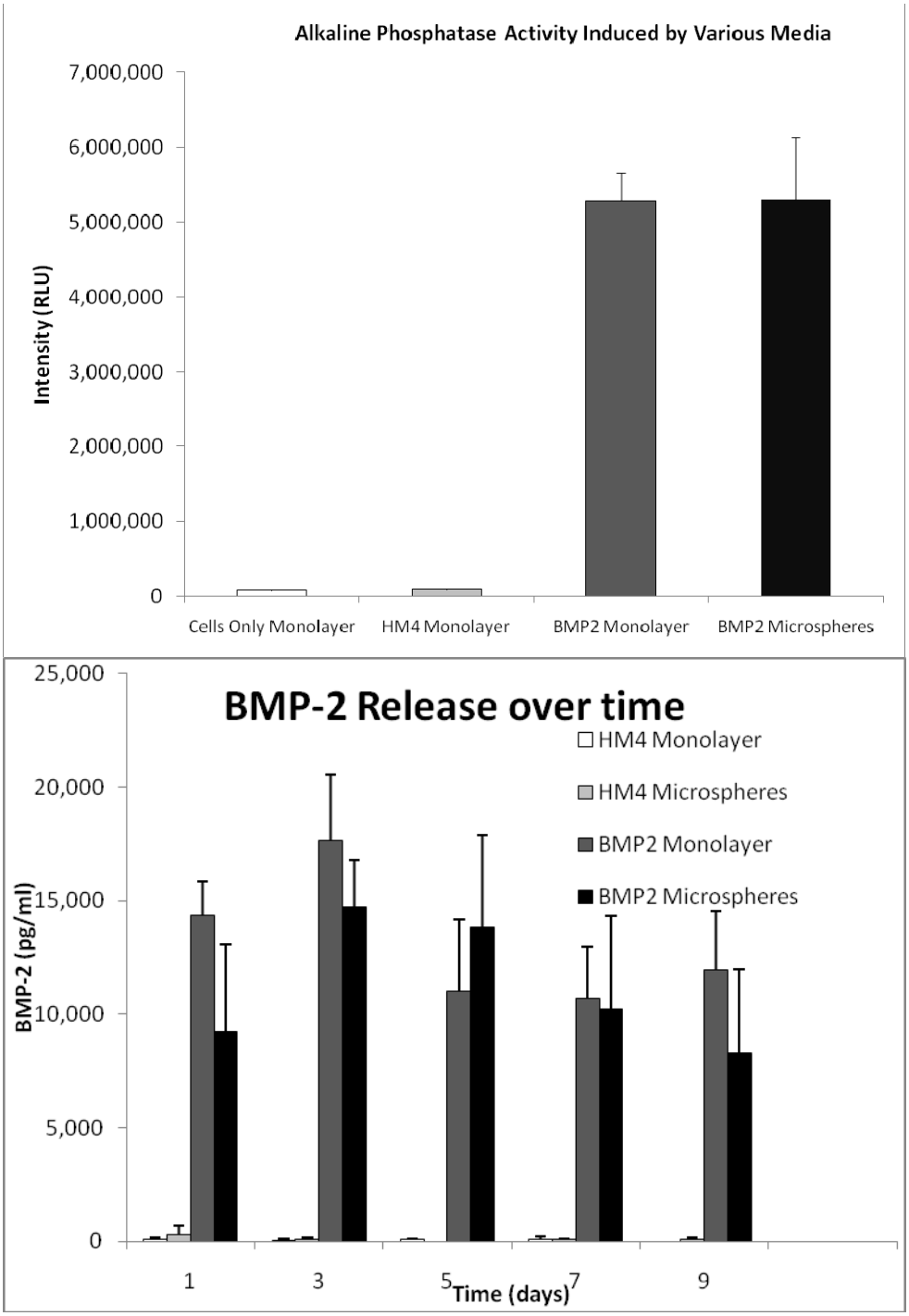

Figure 5. Comparison of BMP2 expression, secretion and activity after PEGDA encapsulation. **A.** BMP2 protein in culture supernatant, taken from AdBMP2 or Adempty cassette transduced cells (25000 vp/cell) (monolayer) or those encapsulated in PEGDA microspheres was quantified daily over one week using an ELISA. **B.** Alkaline phosphatase activity in W20-17 cells after addition of conditioned media from AdBMP2 or Adempty cassette transduced cells (25000 vp/cell) (monolayer) or those encapsulated in PEGDA microspheres. As a negative control, we also included culture supernatant from untransduced cells. Alkaline phosphatase activity is depicted as the average relative chemiluminescences units (RLU) where n=3. Error bars represent means ± SD for n=3. A student t-test was applied to demonstrate significance and all the samples demonstrated significance at the confidence interval $p < 0.05$.

In vivo comparison of transgene expression with and without encapsulation in PEG-DA hydrogel. To determine if the microencapsulation would prevent rapid clearance of the transduced cells and ultimately extend transgene expression, cells were transduced with an adenovirus possessing the reporter gene dsRED or an empty cassette control virus. This adenovirus was similar to the AdBMP2 virus; accept that it possessed a dsRED cassette in place of the BMP-2, and cells were transduced in a similar manner. Cells (5×10^7) were transduced with AddsRED (5000 vp/cell) and remained as a monolayer, or microencapsulated into microspheres, and 24 hours later directly injected into the muscle of the mouse hind limb. As a control, 5×10^7 cells were transduced with Adempty cassette virus (5000 vp/cell) and the encapsulated into microspheres and similarly injected into mouse hind limbs (n=4). Reporter expression within the tissues was then followed by live animal imaging for 2 to 34 days Fluorescent imaging was performed at

excitation and emission wavelengths of 568 nm and 590 +10 nm, respectively (figure 6). The excitation light was supplied by a 200 W Argon/Krypton laser and data were quantified and reported as a target to background ratio, where the specific signal was normalized to any background or autofluorescence.

Two days after the initial injection of cells, dsRED expression was readily detected whether cells were encapsulated or not and in no cases were cells or microspheres detected migrating from the injection site.

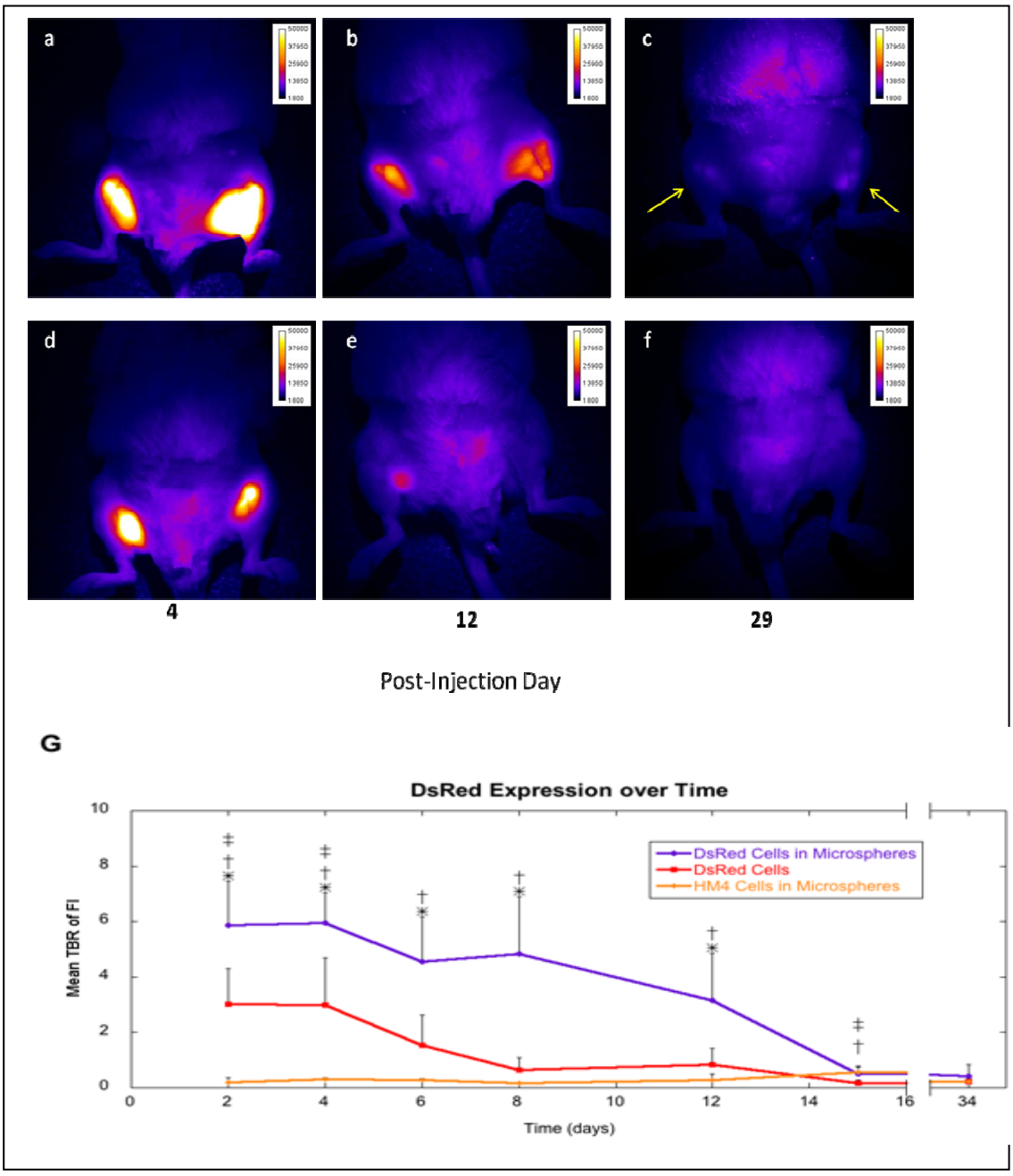

Because solution spread is a function of injection volume, dsRED expression in the tissues receiving the microspheres encompasses a larger volume than the encapsulated counterpart (Figure 6A). However, the magnitude of expression should not be affected by injection volume and dsRED expression was significantly elevated in microencapsulated cells compared to directly injected cells (Figure 6B), suggesting that the directly injected cells may already be starting to be cleared from the tissues. Reporter expression in animals receiving AdBMP2 transduced cells directly injected was substantially reduced after seven days and was indistinguishable from control (Figure

Figure 6. A. Optical fluorescence imaging of mice injected with cells expressing dsRED. Top panels (a through c) are images of a representative mouse (n=4) injected with dsRED-expressing cells encapsulated in microspheres and bottom panels (d through f) are of a mouse injected with dsRED-expressing cells directly, without microspheres. The images were taken at day 4, 12 and 29 post-injection of cells. By day 29, the fluorescent signal is at background levels or was undetectable for the mouse given dsRED-expressing cells without microspheres (f). Whereas, the signal remains detectable in the mouse given dsRED-expressing cells encapsulated in microspheres (c). **B.** Mean Target-to-Background Ratio (TBR) of Fluorescence Intensity (FI) in mice given unencapsulated dsRED Cells, microencapsulated dsRED cells or microencapsulated control cells. * $p \leq 0.05$ for microencapsulated dsRED cells versus microencapsulated control cells; † $p \leq 0.05$ for microencapsulated dsRED cells versus unencapsulated dsRED cells; ‡ $p \leq 0.05$ for unencapsulated dsRED cells versus microencapsulated control cells.

6B). This result was similar to our previous findings where the delivery cells are rapidly cleared. In contrast, the microencapsulated cells continued to be significantly elevated over background (Figure 6B). This was not due to autofluorescence of PEGDA indicated by the absence of signal at 590 ±10 nm in microencapsulated control cells. This 590 ±10 nm dsRED fluorescent signal was significantly elevated over that of microencapsulated cells transduced with Adempty cassette for 15 days (Figure 6B). After 15 days, these levels dropped; however, signal was still detectable (Figure 6A, arrows) in some animals, suggesting that the microencapsulated cells remained viable to express the dsRED transgene. Collectively, the data suggest that microencapsulation prolongs transgene expression within the tissues.

In vivo bone formation with and without microencapsulation in PEGDA hydrogels.

PEGDA microspheres encapsulating AdBMP2 transduced cells were next tested *in vivo* to determine whether prolonged BMP-2 expression could enhance heterotopic bone formation. As with the live animal imaging, similar numbers of AdBMP2

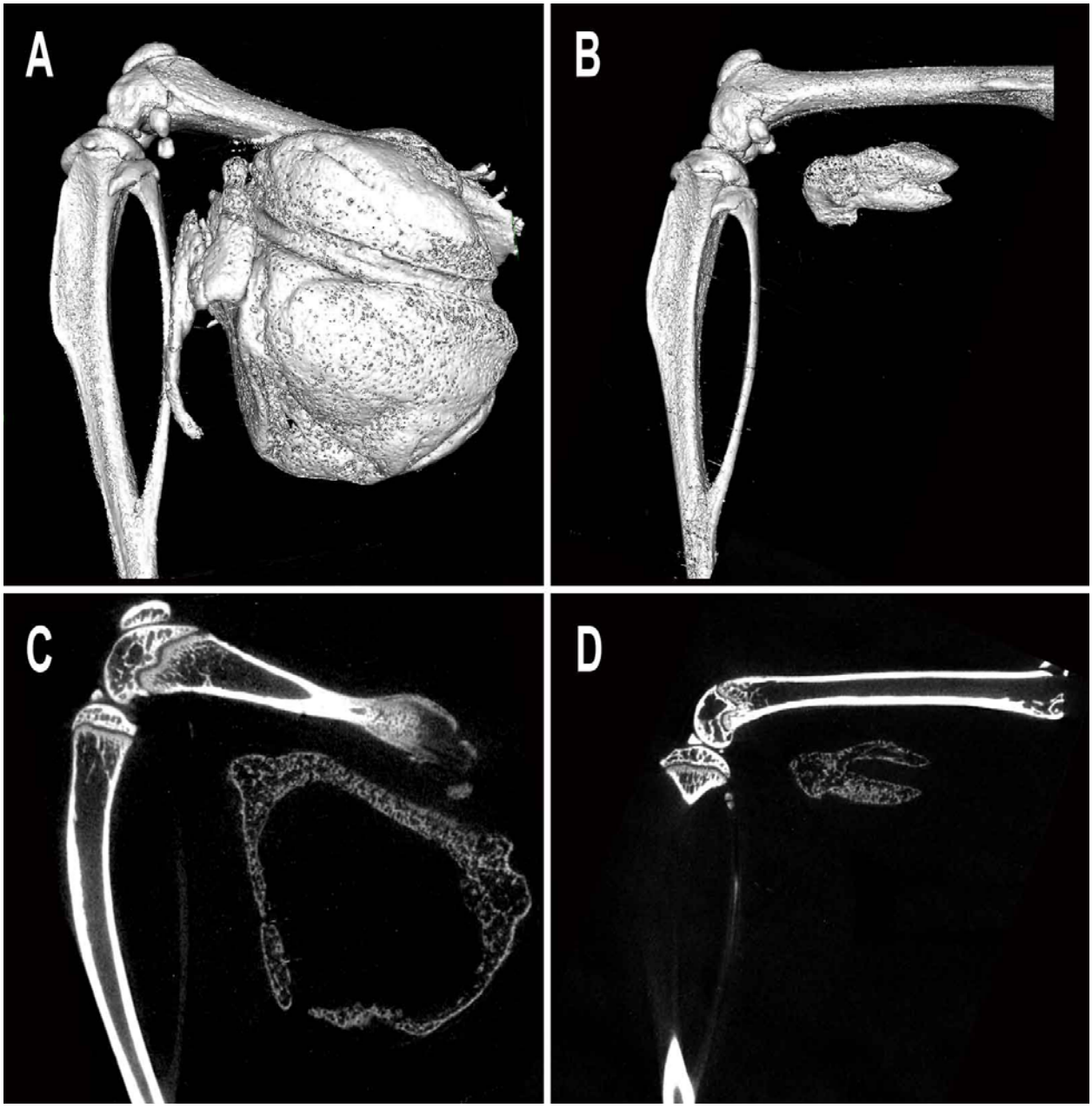

Figure 7 Micro computational analysis of the resultant heterotopic bone formation. Top images (**A, B**) are 3D surface renderings of the resultant heterotopic bone, while bottom images (**C, D**) are cross-sectional slices through the new bone. Panels A, C show the resultant mineralization of the muscle tissues after injection of AdBMP2 transduced cells (2500 vp/cell) and encapsulation into PEGDA microspheres (**A, C**) and/or direct injection (**B, D**). Both have a denser rim of bone, with a hollow interior structure, suggesting that the biomaterial did not alter bone patterning.

transduced cells were either directly or following microencapsulation injected into the muscle in mouse hind limb and the resulting heterotopic ossification was analyzed. MicroCT analysis of the resulting bone showed a significantly greater region or volume of heterotopic ossification in tissues receiving microspheres (Figure 7A, C) than those receiving directly injected cells (Figure 7B, D). Quantification of the groups (n=6) enabled direct comparison. Cross sectional microCT analysis of the newly formed bone revealed a similar architecture between the two samples. Heterotopic bone formed by both the microspheres, and the directly injected cells had a pattern of dense bone surrounding a hollow interior (Figures 7C and D); however the circumference of bone within the directly injected cells was significantly smaller.

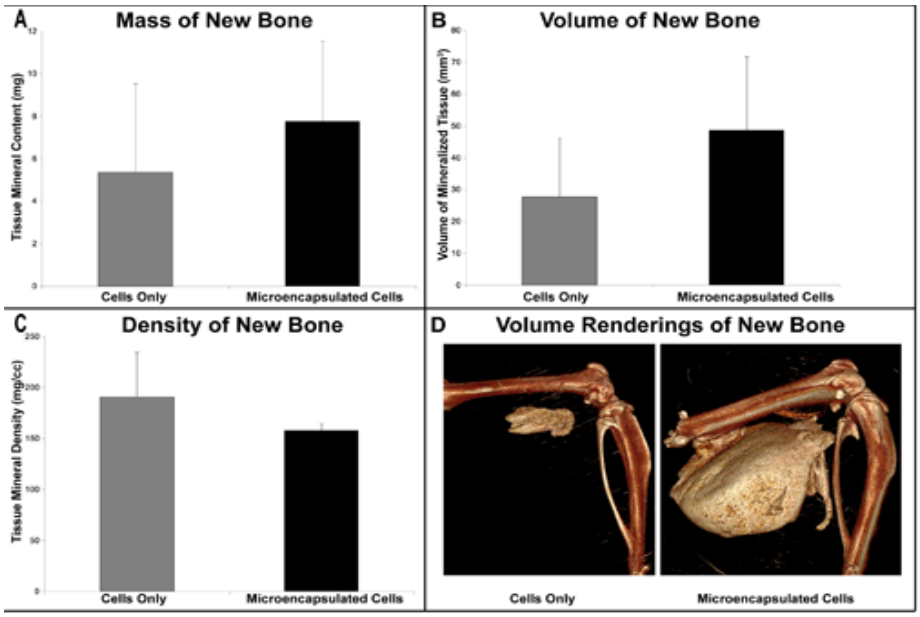

Microencapsulated AdBMP2 transduced cells resulted in approximately twice the bone volume produced when these cells were directly injected (Figure 8B). However, the bone tissue mineral content or mass of the new bone although trending towards an elevation in samples that received the microspheres, was statistically similar between these groups (Figure 8A). Most likely the lack of statistical significance results from the change in tissue mineral density of the new bone (figure 8C). It appears to be slightly less dense, leading to the overall similarity in mass. Interestingly, the less dense bone obtained from

Figure 8. Quantification of the heterotopic ossification using micro computational analysis. Cells were transduced with AdBMP2 and either directly injected or encapsulated into microspheres prior to injection, and the resultant heterotopic bone was analyzed two weeks later. Tissue parameters, **A.** Bone tissue mineral content; **B.** bone volume of mineralized tissue and ; **C.** Bone tissue mineral density were calculated for the newly formed bone (n=6 per group) and the means and standard deviations for each group calculated and compared to one using a one-way analysis of variance. Results indicate that mineral content is statistically equivalent (p=0.2) between the groups, whereas the microspheres had a significantly greater volume (p=0.038) than the AdBMP2 transduced cells directly injected. Alternatively, the bone tissue mineral density was significantly denser for the group receiving the cells directly as compared to the microspheres (p=0.029). Panel **D.** shows a 3D volume rendering of new bone formed in cell only and microencapsulated cells, respectively.

the microspheres, may in part be related to the fact that the microspheres have spread out the area of BMP2 release over a greater volume, and thus effectively diluted the concentration of BMP2 in any given area.

To further analyze the newly formed bone, tissues were processed, paraffin embedded and the new bone was visualized by hematoxylin and eosin staining. Both groups had significant new bone formation within the muscle (Figure 9). In tissues that had received the direct injection of AdBMP2 transduced cells there was a small compact piece of bone forming a ring-like structure encircling what appears to be blood and tentative stroma, and just exterior to this structure was significant adipose (Figure 9A). A similar structure was observed in tissues that had received microspheres (Figure 9B). Since the microspheres do not degrade over time, they appear histologically as gaps or holes within the matrix (Figure 9B). Thus, despite the presence of nondegradable microspheres, both structures were patterned to have a denser bone structure with a bone marrow like cavity on the interior.

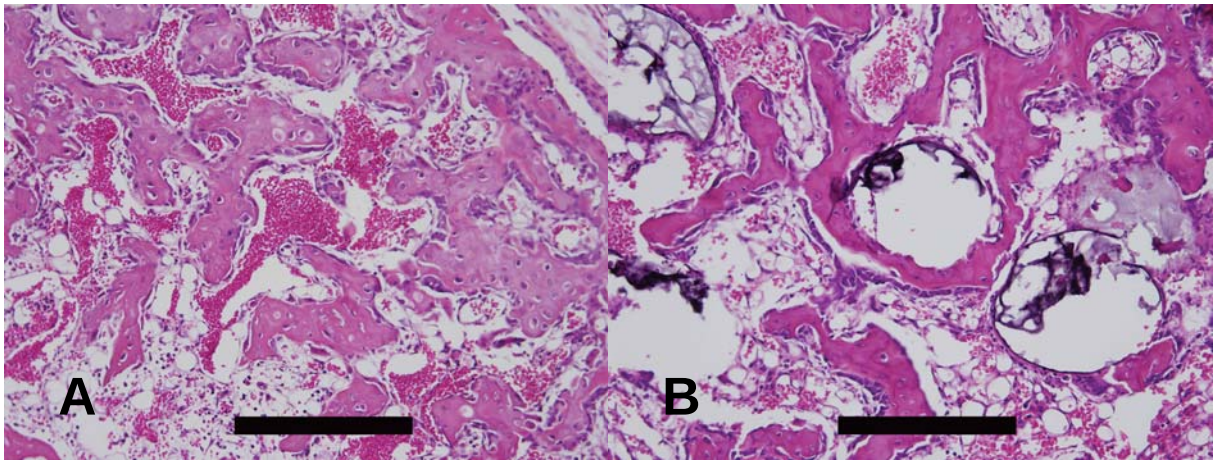

Figure 9. Photomicrographs of heterotopic ossification. Hematoxylin and eosin stains of new bone formation. **A.** direct injection. **B.** Microsphere encapsulated cells. Both groups show small compact pieces of bone forming ring-like structures, encircling what appears to be blood and tentative stroma in the inner region, with significant adipose just exterior to the new bone. Scale bars are 500 μm.

c. *To demonstrate the termination of BMP2 expression using an Ad5F35tet-BMP2-IRESCBRLuc vector in which expression can be tracked through live animal imaging.* ***(Months 12-24)***

We are currently working on this, and our preliminary data shows unequivocally that if we do not have expression of BMP2 sustained for over four days, the targeted heterotopic ossification will not work. Alternatively, we have already shown enhanced bone parameters in the presence of sustained BMP2 expression using the microspheres. Therefore this topic is some what completed. However, it would be potentially beneficial to have the option to eliminate the delivery cells at some point after we have achieved bone formation, therefore, we are working on introducing a caspase gene within our delivery cells, which is regulated and upon activation will force the cell to undergo apoptosis. Thus, AdBMP2 transduced cells can be eliminated at a point after bone formation is complete.

d. *To track BMP2 expression in vivo by identifying cells undergoing BMP2 signaling through confocal imaging which follows the translocation of a Smad 1 to the nucleus.* ***(Months 24-48)***

We initiated these experiments earlier than proposed since the set up of imaging this *in vivo* model is a large undertaking and will require a significant amount of time to validate. Initial experiments have been done to compare and pinpoint the changes in phosphoSmad signaling in tissues receiving the Ad5BMP2 transduced cells, as compared to those receiving cells transduced with control virus. This analysis was done in tissue sections to provide preliminary data before setting up the *in vivo* imaging.

These preliminary experiments will allow us to not only pinpoint locations within the tissues to focus, but also provide us with a time frame of signaling, thus providing incite for the in vivo studies. Figure 10, shows immunohistochemical staining for phosphoSmad using an antibody specific to the active phosphorylated form in tissue sections taken from tissues isolated four days after injection of the transduced cells. These initial experiments were done in wild type (C57BL/6) mice.

The phoshpoSmad reporter mice were generated using a targeting construct to modify the Smad1 genomic locus to express the CFP:Smad1 fusion protein at endogenous levels within cells that normally express Smad1. This construct is designed to insert CFP at the N-terminal end of Smad1 by replacing the start codon in exon 2. Using homologous recombination to generate correctly targeted ES cell lines, we have generated three independent ES clones which have been injected into blastocysts for the production of chimera mice. From these chimera mice, we have now obtained germline transmission in the animals and we have looked for the expression of CFP. Since these mice express the fusion protein reporter at endogenous Smad 1 levels, analysis of the tissues shows an extremely weak to undetectable level of expression. Unfortunately the limited amount Smad in tissues has made this strategy difficult to impossible to implement. Therefore in the coming year, we will focus our efforts on quantifying the responder cells, by immunostaining and nuclear co-localization of phosphoSmad using the current antibodies.

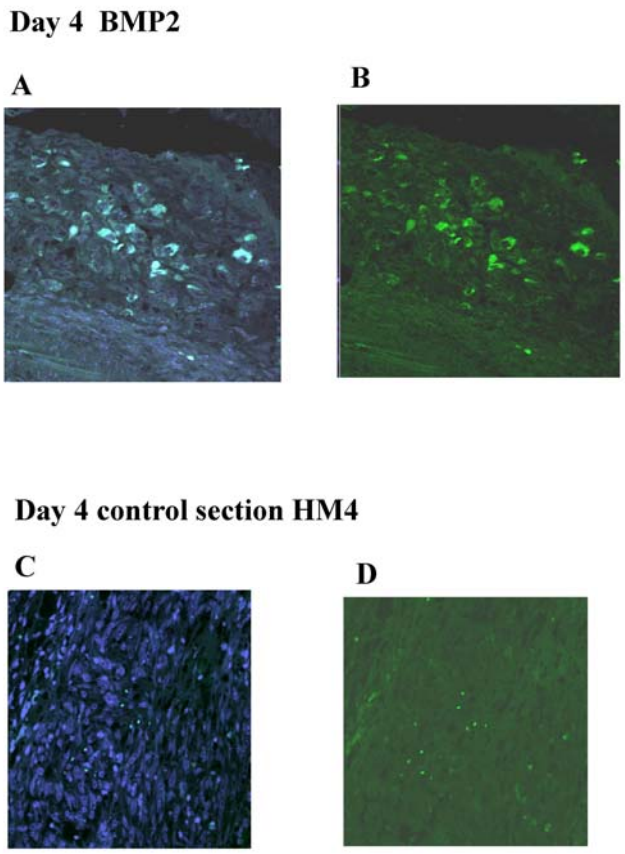

Figure 10: Immnuno-fluorescence staining on tissues isolated four days after receiving Ad5F35BMP2 transduced cells (A and B) or cells transduced with a control virus Ad4F35HM4 (C and D). Sections B and D are stained with Phospho-Smad1/5/8 antibody (1/100 dilution, Cell Signaling technology) and a secondary antibody anti-rabbit Alexa Fluor 488 conjugated. Sections A and C and stained with Phospho-Smad1/5/8 and counterstained with DAPI

e. *Approximately 470 mice will be used in the experiments in this task. NOD\Scid 36 mice/experiment and we request three experiments, plus additional for breeding or 250 total and SMAD 1= 63 mice/experiment and we request three experiments, plus several for breeding or 220 total.*

Task 2: To design an optimal hydrogel material that will rapidly promote endochondral bone formation and be capable of removal through bone remodeling processes.

a. *Optimize and develop a hydrogel that can be specifically degraded by osteoclasts.* ***(Months 0-24)***

Synthesis of Cathepsin K degradable PEGDA hydrogel

- Cathepsin K-sensitive sequence (CTSK):
  - MGPSGPRGK
- Control sequence:
  - MPGSPGGRK
- Conjugate with 3400 Da PEG-SCM

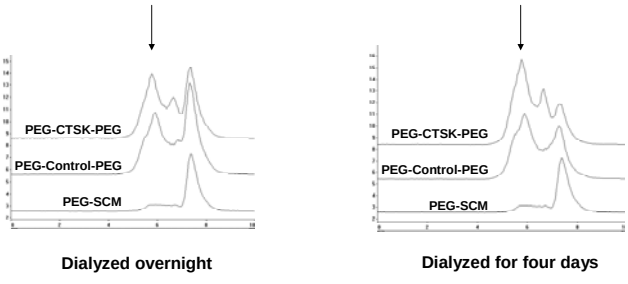

Dialyzed overnight Dialyzed for four days

We have synthesized the peptide MGPSGPRG (Gowen et al;1999) using a 431A solid-phase peptide synthesizer (Applied Biosystems, Foster City, CA). In order to make degradable PEG, we start with PEG-DA-SMC (succinimidyl carbonate). The PEG-SMC is conjugated with our peptide in order to get PEG-PEPTIDE-PEG. So, we expect to obtain three peaks representing the completely conjugated product: PEG-PEPIDE-PEG, incompletely conjugated product: PEG-PEPTIDE and unconjugated product: PEG-SMC (Figure 11).

Figure 11: Results of HPLC analysis of the conjugation of peptide with the PEG-DA hydrogel.

We have run GPC tests on it and the results indicate that there is still unconjugated PEG, ie: we have PEG-Peptide or free PEG in the preparations. We have tried changing the ratio of peptide to PEG, changing the length of conjugation time, increasing the pore size of the dialysis membrane and changing the length we dialyze the conjugation products. These have led to a higher concentration of PEG-PEPTIDE-PEG as indicated by the GPC results (Figure 11). We have cathepsin K (Calbiochem; Cathepsin K, His•Tag®, Human, Recombinant, *E. coli*) and are ready to test their degradability.

The next step in developing this material was to test whether the conjugation of the cathepsin K site is enough to degrade a polymerized peptide. We placed microbeads of the hydrogel in the 25 µL cathepsin K vial (stock solution 0.2 mg/mL cathepsin K) incubated at 37°C. The PEG-peptide-PEG hydrogels (where "peptide" refers to the cathepsin K degradable peptide) were tested for swelling and degradation in PBS and cathepsin K, respectively. A swelling hydrogel typically has a logarithmic curve, like the PBS curve, where the weight of the gel increases and reaches a maximum. A degrading hydrogel will initially show an increase in weight as broken bonds allow more water in, allowing the hydrogel to swell more. Then the swollen weight will drop dramatically. Figure 12A and B shows evidence that the hydrogels are at least partly degradable. However, the results also suggest that the material cannot be completely degraded suggesting the PEG-Peptide-PEG is limiting, or that the sites are not efficiently digested. To circumvent the latter, we are resynthesizing the peptide to include additional 3 glycines on either end to lengthen the protein region and ensure that cathepsin K can reach it efficiently within its PEG backbone. Hopefully with the additional amino acids on the peptide site, any constraints the protease may have in binding for digestion of the site will be alleviated.

We have been recently testing the new protease site which now has a glycine repeat sequence was designed into the peptide in order to act as a spacer. Thus the modified peptide sequence is GGGMGPSGPWGGK, see figure 13. The W is tryptophan that we will use to track the degradation of the hydrogel by measuring tryptophan release into the media by taking Ultra-Violet/Visible (UV/VIS) Spectrophotometry absorbance measurements at 280 nm.

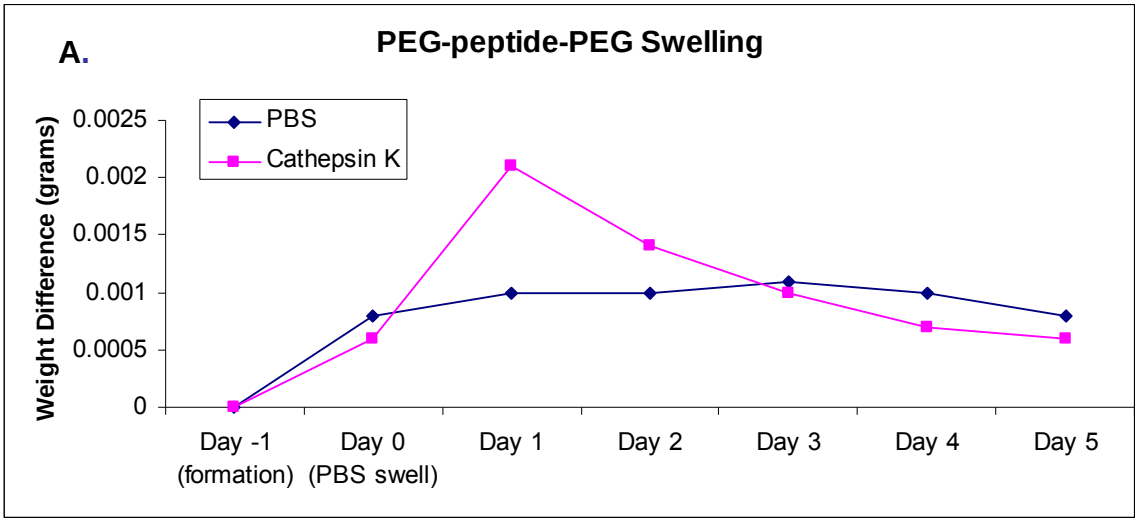

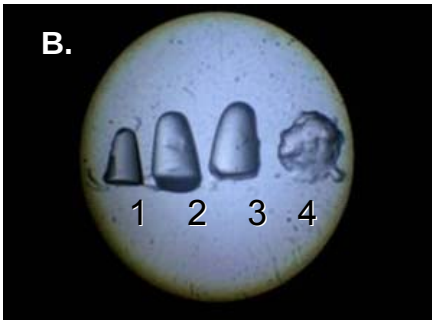

Figure 12 Swelling test of the Cathepsin K degradable peptide. **A.** Weight changes upon swelling during degradation. **B.** Hydrogels after swelling and degradation. (1) PEG-CTSK-PEG in buffer w/o proteinase K; (2) PEG-CTSK-PEG w/ 0.125 mg/ml; (3) PEG-control-PEG w/ 0.125 mg/ml; (4) PEG-CTSK-PEG w/ 0.250 mg/ml after compression.

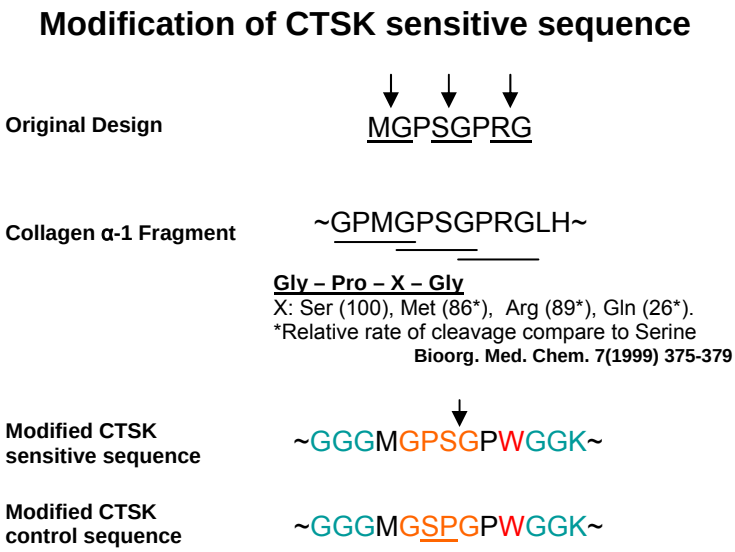

Figure 13: Schematic of the changes made in the peptide to introduce the cathepsin K protease site into the PEG-DA hydrogel.

Rather than incorporate this new peptide immediately into a PEG backbone, it was tested directly. We ran mass spectrometry on the peptide in order to see if the predicted molecular weight (1143.43) of the peptide was present. We found a peak at 1143.9, indicating success of the peptide synthesis. Next, we incorporated the peptide with activated cathepsin K and repeated the mass spectrometry. The 1143.9 peak was now absent, and present were predicted cleavage products (figure 14).

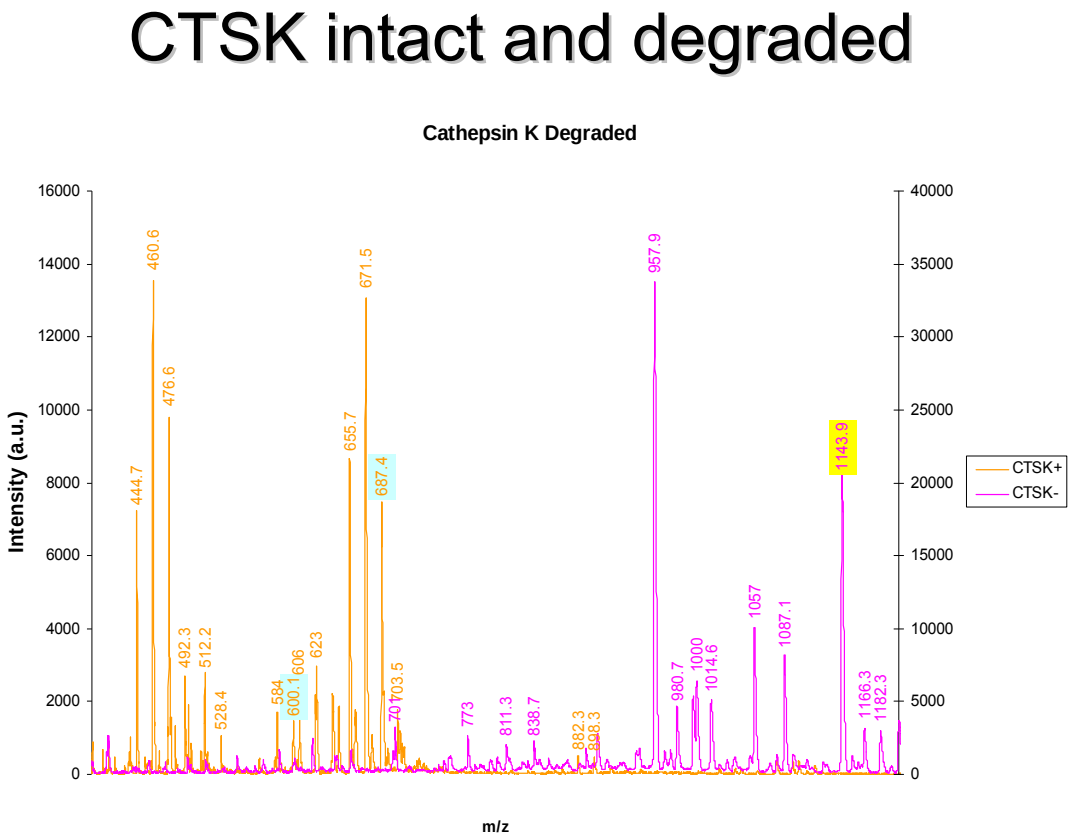

Figure 14: Mass spectrometry of the peptide consisting of the cathepsin K protease site (CTSK) before and after cleavage with the protease.

We proceeded with degradation tests when prepared hydrogels degraded almost immediately in proteinase K. Proteinase K was used as a positive control. While the hydrogel degrades, the peptide that was incorporated into the hydrogel structure will be cleaved by enzymes and gradually release into solution. The degradation profiles of GPSG hydrogels were measured by monitoring the concentration change of tryptophan in solution at UV absorbance of 280 nm. Crosslinkable GPSG hydrogels were polymerized in microcuvettes and incubated with enzyme solutions. After equal swelling in TBS overnight, hydrogels were treated with different enzymes to evaluate the degradation profiles (Figure 15). After incubation with different

enzyme solutions for 24 hr, hydrogels in cathepsin K and proteinase K solutions had similar degradation profiles, both indicating a rapid tryptophan concentration increase within the first hour and reaching about 80% release of total tryptophan at 24 hr. No degradation was observed when hydrogels were incubated in TBS buffer, NaOAc buffer, and plasmin. Hydrogels incubated in nonspecific collagenase I and collagenase III solutions also released 40% of incorporated tryptophan after a 24 hour incubation.

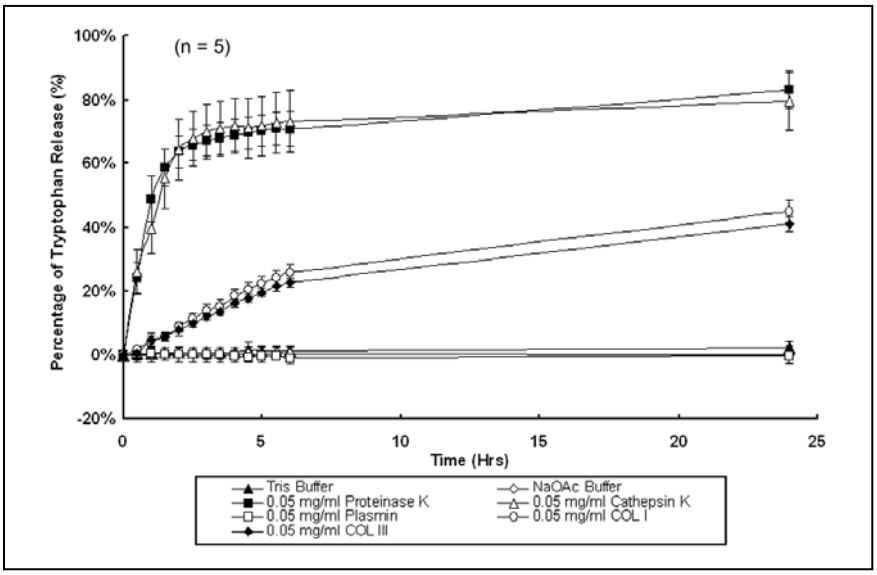

Figure 15: Degradation of hydrogel over time. Degradation profiles of cathepsin K-sensitive GPSG hydrogels. Hydrogel droplets (3 µl) were polymerized in each micro-cuvette and swelled overnight with 250 µl of TBS buffer. Each hydrogel was incubated in buffer or enzyme solution at 0.05 mg/ml at 37^{O}C. UV absorbance at 280 nm was measured over 24 hours to monitor tryptophan release corresponding to the degradation of the GPSP hydrogels.

b. *Engineer cellular binding sights within the hydrogel to determine if this improves cell viability of the transduced cells, and in turn BMP2 expression, and to tentatively enhance the migration of mesenchmyal stem cells to the sight of bone formation.* ***(Months 0-24)***

We have actually been changing this aim to meet the needs of both the encapsulated cells but also allow for the selective degradation. Since the recruitment of osteoclasts often comes from the expression of RANK ligand (RANKL) and degradation requires RGD binding, we have designed a large number of RGD binging sites within the hydrogel material (Yang et al, 2005). This should greatly enhance binding and long term viability of our encapsulated cells, but it will also permit the hydrogel to be degraded by osteoclasts which adhere to the bone surface through RGD, form a ring structure (Figure16) of the ruffled border (Hollberg *et al*, 2005) and then activate a proton pump as well as secrete specific proteases such as cathepsin K. Therefore, RGD is critical to the recruitment, adherence, and resorption of the hydrogel by osteoclasts. RGDS will also aid in recruitment and binding of other cell types to the surface of the biomaterial, and allow for the newly forming bone to be close enough to the surface that it can easily fill in the areas removed by remodeling.

c. *Test addition of proteins that may enhance the BMP2 bone inductive response, such as VEGF-A or -D and compare enhancement of bone formation.* ***(Months 24-36)***

We have a manuscript coming out that shows significant elevation in these VEGF proteins after expression of BMP2 in the tissues (Fouletier-Dilling *et al*, JBMR 2009). Thus we do not believe that this will add anything to our current system. In the event that minimal BMP2 is made, VEGF seems to emphasize the bone reaction, presumably since it is one of the first downstream proteins we observe elevated after addition of the AdBMP2 transduced cells. However, we are getting significant elevation of these proteins through using our cell based gene therapy system, and thus we find combinations of these do not enhance the bone reaction. Therefore we propose to discontinue this testing.

d. *Test these gels in vitro.* ***(Months 12-36)***

We have previously tested the degradation profile of the cathepsin K (CTSK) sensitive-hydrogel *in vitro* with proteinase K, collagenase, and cathepsin K (Figure 16). Before proceeding with the animal study, we first performed a cell based *in vitro* test to demonstrate that the CTSK-sensitive hydrogel can be gradually remodeled by osteoclasts (OCs). We used the RAW264.7 monocyte cell line that has been demonstrated in the literature to undergo fusion and osteoclastogenesis in the presence of 20 ng/ml nuclear factor kB ligand (RANKL). We first differentiated the RAW264.7 cells with 20 ng/ml RANKL in standard tissue culture for 6 days, at which time we observed that multi-nuclei, osteolclast-like cells by the end of the differentiation period. Then 1.5 x 10^5 cells/cm^2 osteoclasts-like cells were seeded on 10% (W/V) hydrogel (100% CTSK-sensitive

hydrogel), which contained 10mM acryl-PEG-RGDS and Alexaflour 680 labeled acryl-PEG-RGDS. The differentiated osteoclasts-like cells were then cultured on the hydrogel surface in RANKL-free medium for 24 hours before further analysis. The cells and gel were than fixed and stained with DAPI and rhodamine phalloidin after 24 hours. Images were taken by LSM-5 LIVE and then processed by Image J and OsiriX (Figure 16).

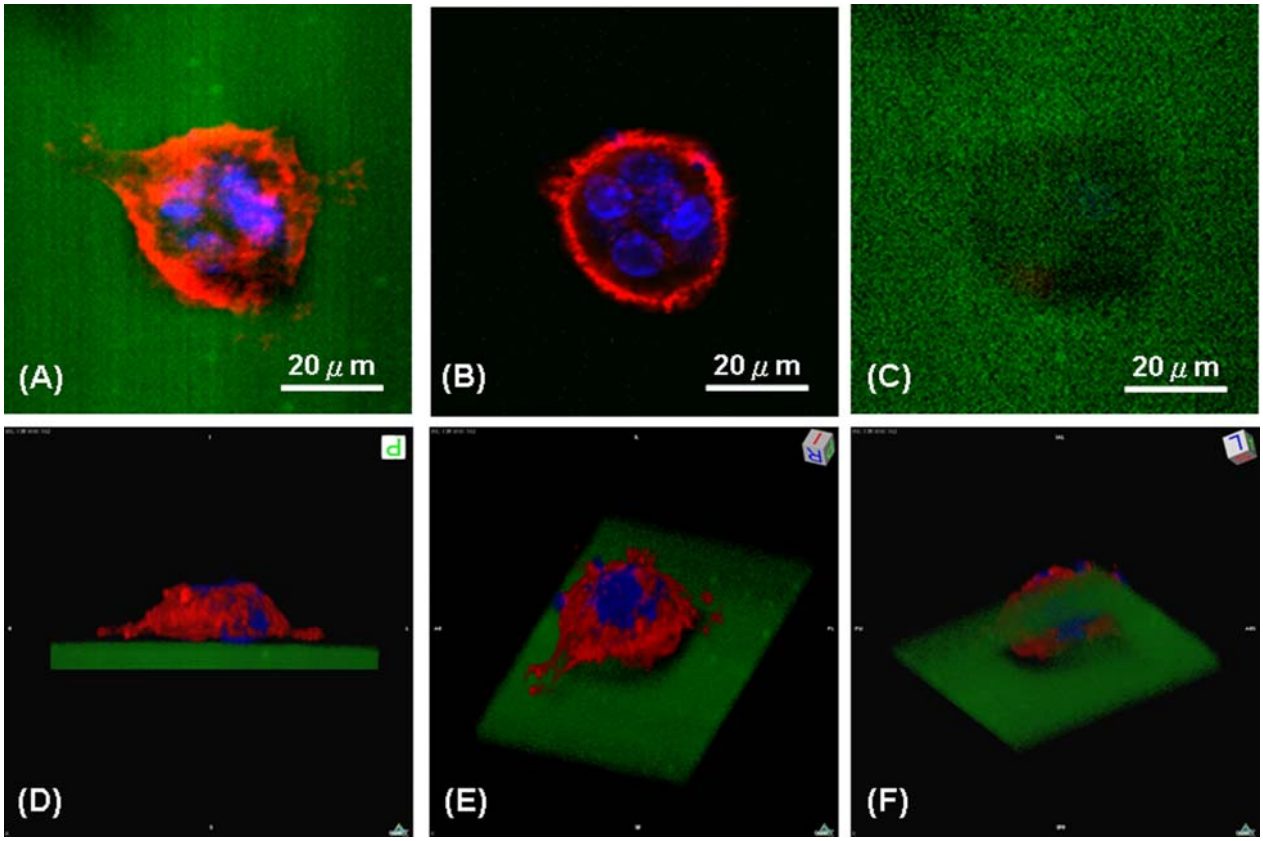

Figure 16: Three-dimensional fluorescent image reconstruction of an active osteoclast on the GPSG hydrogel surface. The GPSG hydrogel was labeled with Alexafluor 680 fluorophore (green), which is conjugated with the acryloyl-PEG-RGDS and incorporated into the hydrogel by photo-polymerization. The cells were fixed and permeabilized before staining the nuclei with DAPI (blue) and F-actin by rhodamine phalloidin (red) 48 hours after seeding. (A) Composed z-stack images of the osteoclast and hydrogel. (B) Sealing ring and multiple nuclei of the osteoclast. (C) GPSG hydrogel with fluorescent signal lost at middle. Z-stack Images were reconstructed using the volume renderings algorithm and presented from (D) side view, (E) orthogonal view from above, and (F) from bottom. The resorption site is located underneath the osteoclast, which was can be observed in the loss of the fluorescent intensity of Alexafluor 680. The resorption pit on the hydrogel surface can be clearly seen from different angles, suggesting that the GPSG hydrogel has been degraded by cathepsin K secreted by osteoclasts.

The resorption site is observed underneath the osteoclast, which was shown by a loss of the fluorescent intensity of Alexafluor 680, but not under osteoblasts cultured on the hydrogel sheets (Figure 17). This demonstrates that the hydrogel is being cleaved by the osteoclasts selectively, and are tunable to the parameters of bone remodeling.

Figure 17: Three-dimensional fluorescent image reconstruction of an active osteoclast on the GPSG hydrogel surface. The GPSG hydrogel was labeled with Alexafluor 680 fluorophore (green), which is conjugated with the acryloyl-PEG-RGDS and incorporated into the hydrogel by photo-polymerization. The cells were fixed and permeabilized before staining the nuclei with DAPI (blue) and F-actin by rhodamine phalloidin (red) 48 hours after seeding. (Left) an osteoclast actively bound to and degrading the hydrogel, while (Right) osteoblasts bound to the hydrogel, are unable to degrade the material, no indentations were observed on the material.

DAPI Rhodamine Phalloidin Alexafluor 680

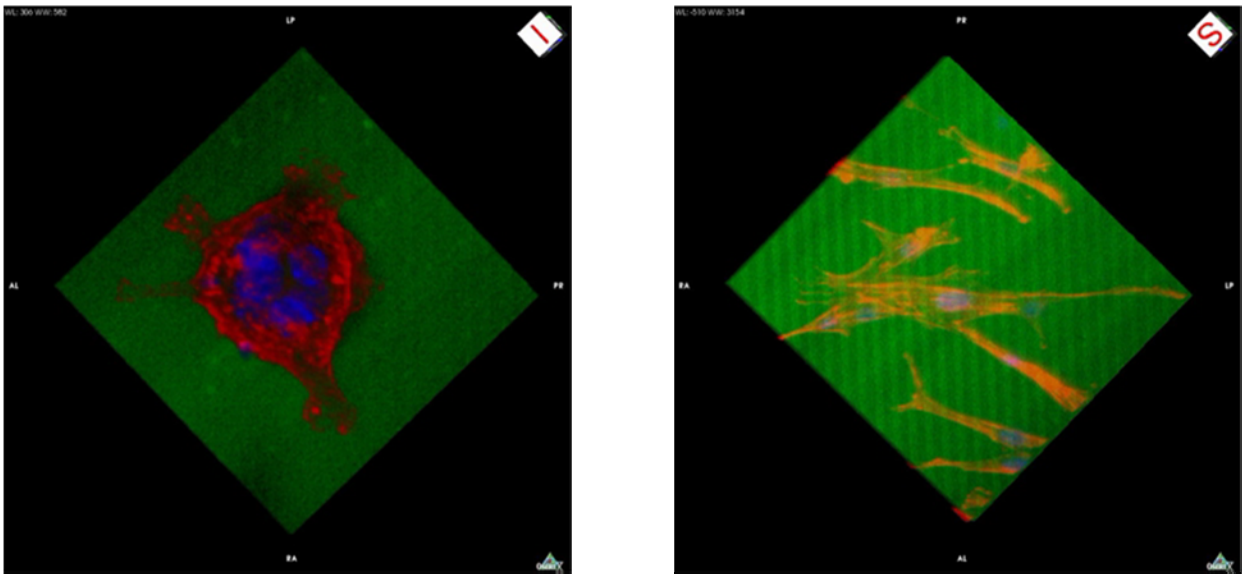

d. *Test these gels in vivo.* ***(Months 36-48)***

Studies to test these hydrogel *in vivo* are just being initiated. These studies are right on track for our time frame. Figure 18 shows preliminary studies in which the degradable beads were placed in the animal to induce heterotopic ossification. As can be seen in figure 18A, the resultant bone, two weeks after induction of bone formation with the degradable beads, shows a bead like structure, while the non-degradable counterpart

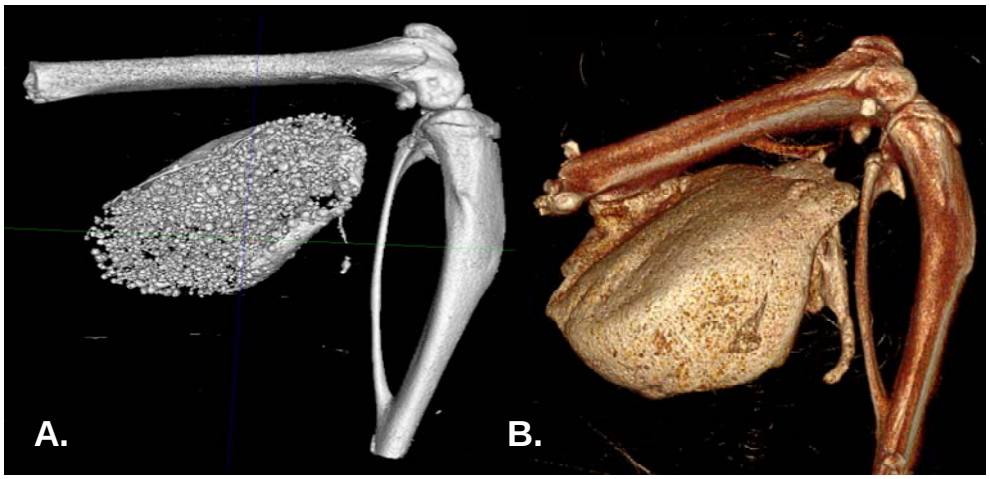

Figure 18: MicroCT Analysis of heterotopic ossification, after induction by AdBMP2 transduced cells encapsulated in **(A)** Cathepsin K degradable PEGDA hydrogel and **(B)** nondegradable PEGDA hydrogel

looks more similar to the skeletal bone, in having a denser bar of bone along the surface. We hypothesize that this is partly due to rapid remodeling of the bead structures with the rapid initial new bone, and thus termination of the experiment prematurely, by early degradation of the beads. However, will need to analyze the bone formation at all stages, and determine the timing of the resorption, the timing of transgene expression and early biological stages of HO, in comparison to HO obtained from nondegradable beads before we can discern the tentative cause. We are currently focused on looking at transgene expression within the tissues using the dsRED reporter system, and live animal imaging, to determine timing of degradation, and length of tentative BMP2 expression within this model. Further we are evaluating these and other samples taken at weekly intervals by both radiological and histological analysis. Depending on the outcome of these results, we can further optimize or tune the degradable beads to degrade more slowly or quickly depending on our findings. This can be achieved by reducing the number of protease sites within the structure, or altering the sites completely.

e. *Approximately 500 mice (NOD\Scid) will be used to complete the experiments in this task. This will provide us with the 468 we need to complete the proposed experiments as well as an additional 32 for breeding stock.*

Task 3: To achieve rapid bone formation by percutaneous injection of the encapsulated Ad5F35BMP2 transduced human bone marrow mesenchymal stem cells (hBM-MSCs) into the adjacent musculature of athymic rats in a model of nonunion.

a. *Obtain approvals through the DOD institutional review board for approval to work with the human mesenchymal stem cells.* ***(Months 0-12)***

We have approval to use human mesenchymal stem cells, and are currently testing these cells for both viability and BMP2 secretion after encapsulation in the PEG-DA hydrogel. Also we have been working on developing the protocols for encapsulation of the rat fibroblasts to confirm maximum BMP2 secretion and viability. Human MSCs are used in the athymic animals but in order to validate this system in immune competent animals we generated a Wistar rat MSCs. Because of the nature of how MSCs are obtained it is impossible to obtain autologous cells, but rather these are allogenic or from litter mates of the recipient animal. We recently generated the rat MSCs and have been working on characterizing them to ensure they possess their stem cell functions. We are also confirming that these cells can express functional BMP2 after transduction with the AdBMP2 virus. Simultaneous to this we rapidly generated skin fibroblast cell lines, both autologous and allogenic to start to characterize the resultant bone formation in wild type rats. We again chose to confirm that these primary cells could secrete functional BMP2 after transduction with an AdBMP2 virus. Figure 19 shows the results of the functional assay, in which culture supernatant is added to the W20-17 cells which is a cell line that responds to functional BMP2 by undergoing differentiation, and elevation in alkaline phosphatase. As seen in Figure 19, all the cell lines could readily secrete functional BMP2 at similar levels to our positive control. We next introduced the cells into the Wistar mice using a heterotopic bone assay. The allogenic cells were injected into the animal in comparison to those encapsulated in the microspheres. Figure 20 shows the resultant x-rays from these experiments. Surprisingly, we did not observe bone formation even at 3 weeks after induction when AdBMP2 transduced allogenic (litter mate) cells were used, while alternatively, we observed new bone formation within two weeks of induction when we used autologous cells. The data suggests that the degree of genetic out breeding within the

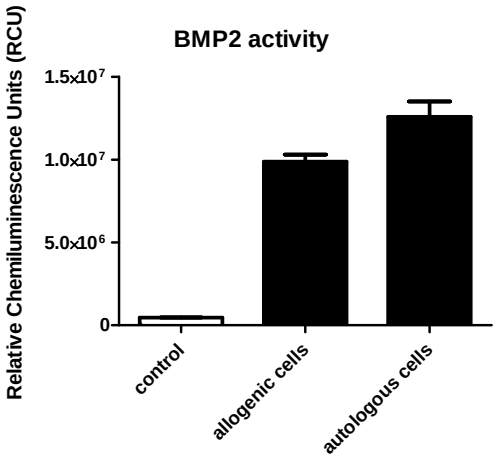

Figure 19: Quantification of BMP2 activity after AdBMP2 transduction of allogenic and autologous Wistar rat skin fibroblasts.

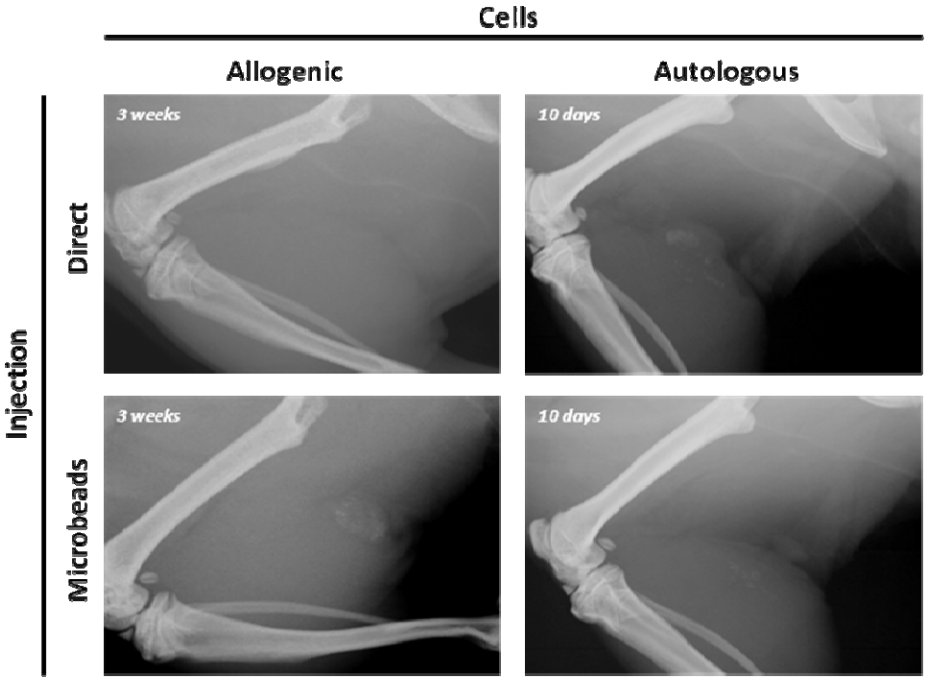

Figure 20: Radiological analysis of heterotopic bone formation after induction with AdBMP2 transduced autologous or allogenic cells either directly injected or encapsulated in microspheres and injected. Tissues receiving autologous cells were analyzed at 2 weeks whereas the tissues receiving allogenic cells were analyzed at 3 weeks.

Wistar rat colony (between littermates) was enough to circumvent the bone formation, whereas the adenoviral transduction does not appear to affect bone formation in these animals. As expected microencapsulation of the either autologous or allogenic cells, alleviated this problem and bone formation was obtained independent of the type of cells (figure 20). Figure 21 shows the resultant bone formation in when allogenic cells were used. We are currently sectioning the tissues which received the AdBMP2 transduced autologous cells. We do observe some giant cells within the newly forming bone, however, we have now traced that phenomena to the mineral oil used to form the microspheres. We have currently developed molds that will avoid the use of oil in production of the microspheres, and we have eliminated the giant cells. In the tissues which received cells directly injected, we observed no changes from normal muscle tissue within this time frame (Data not shown). **This is a major finding for the field of gene and stem cell therapy. We will continue to complete these studies, using the allogenic MSCs either directly or in microspheres, to determine if these cells also lead to immune clearance, and suppression of bone, or whether they are capable of behaving more like autologous cells. Further, the ability to encapsulate these cells, and avoid immune reaction, is a huge addition to all cell based gene therapy systems which want to deliver secreted proteins.** This work should be completed and published within the next 6 months.

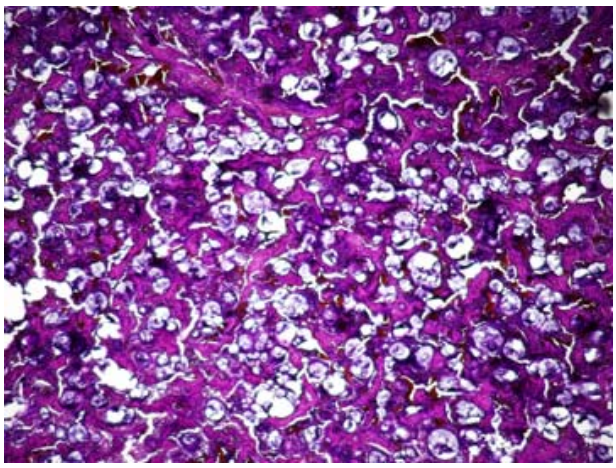

Figure 21: Resulting bone, two weeks after delivery of microspheres containing AdBMP2 transduced cells. Direct injection tissues appeared to be normal muscle with no apparent bone formation or reaction at all (data not shown).

b. *Once the gels have been modified to offer optimal properties for bone formation and removal, we will test these in a rat model of a critical-size defect. We will demonstrate the ability to induce bone healing in the presence of tetracycline.* ***(Months 24-40)***

Approvals have been obtained from Baylor College of Medicine and more recently from the Department of Defense for both the animal experiments and use of the human materials. Because we were able to complete this rapidly, we have initiated the studies using a critical defect rat model. We recently have also been focused on using an alternative to this model, which provides a much faster more reliable critical size defect, for testing of the biomaterials. We have approval for this amendment from the Baylor College of Medicine IACUC committee. In this model, we introduced a 1 to 10 mm defect into the fibula bone, to determine the "critical size" which would not heal on its own. Surprisingly, as seen in figure 22, none of the defects including simple fracture were able to heal, but rather the bone resorbed in all cases to a uniform defect size, within two weeks after induction of bone formation. MicroCt analysis of the samples revealed bone healing at the boundary of the defect. Samples examined at 2 weeks appeared to have a non-mineralized central core, suggesting that the bone had not formed over the defect boundary, whereas at 6 weeks, the end

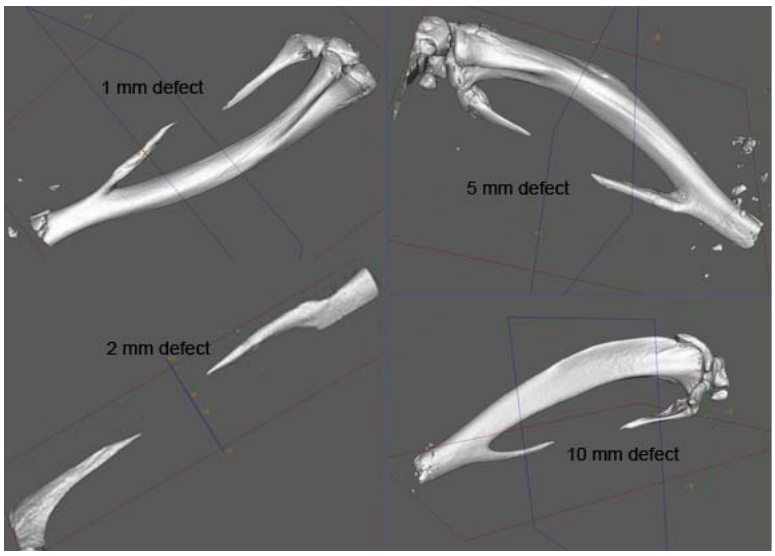

Figure 22: MicroCT analysis of the rat fibula 6 weeks after introduction of varying size defects. The numbers in mm represents the original size defect introduced into each sample. The samples shown are representative of n=3 samples.

of the bone appears to be mineralized with no visible central core. We believe this model is highly relevant for testing our gene therapy system, since in no case was the skeletal bone able to contribute to bone healing. In fact the skeletal bone actually resorbs, and therefore any observed bone formation would be a direct result of the heterotopic bone formation that we launched using our system. In this model, the adjacent tibia remains intact and thus provides the necessary stabilization. Thus no additional hardware is required, and the surgical procedure is quite rapid.

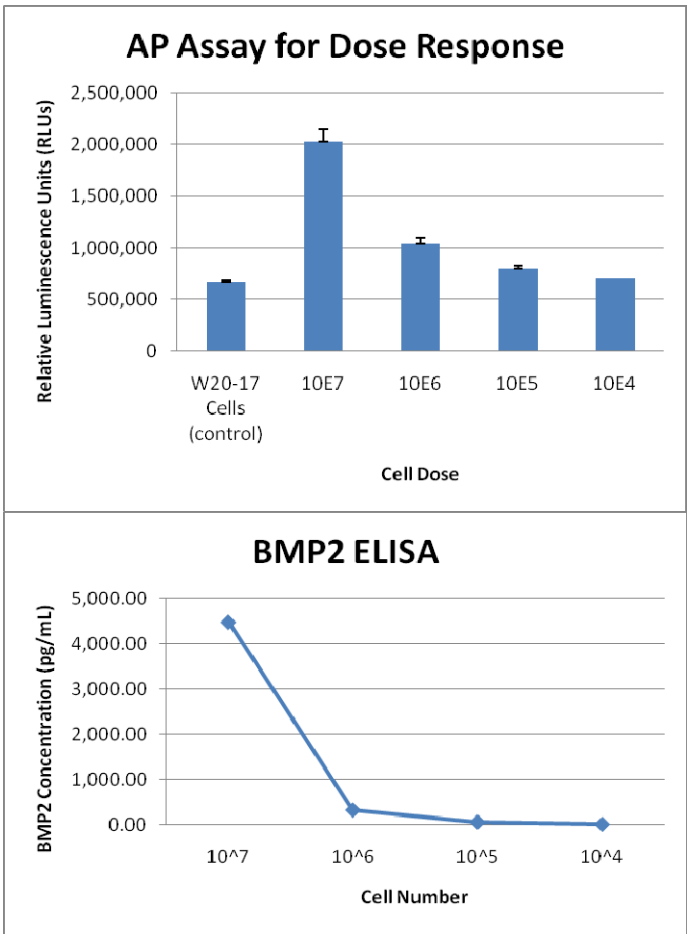

To determine the optimal number of cells that will lead to rapid bone healing we did dose escalation experiments in which we increased the number of cells added to the defect in log increments. Varying numbers of cells were transduced with AdBMP2 (2500 vp/cell) and then culture supernatant harvested and BMP2 quantified. As can be seen in figure 23, the highest number of AdBMP2 transduced cells had more total BMP2 produced as compared to the lower doses. By the lowest dose 1 x 10^4 transduced cells, BMP2 levels are so small that they almost undetectable by these assay, and not statistically elevated over the control.

Figure 23: Quantification of BMP2 protein from escalating numbers of AdBMP2 transduced cells.

As seen in figure 24, the lowest dose 5 x 10^4 cells resulted in no bone healing, but rather resorption as expected with the control. However, all other doses resulted in bone formation; however the next dose of 5 x 10^5 resulted in a small amount of bone formation, unfortunately upon evaluation using microCT, the small amount of bone formed, is adjacent to the skeletal bone, and does not bridge the defect (data not shown). The two highest cell numbers resulted in substantial bridging bone within the defect. Suggesting that at these doses the heterotopic bone could easily fill the void region of the skeletal bone.

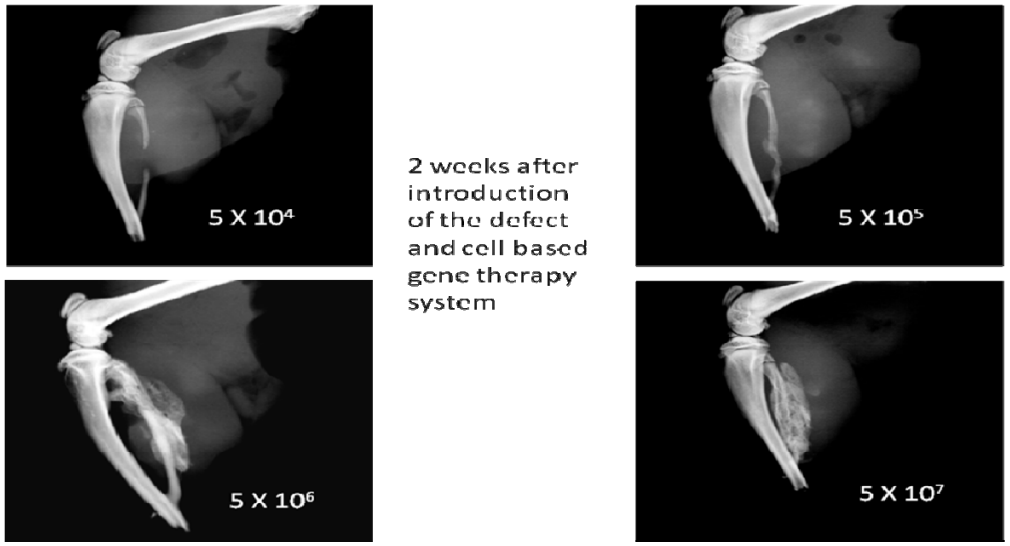

Figure 24: Radiographic analysis of a fibular defect introduced into rats two weeks after AdBMP2 transduced cells were introduced into the defect at varying doses.

c. *Analyze the modified injectable hydrogel for optimal volume, in vivo crosslinking, design, selective degradation, and inflammatory reaction using both live animal imaging and histology.* ***(Months 24-48)***

These experiments are underway; we are introducing a new live animal imaging system based on Infrared fluorescent protein (IFP) (Shu X, et al, Science 2009). This system is more sensitive than the dsRED which unfortunately appears to be shielded by the resultant bone we will introduce this in the rat fibula model to demonstrate expression of the transgene, degradation of the bead, and formation of the new bone. These experiments are currently ongoing and should be completed within the next year. Figure 26 shows the resultant bone formation within the fibula after delivery of the AdBMP2 transduced cells within the

Figure 26: Radiological analysis of new bone formation after delivery of 2 x 10^5 AdBMP2 transduced cells encapsulated in PEGDA microspheres. These microspheres are nondegradable, however the bone appears to remodel over time.

microspheres. As can be see there is a significant amount of bone around the microbeads as expected, however, it is interesting that by 6 weeks, the bone has started to remodel. It is not clear why the bend is within the newly forming bone tissue, but rather important to note that the HO appears to be somewhat fused, and starting to remodel into a contiguous fibular structure.

d. *Bone healing will be tested both biomechanically as well as radiologically using microCT to confirm the fusion.* ***(Months 40-48)***

We also followed repair of skeletal bone with heterotopic bone formation over time, to determine if the large amount of heterotopic bone forming at the defect site would fuse and remodel into the missing fibula structure, if it would remain as the large mass of heterotopic bone, or if would resorb altogether. Therefore we

Figure 27: BMP2 induced heterotopic bone formation in a rat fibula critical size defect model over time. The samples were x-rayed at 2, 4 and 6 weeks after induction of bone formation with the cell based gene therapy system. Extensive heterotopic bone formation appears to remodel and resorb the leaving the regenerated bone within the fibula that has fused to the adjacent skeletal bone.

next set up the assay using 5 x 10^6 cells and added them through an intramuscular injection to the site of the

fibula defect. Figure 27 shows the results of BMP2 protein expression from these cells, demonstrating escalation of cell number was in fact increasing the amount of BMP2 expressed within the tissues. These cells were then injected into the fibula defect in rats, and the resultant bone formation analyzed at 2, 4, and 6 weeks after induction of bone formation. As can be seen in figure 28, the newly forming heterotopic bone is quite extensive as seen in the previous figure, but at two weeks this appears to be considerably resorbed yet still bridging the defect. By 6 weeks again, the bone is bridging, but now fairly small amounts of heterotopic ossification, are observed within the hind limb, but the bone within the fibula, appears to be much more remodeled and contiguous. Cross sectional MicroCT analysis (figure 28) of the samples of bone at 2 and 6 weeks shows that in both cases the bone appears to be bridging the fibular defect, however at two weeks the bone appears to be immature woven bone rather than remodeled lamellar bone. However, by 6 weeks, the bone now appears to have well mineralized cortexes with a more hollow marrow cavity similar to the adjacent skeletal bone. As seen in figure 28, at 6 weeks the bone appears to be well fused, and is contiguous with one side being almost indistinguishable as to where the defect initially lay. This suggests that the bone will remodel to the correct skeletal structure, and result in regeneration of the missing tissue, without unwanted heterotopic bone.

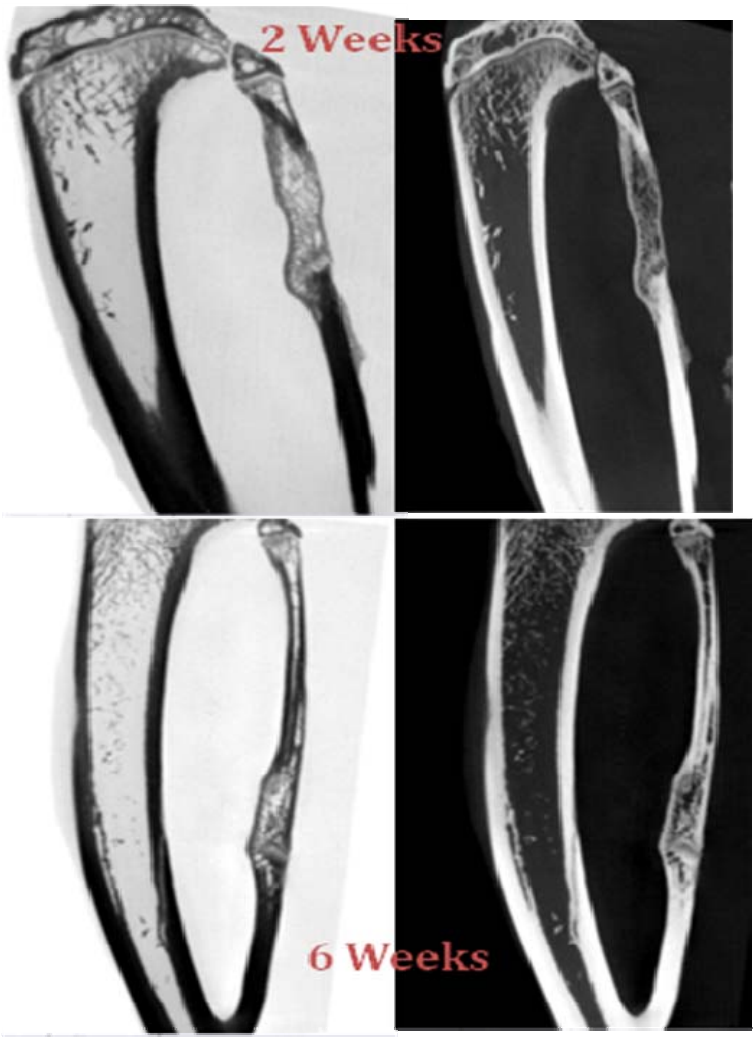

Figure 28: A critical size defect was introduced into the fibula of athymic rats and Ad5BMP2 transduced cells were delivered through intramuscular injection. Approximately 2 and 6 weeks after initial injection of the cells, bone formation was analyzed through microCT analysis. The top two panels show the immature bone bridging the defect in the fibula, with uniform structure. These reflect two different methods for contrasting the microCT of the same representative sample. However, as can be seen in the bottom two panels show the bone is now remodeled into lamellar structure, with more mineralized cortexes, similar to the adjacent skeletal bone. The bone appears to be well fused.

The results suggest that the rate of heterotopic bone formation within the tissues dictates the rate of bone healing and that this is independent of the skeletal bone healing. Further this rate cannot be increased by increasing the number of cells expressing BMP2 delivered to the site. The dose of BMP2 expressing cells appears to alter only the volume of bone produced. However, we are currently working on determining the influence of this rate on weight bearing. Our preliminary data suggests that we may achieve more rapid bone healing and fusion, in bones that are weight bearing rather than bones which are not such as the fibula. As seen in figure 29, we observed substantial new bone formation bridging a critical size defect in the rat femur 3 weeks after induction of bone formation by delivery of AdBMP2 transduced cells. The new bone, although again curved, appears to be well fused and bridging. We are currently completing the microCT analysis and histology of this tissue to confirm our finding. We are also initiating the completed or proposed fibula defect experiments in tandem in the femur as well. Thus we will be able to compare if the bone healing is slowed in models which are repair of non-weight bearing bones.

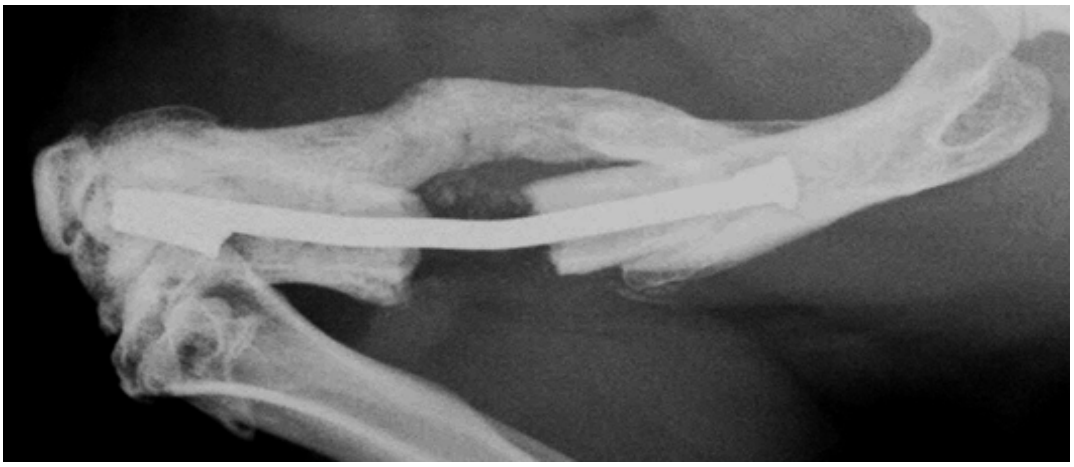

Figure 29: Radiological analysis of new bone formation in a rat femur three weeks after induction of HO using 1 x 10^7 AdBMP2 transduce cells.

e. *Approximately 230 rats total. We request 120 NIH nude athymic rats for experiments and 108 Wistar rats to complete the experiments in this task.*

Key Research Accomplishments:

Task 1: To produce high levels of BMP2 from human mesenchymal stem cells transduced Ad5F35BMP2 adenovirus in the presence of tetracycline carrying a red luciferase reporter gene.

- We have employed a dsRED reporter system for tracking transgene expression in live animals.
- We have obtained and produced vectors for a novel infrared fluorescent protein (IFP) system that will allow us to monitor transgene expression during bone formation, even in the presence of substantial matrix.
- We have initiated experiments to utilize a novel caspase system, patented by a BCM colleague, which can upon induction with a small molecule induce the delivery cells to undergo apoptosis.
- We have a manuscript currently in review which demonstrates that the hydrogel is capable of expanding viability and transgene expression and for the same number of cells and BMP2 form a greater volume of bone. (See appendix)
- We have constructed the Smad-CFP mice, but have found the expression to be below detection limits, so we are currently working with the phosphoSmad antibody to determine the cells which are responding to BMP2.

Task 2: To design an optimal hydrogel material that will rapidly promote endochondral bone formation and be capable of removal through bone remodeling processes.

- We have constructed the cathespin K protease site, and introduced it into the hydrogel material.
- We have initially tested this material and found it to be selectively degraded by cathespin K as compared to other proteases.
- We have shown that osteoclasts will adhere, form ruffled borders, and start to resorb the material, presumably by the production of cathespin K.
- We have introduced RGD peptide binding sites to the hydrogel material to provide adhesion for the osteoclasts, as well as to extend the life span of the cells within the gel.
- We have engineered RANK ligand into the hydrogel material which can be bound by the osteoclast precursors to induce osteoclastogenesis, similar to skeletal remodeling. In normal bone remodeling RANKL is released by the osteoblasts to induced osteoclast differentiation, and resorption. Thus it will aid in allowing the biomaterial to function similar to normal bone matrix.
- We have a manuscript in review which describes the data demonstrating selectable degradation by osteoclasts but not osteoblasts. (See appendix)
- We have filed a disclosure and are moving to patent this material.
- We have currently started to implement the nondegradable and degradable microbeads in both the HO-muscle model as well as the fibula model, and transgene expression will be tracked through live animal imaging of the IFP.

Task 3: To achieve rapid bone formation by percutaneous injection of the encapsulated Ad5F35BMP2 transduced human bone marrow mesenchymal stem cells (hBM-MSCs) into the adjacent musculature of athymic rats in a model of nonunion.

- We have established and set up a reproducible critical size defect model that due to the nature of the site is a tremendously challenging model of bone healing.
- We have demonstrated the ability to transduce both the human cells to express high levels of BMP2, as well as the rat fibroblasts
- We are currently testing the rat MSC primary cells to determine if they can suppress the immune response to allogenic cells within the rat.
- We have shown the absence of HO in wild type rats receiving allogenic (litter mate) cells whereas autologous skin fibroblasts transduced with AdBMP2 appeared to generate a significant amount of bone in two weeks.
- We have demonstrated the ability of PEGDA hydrogel encapsulation to completely stop the rapid immune response to the allogenic cells, and recover bone formation.
- We have initially tested the BMP2 transduced cells to induce both heterotopic bone formation and bone healing in this model and found that heterotopic ossification can be rapidly produced in an immune compromised animal using transduced human fibroblasts expressing high levels of BMP2.
- We are currently continuing to trouble shoot the production of bone formation from the biomaterial, so that we can target the formation more appropriately to allow for rapid healing of the defect. This will

involve not only introducing the biomaterial in vivo, but also analyzing the placement of the material within the defect. We have on going studies in the spine, which demonstrate the need for appropriate placement of the cells and biomaterial for optimal targeting.

Reportable Outcomes:

Manuscripts:

- Dilling CF, Wada A, Lazard Z, Salisbury E, Gannon F, Vadakkan T, Gao L, Hirschi K, Dickinson M, Davis AR**,** Olmsted-Davis E. (2009) Vessel Formation is Induced Prior to the Appearance of Cartilage in BMP2-Mediated Heterotopic Ossification. J Bone Miner Res. 2009 Oct 19. [Epub ahead of print] PMID: 19839764

Manuscripts in Review:

- Chih-Wei Hsu, Ronke M. Olabisi, Elizabeth A. Olmsted-Davis, Alan R. Davis, Jennifer L. West Cathepsin-K sensitive poly(ethylene Glycol) hydrogels for degradation in response to bone formation. (Biomaterials)
- Ronke M. Olabisi, Zawaunyka Lazard, Mary Hall, Eva Sevick, John A Hipp, Alan R. Davis, Elizabeth A. Olmsted-Davis and Jennifer L. West. Hydrogel microsphere encapsulation of a cell based gene therapy system; increases cell survival, transgene expression, and bone volume in a model of heterotopic ossification. (Tissue Engineering)
- Ronke M Olabisi, Zawaunyka Lazard, Michael Heggeness, Kevin M Moran, John A Hipp, Ashvin Dewan, Alan R. Davis, Jennifer L. West and Elizabeth A. Olmsted-Davis. An Injectable Method for Spine Fusion. (Human Gene Therapy)

Manuscripts in Preparation:

- S. Kwon, Z. Lazard, E. Salisbury, E. Rodenberg, M. Merched-Savage, A.R. Davis, E. Sevick, and E. Olmsted-Davis. Development of a non-invasive optical imaging modality for detection of early bone formation. (In preparation)
- Z. Lazard, M. Heggeness, R. M. Olabisi, C. Hsu, J.A. Hipp, F. Gannon, A. R. Davis, J. L. West, and E. Olmsted-Davis. Induction of targeted heterotopic ossification for healing traumatic bone injury. (In preparation)
- E.A. Olmsted-Davis, Z. Lazard, C. Sonnet, F. Gannon, E. Rodenberg and A.R. Davis. Dependence of Heterotopic Ossification on Local Peripheral Nerves. (In preparation)

Presentations were made at the following meetings:

Oral presentation:

Ronke M. Olabisi, Chi-Wei Hsu, **Elizabeth A. Olmsted-Davis**, Jennifer L. West. Cathepsin-K Degradable Poly(ethylene) Glycol Hydrogels for Bone Formation. Federation of South-Western Bioengineering Annual Meeting, 2009, San Antonio TX (Oral Presentation).

E. Olmsted-Davis, Z. Lazard, R. Olabisi, L. Hsu, M. Heggeness, J. Hipp, J. West, A.R. Davis. Non-Invasive Cellular Therapy for Spinal Fusion Treatment. Military Health Research Forum, 2009. Kansas City, MO.

E. Olmsted-Davis, Z. Lazard, M. H. Heggeness, R. Olabisi, L. Hsu., E. Salisbury, C. Fouletier-Dilling, J. Hipp, Ph.D., J. West, A. R. Davis. Cellular Therapy to Accelerate Fracture Healing. Military Health Research Forum, 2009. Kansas City, MO.

E. Olmsted-Davis, E. Rodenberg, Z. Lazard, C. Sonnet. Advances in Mineral Metabolism- American Society of Bone and Mineral Research Young Investigators meeting. April 2010, Snowmass CO.

Poster presentation:

Smith, T J; Gandy, J C; **Olmsted-Davis, E A**; Davis, A R; Sordillo LM; Zachos TA Efficient *In Vitro* Adenoviral BMP-2 Gene Delivery into Canine Bone Marrow-Derived Stem Cells. Orthopedic Research Society Annual Meeting, 2009, San Francisco, CA.

Dewan A K; Calderon N; Dewan R A; Fuentes A; Lazard, Z;; Davis, A; Heggeness, M; **Olmsted-Davis, EA** and Hipp, J. Mechanical Integrity of Spinal Fusion by in situ Endochondral Osteoinduction. Orthopedic Research Society Annual Meeting, 2009, San Francisco, CA.

Z. Lazard, R. Olabisi, L. Hsu, C. Fouletier-Dilling, J. West, F. Gannon, A. Davis, M. Heggeness, **E. Olmsted-Davis**. Non-Invasive Cellular Therapy for Spinal Fusion Treatment. New York Skeletal Society Annual Meeting, 2009, New York, NY.

Merched-Sauvage, M., Kwon, S., Lazard, Z., Salisbury, E, Gannon, F., Davis, A.,Sevick, E, and **Olmsted-Davis, E.** Imaging of heterotopic ossification in advance of bone formation. New York Skeletal Society Annual Meeting, 2009. New York, NY.

E. J. Rodenberg, E. A. Salisbury, Z. W. Lazard, F. H. Gannon, A. R. Davis, and **E. A. Olmsted-Davis.** A Functional Role for Mast Cells in the Production of Brown Adipocytes from Peripheral Nerves in Early Heterotopic Ossification. ASBMR topical meeting, 2009 Bethesda, MD.; Young Investigator Award Winner.

E. Salisbury, Z. Lazard, E. Rodenberg, A.R. Davis, and **E.A. Olmsted-Davis**. Regulation of Early Heterotopic Ossification. ASBMR topical meeting, 2009 Bethesda, MD.; Young Investigator Award Winner.

E. Salisbury, Z. Lazard, E. Rodenberg, A.R. Davis, and **E.A. Olmsted-Davis**. The role of brown adipose in heterotopic ossification. Texas Bone Program Annual Meeting, 2009. Houston TX. Second place winner for best presentation.

E. Olmsted-Davis, Z. Lazard, R. Olabisi, L. Hsu, M. Heggeness, J. Hipp, J. West, A.R. Davis. Non-Invasive Cellular Therapy for Spinal Fusion Treatment. Military Health Research Forum, 2009. Kansas City, MO.

E. Olmsted-Davis, Z. Lazard, M. H. Heggeness, R. Olabisi, E. Salisbury, C. Fouletier-Dilling, J. Hipp, Ph.D., J. West, A. R. Davis. Cellular Therapy to Accelerate Fracture Healing. Military Health Research Forum, 2009. Kansas City, MO.

This past year we have collected data for seven manuscripts. The first is in press; the second three manuscripts are in review at various journals (see appendix) and the remaining three are currently being assembled. We have made significant progress towards developing this system for clinical use. We have found that our system generates significant new vessels presumably through the elevated expression of VEGF from brown adipose rapidly generated within the tissues. From this we have turned our focus from trying to engineer VEGF expression into the polymer. We have completed our work to develop a tunable polymer, that can be removed through normal bone remodeling principals and shown this to function as predicted *in vitro* (appendix). We have also show that the heterotopic bone can fuse over time and remodel into a contiguous structure with skeletal bone (appendix), and the fusion is strong enough to restrict bone growth within the spine. Finally we have demonstrated the ability to encapsulate the transduced cells and deliver them to both mice and rats for the formation of bone. Comparison of the resultant bone formation in animals receiving similar levels of either AdBMP2 transduced cells encapsulated or unencapsulated resulted in a significant increase in bone volume with a slight drop in density in the former versus the latter. The resultant heterotopic ossification, showed similar structures or patterns to the HO regardless of the microbeads. This data shows that although we only observed bone formation surrounding the microspheres, some of the beads which are within the central marrow cavity did not have bone formed around them, suggesting that other patterning forces are at invoked. Finally, we have initiated testing of these materials two different long bone models, and preliminary data using both autologous and allogenic cells for delivery of the BMP2, suggest the essential nature of the PEGDA microspheres.

I have presented the work at the Department of Defense (CDMRP) research forum, and have been asked to present the work at the upcoming Advances in Mineral Metabolism Meeting in Snowmass CO. We have also presented the work through poster-presentations through a number of different forums, including the upcoming AAOS meeting.

Finally we have filed two disclosures describing first the gene therapy system and are moving towards patenting this system for the use of heterotopic ossification for the healing of critical size defects, and secondly the osteoclast specific degradable PEG-DA hydrogel material.

Conclusions:

We have made significant progress for this second year of the four year proposed study. In the upcoming years we hope to complete the studies described in aim 1, using the BMP2- DsRED vectors to compare temporal and spatial expression of BMP2 on endochondral bone formation. We are currently completing and publishing the *in vitro* phase for developing the osteoclast degradable hydrogel material, through the principles of bone remodeling. Finally we have not only established a challenging model of non-union critical size defects in rats, but also have preliminary data that BMP2 is capable of healing or producing bone under these circumstances. Although we have just started this work the rapid new bone within two weeks, and the large amount of new bone filling the defects, suggests the gene therapy based system holds much promise. We believe in the upcoming year that we will further optimize this system to obtain the rapid and complete healing of the defect. Further, we will determine if this is due to heterotopic bone formation fusing into the orthotopic, or stimulation of the orthotopic bone by BMP2 to induce healing. We will start to test the biodegradable hydrogel structures in the critical size defect model. We will also optimize the placement of the biomaterial for optimal healing. Since ultimately this material will be injectable, we want to determine the number of injections and exact locations for optimal healing. We would like to introduce a second model for critical size defect in the tibia, in which we will fix the bone by plating, and thus allow for us to compare our healing in the fibula to that in a more weight bearing bone. Thus we have considerable challenges in the third year of this proposal, but have had significant achievements in the first two years, to develop the tools necessary for completing the experiments. In accordance with our projected timeline we are exactly on schedule. Thus the substantial preliminary data, from the first two years, suggests success in our endeavors.

References:

1. Gowen, M., et al. (1999). Cathepsin K knockout mice develop osteopetrosis due to a deficit in matrix degradation but not demineralization. *J Bone Miner Res* 14: 1654-1663.
2. Hollberg, K., Nordahl, J., Hultenby, K., Mengarelli-Widholm, S., Andersson, G., and Reinholt, F. P. (2005). Polarization and secretion of cathepsin K precede tartrate-resistant acid phosphatase secretion to the ruffled border area during the activation of matrix-resorbing clasts. *J Bone Miner Metab* 23: 441-449.
3. Yang, F., Williams, C. G., Wang, D. A., Lee, H., Manson, P. N., and Elisseeff, J. (2005). The effect of incorporating RGD adhesive peptide in polyethylene glycol diacrylate hydrogel on osteogenesis of bone marrow stromal cells. *Biomaterials* 26: 5991-5998.
4. Fouletier-Dilling, CM. et al. (2005). Novel compound enables high-level adenovirus transduction in the absence of an adenovirus-specific receptor. *Hum Gene Ther* 16: 1287-1297.
5. Fouletier-Dilling CM, Gannon F, Olmsted-Davis EA, Lazard Z, Heggeness MH, Shafer JA, Hipp JA, and A.R. Davis. (2007) Efficient and Rapid Osteoinduction in an Immune Competent Host. Hum Gene Ther 18(8):733-45 (Fast Track publication and Cover).
6. Olmsted-Davis, EA, *et al.* (2002). Use of a chimeric adenovirus vector enhances BMP2 production and bone formation. *Hum Gene Ther* 13: 1337-1347.
7. Bikram M, Fouletier-Dilling CM, Hipp JA, Gannon F, Davis AR, Olmsted-Davis EA, and West JL (2007) Endochondral Bone Formation from Hydrogel Carriers Loaded with BMP2-Transduced Cells. Ann Biomed Eng. 35(5):796-807.
8. Olmsted, EA. *et al.* (2001). Adenovirus-mediated BMP2 expression in human bone marrow stromal cells. *J Cell Biochem* 82: 11-21.
9. Gugala, Z., Davis, A.R., Fouletier-Dilling, C, F. Gannon, Lindsey, R.W., Olmsted-Davis, EA (2007) Adenovirus BMP2-Induced Osteogenesis in combination with various collagen carriers. Biomaterials, 28(30):4469-79.
10. Shu X, Royant A, Lin MZ, Aguilera TA, Lev-Ram V, Steinbach PA, Tsien RY (2009) Mammalian expression of infrared fluorescent proteins engineered from a bacterial phytochrome. Science, 8;324(5928):804-7.

Appendix:

Manuscripts:

1. Dilling CF, Wada A, Lazard Z, Salisbury E, Gannon F, Vadakkan T, Gao L, Hirschi K, Dickinson M, Davis AR**,** Olmsted-Davis E. (2009) Vessel Formation is Induced Prior to the Appearance of Cartilage

in BMP2-Mediated Heterotopic Ossification. J Bone Miner Res. 2009 Oct 19. [Epub ahead of print] PMID: 19839764

2. Chih-Wei Hsu, Ronke M. Olabisi, Elizabeth A. Olmsted-Davis, Alan R. Davis, Jennifer L. West Cathepsin-K sensitive poly(ethylene Glycol) hydrogels for degradation in response to bone formation. (Biomaterials)
3. Ronke M. Olabisi, Zawaunyka Lazard, Mary Hall, Eva Sevick, John A Hipp, Alan R. Davis, Elizabeth A. Olmsted-Davis and Jennifer L. West. Hydrogel microsphere encapsulation of a cell based gene therapy system; increases cell survival, transgene expression, and bone volume in a model of heterotopic ossification. (Tissue Engineering)
4. Ronke M Olabisi, Zawaunyka Lazard, Michael Heggeness, Kevin M Moran, John A Hipp, Ashvin Dewan, Alan R. Davis, Jennifer L. West and Elizabeth A. Olmsted-Davis. An Injectable Method for Spine Fusion. (Human Gene Therapy)

Editorial Manager(tm) for Journal of Bone and Mineral Research
Manuscript Draft

Manuscript Number: J0903197R2

Title: Vessel formation is induced prior to the appearance of cartilage in BMP2-mediated heterotopic ossification

Article Type: Original Study

Section/Category: Basic

Keywords: Bone morphogentic protein type2; heterotopic ossification; vessel formation

Corresponding Author: Dr. Alan R. Davis, Ph.D

Corresponding Author's Institution: Baylor College of Medicine

First Author: Christine Fouletier Dilling, Ph.D.

Order of Authors: Christine Fouletier Dilling, Ph.D.; Aya Wada, Ph.D.; Zawaunyka Lazard, BSEE; Elizabeth A Salisbury, BA; Tegy Vadakkan, PhD; Alan R. Davis, Ph.D; Liang Gao, BA; Francis Gannon, MD; Karen Hirschi, Ph.D.; Mary Dickinson, PhD; Elizabeth Olmsted-Davis, PhD

Abstract: Heterotopic ossification (HO) or endochondral bone formation at non-skeletal sites, often results from traumatic injury, and can lead to devastating consequences. Alternatively the ability to harness this phenomenon would greatly enhance current orthopedic tools for treating segmental bone defects. Thus understanding the earliest events in this process would potentially allow us to design more targeted therapies to either block or enhance this process. Using a murine model of HO induced by delivery of adenovirus transduced cells expressing bone morphogenetic protein 2, BMP2, we show here that one of the earliest stages in this process is the establishment of new vessels prior to the appearance of cartilage. As early as 48 hours after induction of HO, we observed the appearance of brown adipocytes expressing VEGFs, simultaneous with endothelial progenitor replication. This was determined by using a murine model, which possesses the VEGF receptor 2 (flk-1) promoter containing an endothelial cell enhancer, driving the expression of nuclear-localized yellow fluorescent protein (YFP). Expression of this marker has previously been shown to correlate with the establishment of new vasculature (1) and the nuclear localization of YFP expression allowed us to quantify changes in endothelial cell numbers. We found a significant increase in Flk1-H2B::YFP cells in BMP2-treated animals as compared to controls. The increase in endothelial progenitors occurred three days prior to the appearance of early cartilage. The data collectively suggests that vascular remodeling and growth may be essential to modify the microenvironment and enable engraftment of the necessary progenitors to form endochondral bone.

Response to Reviewers:

Revised Manuscript

Vessel formation is induced prior to the appearance of cartilage in BMP2-mediated heterotopic ossification

C. Fouletier Dilling[1], A.M. Wada[2], Z.W. Lazard[1], E.A. Salisbury[1], F.H. Gannon[3], T. J. Vadakkan[2], L. Gao[2], K. Hirschi[1,4], M.E. Dickinson[2], A.R. Davis[1,5], E.A. Olmsted-Davis

[1]Center for Cell and Gene Therapy, Baylor College of Medicine, Houston, TX [2]Departments of Molecular Physiology and Biophysics, and Medicine, Baylor College of Medicine, Houston, TX [3]Department of Pathology, Baylor College of Medicine, Houston TX [4]Department of Pediatrics, Pediatrics-Nutrition, Baylor College of Medicine, Houston, TX [5]Department of Pediatrics, Hematology-Oncology, Baylor College of Medicine, Houston, TX

Funded in part by RO1EB005173-01, USMRMC 06135010 and USMRMC 06136005

Running title: Vessels form prior to cartilage

cdillingdk@yahoo.com, wada@bcm.tmc.edu, zwl@bcm.tmc.edu, salisbur@bcm.tmc.edu, fgannon@bcm.tmc.edu, vadakkan@bcm.tmc.edu, liangg@bcm.tmc.edu, mdickins@bcm.tmc.edu, khirschi@bcm.tmc.edu ardavis@bcm.tmc.edu, edavis@bcm.tmc.edu

Corresponding Author Alan R. Davis Center for Cell and Gene Therapy One Baylor Plaza Houston, TX 77030 Ph 713-798-1237 Fax 713-798-1230 ardavis@bcm.tmc.edu ar

Word count: Number of figures Abstract: 249
Black and White: 1 Manuscript: 6754 Color: 5

All authors have no conflicts of interest

Abstract

Heterotopic ossification (HO) or endochondral bone formation at non-skeletal sites, often results from traumatic injury, and can lead to devastating consequences. Alternatively the ability to harness this phenomenon would greatly enhance current orthopedic tools for treating segmental bone defects. Thus understanding the earliest events in this process would potentially allow us to design more targeted therapies to either block or enhance this process. Using a murine model of HO induced by delivery of adenovirus transduced cells expressing bone morphogenetic protein 2, BMP2, we show here that one of the earliest stages in this process is the establishment of new vessels prior to the appearance of cartilage. As early as 48 hours after induction of HO, we observed the appearance of brown adipocytes expressing VEGFs, simultaneous with endothelial progenitor replication. This was determined by using a murine model, which possesses the VEGF receptor 2 (flk-1) promoter containing an endothelial cell enhancer, driving the expression of nuclear-localized yellow fluorescent protein (YFP). Expression of this marker has previously been shown to correlate with the establishment of new vasculature (1) and the nuclear localization of YFP expression allowed us to quantify changes in endothelial cell numbers. We found a significant increase in Flk1-H2B::YFP cells in BMP2-treated animals as compared to controls. The increase in endothelial progenitors occurred three days prior to the appearance of early cartilage. The data collectively suggests that vascular remodeling and growth may be essential to modify the microenvironment and enable engraftment of the necessary progenitors to form endochondral bone.

Keywords: Bone morphogentic protein type2; heterotopic ossification; vessel formation

Introduction

Endochondral bone formation is thought to proceed through an ordered series of events, starting with the proliferation and “condensation” of presumptive mesenchymal cells to form avascular cartilage. Hence it is presumed that the lack of vasculature and associated cellular replication creates the hypoxic environment necessary for chondrogenic differentiation. However, recent data from our laboratory using a model of heterotopic ossification, suggests that vessels may play an essential role in the induction of chondrogenesis (2).

It has been well established that vessel formation plays a key role in late events during the process of bone formation. Vessels invade the perichondrium and hypertrophic zone and are required for the replacement of cartilage by bone (3). The angiogenic factor, vascular endothelial growth factor (VEGF) promotes vascular invasion via specific receptors, including Flk1 (VEGF-receptor 2) expressed in endothelial cells, in the perichondrium or surrounding tissue (4) (5). These events of cartilage matrix remodeling and vascular invasion are necessary for the migration and differentiation of osteoblasts and osteoclasts which remove mineralized cartilage matrix and replace it with bone. However, much less is known about the role of vessel formation prior to the appearance of the pre-cartilage tissue.

During normal wound repair, a series of cell signaling events are induced by the hypoxic state of the tissues, resulting in up-regulation of hypoxia inducible factor (HIF1) that in turn up-regulates a series of factors including several VEGFs (A, B, and D), leading to vessel formation. Hypoxia-induced angiogenesis has been proposed to be necessary for creating specialized vessels that facilitate progenitor homing and engraftment into damaged

tissues (6). Little is known as to whether such a process plays a key role in the repair of bone. Using a model of *de novo* bone formation to identify the earliest events in this process, we have demonstrated that myelo-mesenchymal stem cells are recruited to the tissues to form the early cartilage (7). One of the earliest events in this model is the appearance of brown adipocytes. These cells are capable of utilizing their uncoupled aerobic respiration to reduce localized oxygen tension and effectively pattern the newly forming cartilage condensations (8). This is consistent with *in vitro* data where bone marrow derived mesenchymal stem cells can undergo chondrogenesis in the presence of bone morphogenetic protein 2 (BMP2) and low oxygen (9). We also observed the appearance of vessels lining the edges of the perichondrial region, separated only by brown adipose, suggesting that perhaps the reduction in oxygen tension coordinately activates new vessel formation in the region (8). Thus, these progenitors may indeed be recruited to the site of new bone formation through the vasculature. In this study we focused on defining this tentative early vessel formation.

To determine this, we chose to employ a transgenic mouse model which expresses the fusion protein, human histone H2B with enhanced yellow fluorescent protein (EYFP) (H2B:YFP) in endothelial cells under the regulation of a Flk1 promoter/enhancer fragment (Flk1-H2B::YFP) (1). Recent improvements in genetically encoded fluorescent protein expression in animal models along with advances in optical imaging and image analysis software have enabled the analysis of many aspects of tissue development at a cellular level (10). Previous studies using this transgenic animal indicates that Flk1-H2B::YFP expression is restricted to endothelial cells of smaller and/or newly forming vessels (8), thus providing a mechanism for quantification of new vessels.

Here we demonstrate new vessel formation within the tissues prior to the appearance of the presumptive cartilage. Quantification of the number of endothelial cells shows that one of the first steps of bone formation is to induce additional endothelial cell proliferation. Histological analysis shows that increases in endothelial cell numbers are evident, just prior to the influx of chondrocytic progenitors. Immunohistochemical analysis of the tissues prior to the mesenchymal condensations, revealed a rapid and transient expression of VEGFA and D from the brown adipocytes. The data collectively, suggests that the brown adipocytes may play a key role in establishing patterning of the cartilage through regulation of oxygen tension within the tissues, through induction of both aerobic respiration, as well as early angiogenesis.

MATERIALS AND METHODS

Cell culture: A murine C57BL/6 derived cell line (MC3T3-E1) was obtained from American Type Culture Collection, propagated in αMEM supplemented with 10% fetal bovine serum (Hyclone, Logan, UT), 100 units/ml penicillin, 100 µg/ml streptomycin, and 0.25 µg/ml amphotericin B (Life Technologies Inc., Gaithersburg, MD). Briefly, the cells were grown in DMEM supplemented as described above and cultured at a subconfluent density in order to maintain the phenotype. All cell types were grown at 37□C and 5% CO_2 in humidified air.

Transduction of cells with adenovirus in the presence of GeneJammer®

***Adenoviruses*:** Replication defective first generation human type 5 adenovirus (Ad5) deleted in regions E1 and E3 was constructed to contain the cDNA for BMP2 in the E1 region of the viral genome (11). The virus particles (vp) to plaque forming unit (pfu) ratios

were: 55 and 200 for Ad5BMP2 and Ad5-empty respectively, and all viruses were shown to be negative for replication competent adenovirus.

The C57BL/6 cell line or MC3T3-E1 (1×10^6), were transduced with Ad5BMP2 or Adempty cassette control virus at a concentration of 5000 vp/cell with 1.2% GeneJammer® as previously described (12).

Heterotopic bone assay: The transduced cells were resuspended at a concentration of 5×10^6 cells/100 µl PBS, and then delivered through intramuscular injection into the hind limb quadriceps muscle of Flk1 mice. Animals were euthanized at daily intervals and hind limbs were harvested, embedded and placed at -80°C. All animal studies were performed in accordance with standards of the Baylor College of Medicine, Department of Comparative Medicine after review and approval of the protocol by the Institutional Animal Care and Use Committee (IACUC).

Histological analysis and staining analysis:

Soft tissues encompassing the site of new bone formation were isolated from the rear hind limb of the mice. Both the skin and skeletal bone were removed from the tissues prior to freezing. Serial sections (15 µm) were prepared that encompassed the entire tissues (approximately 50 sections per tissue specimen). We then performed Hematoxylin and Eosin staining on every 5^{th} slide which allowed us to locate the region containing either our delivery cells or the newly forming endochondral bone. Serial unstained slides were used for immunohistochemical staining (either single or double-antibody labeling). For double antibody labeling, samples were treated with both primary antibodies simultaneously

followed by washing and incubation with respective secondary antibodies, used at 1:500 dilution to which Alexa Fluor 488, 594, or 647 were conjugated. Primary antibodies were used as follows: SMA mouse monoclonal used at 1:200 dilution; Sigma Chem Co, St Louis, MO), CD31 (rat monoclonal used at 1:75 dilution; BD Pharmingen, San Diego, CA), Flk1 (goat polyclonal used at 1:100 dilution; R&D systems, Minneapolis, MN), Ki67 (rat monoclonal used at 1:100, Dako, Carpinteria, CA), VEGF-D (goat polyclonal used at 1:100 dilution, Santa Cruz Biotechnology, INC, Santa Cruz, CA). Stained tissue sections were examined by confocal microscopy (Zeiss Inc, Thornwood, NY, LSM 510 META) using a 20x/0.75NA objective lens.

Flk1 positive cell quantification in BMP -induced tissues: To quantify the increase in YFP positive cells in the BMP-induced tissues, frozen sections across these tissues were counterstain with DAPI and the YFP expression was compared to that obtained in the control tissues. First, a series of low magnification (5.4x and 12x) bright field images of a tissue section were taken and overlapped to reconstruct the tissue section using Adobe Photoshop CS3. The reconstructed montage image was used to measure the area of the tissue section using a manual contour tracing method (Zeiss Axiovision). The area of each of the frozen sections was calculated in a similar manner. Area measurements are used to determine the density of labeled cells as indicated below.

High resolution (10X/NA0.45, 1024x1024 pixels), dual channel images of tissue sections nuclear stained with DAPI were taken using a confocal microscope (Zeiss LSM 510 META). In each image, the number of nuclei in the DAPI and YFP channels was counted using a modified watershed segmentation algorithm (FARSIGHT, RPI) which makes use of both intensity and volume thresholds to distinguish two nuclei as separate. All

the nuclei counted using the software were DAPI positive. The fraction of DAPI stained nuclei marked by YFP were counted as YFP positive. The density of YFP positive cells in a tissue section was defined as the ratio of the number of YFP positive nuclei in the tissue section measured from the high magnification images to the area of the tissue section measured from the low magnification images. The density of the YFP positive nuclei was calculated for a number of control and BMP treated tissues at 2 and 4 days after injection. The ratios were then averaged over the various control and BMP2-treated tissues. The p-values were calculated using a Student's t-test.

Flk1-YFP positive cell association analysis:

To characterize the cell type(s) that express YFP in the adult muscle tissue, we performed immunoflourescent studies using endothelial cell marker CD31 and Flk1 antibodies; for vascular smooth muscle cells -smooth α actin (SMA). Association of cells expressing YFP with immuno-labeled cells was analyzed using (FARSIGHT, RPI, NY) and a custom program written in MATLAB (MathWorks, Natick, MA). After identification of each nucleus by DAPI staining, YFP positive and negative cells were then analyzed for association with fluorescent signals of each antibody. An intensity threshold was applied to the red channel in each image to identify a cell positive or negative for the immunofluorescent signal. Each identified nucleus and overlapping red channel were counted as CD31, Flk1, or SMA positive and then as either YFP negative and positive. Co-localization percentages are shown in the supplemental data section (Table S-1) and describe in detail the YFP positive cell types. The number of YFP+/Ki67+ nuclei in an area of the tissue was calculated by adding the YFP+/Ki67+ in each of the confocal images taken within the area. The area

fraction of YFP+/Ki67+ was defined as the total number of YFP+/Ki67+ in the images taken within the area divided by the number of images. The area fraction was measured for five different areas and the average area fraction was calculated for control and BMP treated tissues for every 5th slide sectioned throughout the entire hindlimb. The area fractions of YFP+/Ki67+ nuclei in the control and the BMP treated tissues on day 2 were 3.97 ± 2.96 and 6.11 ± 1.76 respectively. The area fractions for day 4 were 5.04 ± 0.72 and 6.41 ± 1.41 in the control and the BMP treated tissues. Based on the Student's t-test, the p value for the day 2 data was 0.21 and that for the day 4 data was 0.10. Taken together, the data supports the trend that YFP+/Ki67+ population increases on day 2 and day 4 after the BMP treatment.

Q-RT-PCR: Non-skeletal tissues (n=4 per group) surrounding the site of injection of the AdBMP2 or Adcontrol transduced cells were isolated at daily intervals for 7 days and prepared as total RNA using a Trizol reagent (Life Technologies, Carlsbad, CA) in accordance with the manufacturer's specifications. The two groups of RNAs were subjected to Q-RT-PCR analysis in parallel and the Ct values obtained normalized to both internal 18S ribosomal RNA used in multiplexing, and to each other to remove changes in gene expression common to both the BMP2 and control tissues by using the ® method of ΔΔCt along with Taqmanprimers and probes (Applied Biosystems, Carlsbad, CA) as previously described (8).

RESULTS

Upregulation of vessel markers prior to the onset of chondrogenesis:

We have previously described a model of rapid endochondral bone formation (13) in which mineralized bone is observed 7 days after the initial induction with BMP2. Observation of vessels lining the newly forming perichondrium suggests that vessels may undergo replication prior to chondrogenesis. To confirm this hypothesis, we examined tissues, at 24 hour intervals over the period leading up to chondrogenesis (day 5), for the presence or absence of endothelial cell replication. Figure 1 shows the co-expression of the endothelial cell specific factor, von Willibrand factor (VWF) (red) and Ki67 (green), a marker of cellular replication (14) in the vessels from tissues that received AdBMP2 transduced cells, starting 24 hours to 5 days (panels A-E, respectively). As can be seen in Figure 1, panel B, we did observe overlap of these two markers (yellow color), in tissues receiving the AdBMP2 transduced cellswhereas no replicating endothelial cells were observed in the control tissues (Panel F). We did not attempt to quantify the amount and apparent timing of replication using this method, because VWF is an extracellular matrix protein. Instead we employed the Flk1H2B::YFP model for quantifying endothelial progenitor replication over the course of early bone formation.

Flk1-H2B::YFP in vessels:

We next determined if there was a significant increase in the number of Flk1+ endothelial progenitors during bone induction, consistent with new vessel formation, prior to chondrogenesis. We chose to utilize the Flk1-H2B::YFP mouse model (1), in which new vessel formation could be readily quantified within the muscle tissues. Flk1 is a VEGF

receptor transiently expressed on endothelial cells, and is presumably thought to contribute to VEGF induced endothelial cell replication (15). Therefore quantification of the nuclear YFP expression within tissues from animalsreceiving either AdBMP2 or Adempty transduced cells allowed us to to quantify increases in the number of endothelial progenitors within the muscle prior to cartilage formation. We previously quantified the association of Flk1-H2B::YFP with other endothelial cells markers such as CD31, and found them to be 95% overlapping (supplemental data). Frozen sections were prepared by serial sectioning from Flk1-H2B::YFP adult hind limb soft tissue (n=4 per group) consisting of three groups, those receiving: (1) cells transduced with Ad5BMP2, (2) cells transduced with Ad5empty cassette control virus, and (3) normal mouse muscle. To ensure uniform quantification and adequate sampling, the entire region of soft tissues in the hind limb was sectioned and approximatelyever fifth section was for analyzed for YFP expression.

To quantify differences in the number of endothelial progenitors, the number of YFP+ cells per the total number of DAPI+ cells was determined using automated segmentation methods (see Materials and Methods). The total YFP+ cells was also quantified per total area of the tissue section to ensure there was no bias in the fields of view chosen for image analysis (see Materials and Methods). The total area of each tissue section was determined using a montage of images that were collected using wide-field microscopy (panels A and F) (figure 2). As can be seen in Figure 2, we found Flk1-H2B::YFP positive cells in both tissues receiving Adempty transduced cells (panels B-E) and AdBMP2 transduced cells (panels G-O). These panels are higher magnification confocal images of the region within the corresponding white box on the lower magnification high resolution wide-field montage of the entire tissues (panels A;

control and F; BMP2). The results of the quantification, (figure 3), shows the average number of Flk1H2B::YFP+ cells on day 2 and day 4. Analysis of the entire soft tissue within several mice showed a significant elevation in tissues receiving the AdBMP2 transduced cells ($p=0.017$, day 2 (Fig 3A) and $p=0.006$, day 4 (Fig 3B) as compared to the control, on both days 2 and 4. The peak was approximately 2 days after induction of bone formation with no statistically significant difference between these results and those obtained in tissue sections isolated 4 days after induction.

Endothelial progenitors undergo replication in tissues receiving AdBMP2 transduced cells: In the tissues receiving cells transduced with a control adenoviral vector, we observed randomly scattered YFP+ cells along the vessel structures, while in the tissues receiving AdBMP2 transduced cells we see clustering of the YFP+ cells (Figure 2). This prompted us to question whether the Flk1-H2B::YFP progenitors could be replicating, so we next quantified the number of Flk-H2B::YFP positive cells in these tissues. Representative images used for quantification of YFP positive cell proliferation activity are shown in Figure 4. Replicating endothelial progenitors were defined as nuclei positive for both Flk1-H2B::YFP (yellow) and the cell proliferation marker, Ki67 (red; figure 4). In both control and treated animals, we also observed proliferating cells, positive for Ki67, that did not overlap with Flk1-H2B::YFP. Quantification of cells positive for both Flk1-H2B::YFP and Ki67 (figure 4) indicates a large number of replicating endothelial progenitors in both control and BMP2 treated tissues at two days after induction. Therefore the percentage of dual positive cells was not significant at this early time point as compared to the control. However, by four days after induction with BMP2, we observed much fewer replicating Flk1-H2B::YFP cells in the control and significantly more in the experimental group (figure

4). This difference was found to be statistically signifcant.

Vascular Endothelial Growth Factor (VEGF) mRNA expression:

Endothelial progenitor replication appeared to start within 48 hours of induction with BMP2. This correlated with a significant elevation in the vascular endothelial growth factor, VEGF-D (also termed fos-induced growth factor, FIGF) and VEGFA, RNA expression (figure 5). Figure 5 show the changes in VEGF mRNA expression from day 1 after injection of AdBMP2-transduced cells until day 6 as determined by real time reverse transcription PCR (Q-RT-PCR). Both VEGF-A and VEGF-D mRNA expression was significantly increased on days 2 and 4 after induction of bone formation. VEFG-B and VEGF-C however, remained on the same level throughout the time course. Although the data cannot differentiate between expansion of cells expressing VEGF-A and -D elevated transcription within cells residing in the area, the results suggest that these potent endothelial growth factors are rapidly and transiently increased within the site of new bone formation prior to the onset of cartilage.

Role of brown adipose in vessel formation:

The data collectively suggests that vessel replication is occurring simultaneously with elevated expression of VEGFs within the tissues. Since one of the earliest events observed in our model, is the recruitment and expansion of brown adipocytes (8) we next chose to determine if these cells might be expressing the VEGFs.

Immunohistochemical analysis of Flk1-H2B::YFP tissues that received either

AdBMP2 or Adempty transduced cells, showed co-localization of VEGF-D (green; fig 6, panel c) and the brown adipocyte specific marker uncoupling protein 1 (UCP1; red; fig 6, panel d) (day 2). As can be seen in figure 6, panel e, the expression of UCP1 overlaps expression of VEGF-D, in cells which are adjacent to the Flk1-H2B::YFP+ endothelial progenitors, suggesting that the brown adipocytes may be contributing to the new vessel formation. We observed additional fluorescence within the surrounding muscle, which appears to be punctate, and not cell associated. This staining may represent secreted VEGF-D protein, in the tissues. To confirm the cell specific expression of VEGF-D in the brown adipocytes, we performed additional immunostaining, (Figure 6f). Positive expression of VEGF-D (brown staining) was observed only in the brown adipocytes, again suggesting that these cells may play a role in the regulation of new vessels.

Discussion

Similar physiological steps lead to bone formation during embryonic development and in adult organisms, for instance in fracture repair or heterotopic ossification. In both cases, bone formation begins with mesenchymal condensations and ends with maturation of the growth plate, recruitment of osteoblasts and the production of bone. Vascularization has been shown to play a critical role in this process, through the infiltration into cartilage to form vascularized bone (16). Here we present data that show that vessels play a much earlier role in patterning of the cartilage and bone. The results show the presence of new vessel formation prior to the onset of mesenchymal condensations and cartilage.

We have previously reported the presence of brown adipocytes within the tissues, two days after the initial induction. We have also shown that these cells regulate localized

oxygen tension through their unique metabolism (8). In this study we extend our knowledge of the functional role of brown adipocytes, to include their rapid and transient expression of the potent angiogenic factors VEGFA and D. Interestingly a similar rapid and transient expression of VEGFD has also been demonstrated in limb development and shown to be critical for patterning (17). We observed a biphasic expression pattern for VEGF-A and -D, suggesting multiple roles for this factor in bone formation. The second peak of expression correlates nicely with the transition of cartilage to bone formation which has been highly documented (16,18) However the first phase is less well studied, and in our model and appears to correlate with the establishment of new vessels just prior to the onset of chondrogenesis. Zelzer, *et al*, also reported a similar biphasic expression of VEGF-A during embryonic bone formation (19). In these studies, they showed two functional roles for VEGFA one prior to cartilage and one during the transition of cartilage to bone similar to our own observation in our model. The data collectively, suggests that the brown adipocytes may induce the synthesis of new vessels, as a component for patterning the newly forming cartilage. In the proposed model, the brown adipocytes induce new vessels, facilitating the recruitment of chondrogenic precursors, while at the same time lowering localized oxygen tension to allow for chondrogenic differentiation. In support of this mechanism, we show in this study, the presence of brown adipocytes, expressing VEGF-D only in areas adjacent to our newly expanding vessels as marked by Flk1H2B::YFP.

Using a model of rapid endochondral bone formation, we show the immediate expansion of vessels within the tissues in response to delivery of BMP2. Although BMP2/4 play a critical role in the patterning of cartilage and bone in the embryo (20), much evidence now links the bone morphogenetic proteins to a host of other earlier physiological functions

including vascularization of the early embryo (21) Thus it may not be surprising that the earliest stage of bone formation in our model is the induction of new vessel formation.

Upon BMP2 stimulation, the Flk-1-H2B::YFP endothelial progenitors expand, as the total number of positive cells per tissue area increases. The Flk1-H2B::YFP positive cells are clustered along individual vessels suggesting that these vessels are extending or remodeling in response to BMP2. At this point we can not determine whether this increase occurs via replication of tissue resident endothelial progenitors or the recruitment of progenitors to the site of new bone formation. Our data suggests that the expansion of these progenitors, at least in part, is due to the replication, since we observed an increase in the area of replicating endothelial cells within the tissues receiving AdBMP2 transduced cells on day 4 as compared to the control tissues. However, we can not rule out the possibility that at least some of these cells are recruited from either the circulation of surrounding tissues. Interestingly, their were significant clusters of replicating Flk1-H2B::YFP cells on day 2 in both tissue receiving the AdBMP2 and Adempty cassette transduced cells, suggesting that perhaps the initial inflammatory reponse may be somewhat masking the significance of the replication at this early time point. Alternatively, the increase in replication of the Flk1-H2B::YFP cell population at four days after induction of bone formation may represent the need for vascularization to recruit new chondro-osseous progenitors, since this coincides with the appearance of these cells within the tissues (22). However, recruitment from the surrounding tissue is equally likely, since recently, Kaplan *et al* (34) showed local stem and progenitor contribution to heterotopic bone formation in a murine model of stem cell transplantation, and this process may require new vessel formation for establishment of these cells.

Vascular endothelial growth factors (VEGFs) have been shown to be essential to expansion of both endothelial cells as well as vascular smooth muscle cells which assemble to form the vessel structure. Although VEGFA has been most commonly shown to be responsible for angiogenesis in most systems, recent studies in murine muscle, have found VEGF-D to be an extremely potent angiogenic factor (23). This family member is better known for its critical role in the expansion of lymphatic vasculature (23). In our model we see both factors highly expressed in the tissues receiving the BMP2 transduced cells, as compared to those receiving control cells. Again the rapid but transient elevation in VEGF expression suggests that these factors may be driving the endothelial cell replication. Knockout studies have confirmed that BMPs regulate vasculogenesis during embryonic development (24). Functional deletion of BMP-4 and the BMP I receptor in mice leads to impaired mesoderm precursors required for vascular development (25) (26). It has also been shown that addition of BMP neutralizing antibodies or noggin suppresses endothelial cell formation during development while addition of rhBMP4 promotes it (27).

We and others have recently shown the chondrocyte to be of myeloid original, which circulates to the site of new bone formation (28) (22). These cells must then recruit and pass from the vessels into the tissues, through a process known as extravasation (29) This process has been shown to require small vasculature, which has a reduced blood flow (29) Thus it is conceivable that brown adipocytes express the VEGFs to form new vessels, capable of permitting recruitment of chondrocytic progenitors to the correct location for endochondral bone formation. Since vascular invasion of the growth plate has been well documented to precede the recruitment of osteoblast progenitors to form the new bone (16,18,29,30), it would not be surprising to have an earlier phase of this process that

recruited the chondrocytic progenitors. We have previously shown that the brown adipocytes are capable of inducing hypoxia in the local environment which in the presence of BMP2 has been shown to induce chondrogenesis (8). Thus we propose that the brown adipocytes are capable of patterning the newly forming cartilage by inducing new vessel formation, while simultaneously removing oxygen through uncoupled aerobic respiration. Once the progenitors differentiate into chondrocytes, they then express a number of anti-angiogenic proteins, to prevent in growth of new vessels, thus momentarily attenuating this early wave of angiogenesis (31) (32) (33) (35). Thus the results presented in this study extend our knowledge about the critical nature vascularization plays not only in bone formation but in cartilage as well. The data collectively shows a novel process for patterning of new endochondral bone, in adult organisms. Further, this is one of the first studies that attempt to understand the biology of tissue engineering of cartilage. Surprisingly one of the critical components we have identified is contradictory to our current dogma, that cartilage does not require vessels. The study suggests that brown adipose may play a pivotal role in establishing new vessels, essential for recruitment of chondrogenic progenitors, and patterning of the tissues. These findings may ultimately play an important role in our efforts to replace damaged cartilage through tissue engineering.

Figure Legends:

Figure 1: Immunohistochemical analysis of endothelial cell replication in tissues isolated at daily intervals after induction of bone formation with cells expressing BMP2. (A-E) days 1, 2, 3 , 4, and 5 respectively, after injection of BMP2-producing cells, paraffin sections were prepared and stained with an antibody against Ki-67 followed by as secondary antibody conjugated to Alexa fluor 488 (green) mixed with an anti-Von Willibrand Factor (VWF) antibody followed by a secondary antibody conjugated to Alexa fluor 547 (red). **Panel F** shows a representative image, similar staining, taken from tissues isolated from mice injected with cells transduced with a control vector (Adempty).

Figure 2: Wide-field and confocal images of whole tissue sections and quantification of Flk1-H2B::YFP cells. (A,F) Representative montages of low magnification grayscale images (1 pixel = 0.003mm) used for calculating total area for tissue sections. A single representative tissue section is depicted after the entire hind limb muscles which encompassed the injection site were isolated 2 after receiving an intramuscular injection of cells transduced with either Ad empty control vector **(panel A)** or AdBMP2 **(panel B)** and sectioned at 15 uM thickness. Although every 5th section across the entire tissue was analyzed, we show only a single representative image of each type. The corresponding regions with positive YFP signal, shown by the boxed areas, were imaged by confocal microscopy (panels B-E, G-O) for counting the YFP positive cell numbers.

Figure 3: Increase in Flk-H2B::YFP positive cells in BMP2-induced tissue at Day 2 and 4. Quantification of Flk1-H2B::YFP cells within the tissues, two and four days afterinduction with AdBMP2 transduced or control cells. YFP nuclei were counted and reported as ratio of the total area of the tissue section determined using the wide-field montage. Flk-H2B::YFP positive cells were significantly elevated in the tissues receiving BMP2 as compared to the controls. The graph depicts the average number of Flk-H2B::YFP positive cells in 5 sections for Day 2 control, 7 sections for Day 2 BMP, 8 sections for Day 4 control, and 6 sections for Day 4 BMP. The number of images taken in each section ranged from 4 through 22.* denotes a significant difference as determined by the Student's t-test.

Figure 4: Quantification of YFP positive cell proliferation. Representative images of Flk1-H2B::YFP and the cell proliferation marker Ki-67. Co-localization of Flk1H2B::YFP (yellow) and Ki-67 (red), was detected in BMP2-treated and control tissues. Graphs show the total number of YFP+/Ki67+ in the images taken within the area divided by the number of images analyzed. The area fraction was measured for nine at day 2, five at day 4 BMP and eight at day 2, four at day 4 control different areas and the average area fraction was calculated for control and BMP treated tissues. The area fractions of YFP+/Ki67+ nuclei in the control and the BMP treated tissues on day 2 were 7.32 ± 3.26 and 10.20 ± 6.95 respectively. The area fractions for day 4 were 6.97 ± 2.32 and 11.26 ± 2.58 in the control and the BMP treated tissues. Based on the Student's t-test, the p value for the day 2 data was 0.29 and that for the day 4 data was 0.035. Taken together, the data showed that significant YFP+/Ki67+ population increases by day 4 after the BMP treatment, however, at day 2, there are no significant differences in dividing YFP cell population between control and BMP treated tissues.

Figure 5: Expression of VEGF-D during the early stages of endochondral bone formation. Results of real time quantitative RT-PCR analysis of *VEGF-A,-B,-C, and -D* mRNA levels in tissues surrounding the lesional site that received either the AdBMP2or Adempty cassette-transduced cells isolated at daily intervals for up to 7 days after initial injection. Four biological replicates were run in triplicate and the averages normalized against an internal standard (ribosomal RNA). The samples receiving AdBMP2 transduced cells were then compared to those obtained from the tissues receiving cells transduced with Adempty cassette virus. Therefore the graph depicts the fold changes in VEGF RNAs in the BMP2 samples over time as compared to the control tissues. Error bars depict ± one standard deviation unit. * denotes samples that had a statistically significant ($p < 0.05$) difference from all other samples by the ANOVA test.

Figure 6: Immunohistochemical staining for brown adipocytes expressing VEGFD (green color, c) in tissues isolated from the Flk1-H2B::YFP mice 4 days after receiving MC3T3 cells transduced with Ad5BMP2. Brown adipocytes were identified as cells expressing uncoupling protein 1 (UCP 1; **d,** red color) and the yellow color (**b**) represents the Flk-yfp+ endothelial cells within the muscle. The tissues were also stained with VEGFD antibodies (**c**) and counterstained with dapi (blue color, **a**) that stains the nucleus of cells. A merger of these stains (UCP-1, VEGF-D, and YFP) is shown in panel **e**. In panel **f** a paraffin section taken 4 days after injection of BMP2producing cells, was stained with an antibody against UCP1 and staining was visualized using 3,3'-Diaminobenzidine (DAB) as previously described (8). No staining was observed on a paraffin section taken 4 days after injection of cells transduced with the empty control vector Ad5HM4 (data not shown).

REFERENCES

1. Fraser ST, Hadjantonakis AK, Sahr KE, Willey S, Kelly OG, Jones EA, Dickinson ME, Baron MH 2005 Using a histone yellow fluorescent protein fusion for tagging and tracking endothelial cells in ES cells and mice. Genesis **42**(3)**:**162-71.

2. Shafer J, Davis AR, Gannon FH, Fouletier-Dilling CM, Lazard Z, Moran K, Gugala Z, Ozen M, Ittmann M, Heggeness MH, Olmsted-Davis E 2007 Oxygen tension directs chondrogenic differentiation of myelo-monocytic progenitors during endochondral bone formation. Tissue Eng **13**(8)**:**2011-9.

3. Colnot C, Lu C, Hu D, Helms JA 2004 Distinguishing the contributions of the perichondrium, cartilage, and vascular endothelium to skeletal development. Dev Biol **269**(1)**:**55-69.

4. Maes C, Stockmans I, Moermans K, Van Looveren R, Smets N, Carmeliet P, Bouillon R, Carmeliet G 2004 Soluble VEGF isoforms are essential for establishing epiphyseal vascularization and regulating chondrocyte development and survival. J Clin Invest **113**(2)**:**188-99.

5. Gerber HP, Vu TH, Ryan AM, Kowalski J, Werb Z, Ferrara N 1999 VEGF couples hypertrophic cartilage remodeling, ossification and angiogenesis during endochondral bone formation. Nat Med **5**(6)**:**623-8.

6. Li J, Zhang YP, Kirsner RS 2003 Angiogenesis in wound repair: angiogenic growth factors and the extracellular matrix. Microsc Res Tech **60**(1)**:**107-14.

7. Fouletier-Dilling CM, Gannon FH, Olmsted-Davis EA, Lazard Z, Heggeness MH, Shafer JA, Hipp JA, Davis AR 2007 Efficient and rapid osteoinduction in an immune-competent

host. Hum Gene Ther **18**(8)**:**733-45.
8. Olmsted-Davis E, Gannon FH, Ozen M, Ittmann MM, Gugala Z, Hipp JA, Moran KM, Fouletier-Dilling CM, Schumara-Martin S, Lindsey RW, Heggeness MH, Brenner MK, Davis AR 2007 Hypoxic adipocytes pattern early heterotopic bone formation. Am J Pathol **170**(2)**:**620-32.
9. Shen M, Yoshida E, Yan W, Kawamoto T, Suardita K, Koyano Y, Fujimoto K, Noshiro M, Kato Y 2002 Basic helix-loop-helix protein DEC1 promotes chondrocyte differentiation at the early and terminal stages. J Biol Chem **277**(51)**:**50112-20.
10. Hadjantonakis AK, Dickinson ME, Fraser SE, Papaioannou VE 2003 Technicolour transgenics: imaging tools for functional genomics in the mouse. Nat Rev Genet **4**(8)**:**613-25.
11. Olmsted EA, Blum JS, Rill D, Yotnda P, Gugala Z, Lindsey RW, Davis AR 2001 Adenovirus-mediated BMP2 expression in human bone marrow stromal cells. J Cell Biochem **82**(1)**:**11-21.
12. Fouletier-Dilling CM, Bosch P, Davis AR, Shafer JA, Stice SL, Gugala Z, Gannon FH, Olmsted-Davis EA 2005 Novel compound enables high-level adenovirus transduction in the absence of an adenovirus-specific receptor. Hum Gene Ther **16**(11)**:**1287-97.
13. Olmsted-Davis EA, Gugala Z, Gannon FH, Yotnda P, McAlhany RE, Lindsey RW, Davis AR 2002 Use of a chimeric adenovirus vector enhances BMP2 production and bone formation. Hum Gene Ther **13**(11)**:**1337-47.
14. Gerdes J, Schwab U, Lemke H, Stein H 1983 Production of a mouse monoclonal antibody reactive with a human nuclear antigen associated with cell proliferation. Int J Cancer **31**(1)**:**13-20.
15. Sato Y, Kanno S, Oda N, Abe M, Ito M, Shitara K, Shibuya M 2000 Properties of two VEGF receptors, Flt-1 and KDR, in signal transduction. Ann N Y Acad Sci **902:**201-5; discussion 205-7.
16. Reddi AH 1994 Bone and cartilage differentiation. Curr Opin Genet Dev **4**(5)**:**737-44.
17. Trelles RD, Leon JR, Kawakami Y, Simoes S, Belmonte JC 2002 Expression of the chick vascular endothelial growth factor D gene during limb development. Mech Dev **116**(1-2)**:**239-42.
18. Reddi AH 1992 Regulation of cartilage and bone differentiation by bone morphogenetic proteins. Curr Opin Cell Biol **4**(5)**:**850-5.
19. Zelzer E, McLean W, Ng YS, Fukai N, Reginato AM, Lovejoy S, D'Amore PA, Olsen BR 2002 Skeletal defects in VEGF(120/120) mice reveal multiple roles for VEGF in skeletogenesis. Development **129**(8)**:**1893-904.
20. Li X, Cao X 2006 BMP signaling and skeletogenesis. Ann N Y Acad Sci **1068:**2640.
21. Hogan BL 1996 Bone morphogenetic proteins in development. Curr Opin Genet Dev **6**(4)**:**432-8.
22. Shafer J DA, Gannon FH, Fouletier-Dilling CM, Lazard Z, Moran K, Gugala Z, Ozen M, Ittmann M, Heggeness MH, Olmsted-Davis E 2007 Oxygen tension directs chondrogenic differentiation of myelo-monocytic progenitors during endochondral bone formation. Tissue Eng **13**(8)**:**2011-9.
23. Rissanen TT, Markkanen JE, Gruchala M, Heikura T, Puranen A, Kettunen MI, Kholova I, Kauppinen RA, Achen MG, Stacker SA, Alitalo K, Yla-Herttuala S 2003 VEGF-D is the strongest angiogenic and lymphangiogenic effector among VEGFs delivered into skeletal muscle via adenoviruses. Circ Res **92**(10)**:**1098106.
24. Moser M, Binder O, Wu Y, Aitsebaomo J, Ren R, Bode C, Bautch VL, Conlon FL,

Patterson C 2003 BMPER, a novel endothelial cell precursor-derived protein, antagonizes bone morphogenetic protein signaling and endothelial cell differentiation. Mol Cell Biol **23**(16)**:**5664-79.
25. Mishina Y, Suzuki A, Gilbert DJ, Copeland NG, Jenkins NA, Ueno N, Behringer RR 1995 Genomic organization and chromosomal location of the mouse type I BMP-2/4 receptor. Biochem Biophys Res Commun **206**(1)**:**310-7.
26. Winnier G, Blessing M, Labosky PA, Hogan BL 1995 Bone morphogenetic protein-4 is required for mesoderm formation and patterning in the mouse. Genes Dev **9**(17)**:**2105-16.
27. Kelly MA, Hirschi KK 2009 Signaling Hierarchy Regulating Human Endothelial Cell Development. Arterioscler Thromb Vasc Biol.
28. Zhao Y, Glesne D, Huberman E 2003 A human peripheral blood monocyte-derived subset acts as pluripotent stem cells. Proc Natl Acad Sci U S A **100**(5)**:**2426-31.
29. Ruster B, Gottig S, Ludwig RJ, Bistrian R, Muller S, Seifried E, Gille J, Henschler R 2006 Mesenchymal stem cells display coordinated rolling and adhesion behavior on endothelial cells. Blood **108**(12)**:**3938-44.
30. Otsuru S, Tamai K, Yamazaki T, Yoshikawa H, Kaneda Y 2007 Bone marrow-derived osteoblast progenitor cells in circulating blood contribute to ectopic bone formation in mice. Biochem Biophys Res Commun **354**(2)**:**453-8.
31. Pufe T, Petersen WJ, Miosge N, Goldring MB, Mentlein R, Varoga DJ, Tillmann BN 2004 Endostatin/collagen XVIII--an inhibitor of angiogenesis--is expressed in cartilage and fibrocartilage. Matrix Biol **23**(5)**:**267-76.
32. Oshima Y, Sato K, Tashiro F, Miyazaki J, Nishida K, Hiraki Y, Tano Y, Shukunami C 2004 Anti-angiogenic action of the C-terminal domain of tenomodulin that shares homology with chondromodulin-I. J Cell Sci **117**(Pt 13)**:**2731-44.
33. Hayami T, Funaki H, Yaoeda K, Mitui K, Yamagiwa H, Tokunaga K, Hatano H, Kondo J, Hiraki Y, Yamamoto T, Duong le T, Endo N 2003 Expression of the cartilage derived anti-angiogenic factor chondromodulin-I decreases in the early stage of experimental osteoarthritis. J Rheumatol **30**(10)**:**2207-17.
34. Kaplan FS, Glaser DL, Shore EM, Pignolo RJ, Xu M, Zhang Y, Senitzer D, Forman SJ, Emerson SG 2007 Hematopoietic stem-cell contribution to ectopic skeletogenesis. J Bone Joint Surg Am **89**(2)**:**347-57.
35. Shukunami C, Iyama K, Inoue H, Hiraki Y 1999 Spatiotemporal pattern of the mouse chondromodulin-I gene expression and its regulatory role in vascular invasion into cartilage during endochondral bone formation. Int J Dev Biol **43**(1)**:**39-49.

Supplemental data:

To verify that the Flk-H2B::EYFP was restricted to endothelial cells, we first analyzed the normal adult muscle to examine that the Flk-1-H2B::EYFP expressed in the endothelial cells. YFP positive cells appeared to be association with the endothelial cells labeled by antibodies against CD31 and Flk1 (figure1). When endogenous Flk1 positive cells are immunolabled, smaller vessels showed co-localization of YFP and Flk1 positive cells,

however, not all the Flk1 positive vessels contained YFP positive cells. Since vascular smooth muscle actin (SMA) is also expressed by cell surrounding vascular endothelial cells, we examined whether the YFP expression is associated with the smooth muscle cells using SMA antibody for immuostaining, and we do see the YFP expression in smooth muscle positive vasculature (figure. 1). From our immunolocalization analysis, the endothelial marker VE-cadherin (data not shown) and CD31 marker also exhibit a similar localization pattern with YFP positive cells (figure. 1, table 1).

Using image analysis software, FARSIGHT (RPI, New York), we performed segmentation analysis on RGB images, where we associated immunostaining signals to the red channel, YFP to the green channel, and DAPI to the blue channel. First, DAPI stained nuclei in the blue channels were segmented using FARSIGHT. The total number of segmented nuclei was defined as the total number of cells. Similarly, YFP positive nuclei in the green channels were segmented and counted as YFP positive cells (figure. 1). The fraction of cells that were immumostaining positive was counted by taking the ratio of DAPI stained nuclei that were immumostaining positive (red channel) to the total number of DAPI stained nuclei. Then, the immuno-stained positive cells were classified as YFP positive cells and YFP negative cells. Data sets were quantified and described in the table 1. From this analysis, we demonstrated that adult muscle tissue express H2B::EYFP in the endothelial cells, however, they represents a subset of endothelial cells.

CD31 (8 pictures)	CD31+/DAPI+	YFP+ CD31+/YFP+	YFP+ CD31+/CD31+
Mean	84.56%	100.00%	20.74%
Stv	10.87%	†	16.95%
Confident Interval (95%)	7.10%	†	11.07%

Figure.1

Table.1

All nucleus → DAPI+ DAPI with CD31+ and YFP-→CD31+ DAPI with CD31-and YFP+ →YFP+

CD31 (8 pictures)	CD31+/DAPI+	YFP+ CD31+/YFP+	YFP+ CD31+/CD31+
Mean	84.56%	100.00%	20.74%
Stv	10.87%	†	16.95%
Confident Interval (95%)	7.10%	†	11.07%
VE-Cad (6 pictures)	**VE-Cad+/DAPI+**	**YFP+ VE-Cad +/YFP+**	**YFP+VE-Cad +/VE-Cad +**
Mean	87.67%	100.00%	8.61%
Stv	6.59%	†	3.67%
Confident Interval (95%)	4.31%	†	2.40%
FLK1 (6 pictures)	**FLK1+/DAPI+**	**YFP+ FLK1 +/YFP+**	**YFP+ FLK1 +/FLK1 +**
Mean	94.93%	100.00%	16.94%
Stv	5.22%	†	7.02%
Confident Interval (95%)	4.18%	†	5.61%
SMA (12 pictures)	**SMA +/DAPI+**	**YFP+ SMA +/YFP+**	**YFP+ SMA +/ SMA +**
Mean	62.64%	93.31%	23.53%
Stv	16.71%	10.04%	14.14%

CD31 (8 pictures)	CD31+/DAPI+	YFP+ CD31+/YFP+	YFP+ CD31+/CD31+
Mean	84.56%	100.00%	20.74%
Stv	10.87%	†	16.95%
Confident Interval (95%)	7.10%	†	11.07%
VE-Cad (6 pictures)	**VE-Cad+/DAPI+**	**YFP+ VE-Cad +/YFP+**	**YFP+VE-Cad +/VE-Cad +**
Mean	87.67%	100.00%	8.61%
Stv	6.59%	†	3.67%

DAPI with CD31+ and YFP+ →CD31+YFP+

Figure 1

Click here to download high resolution image

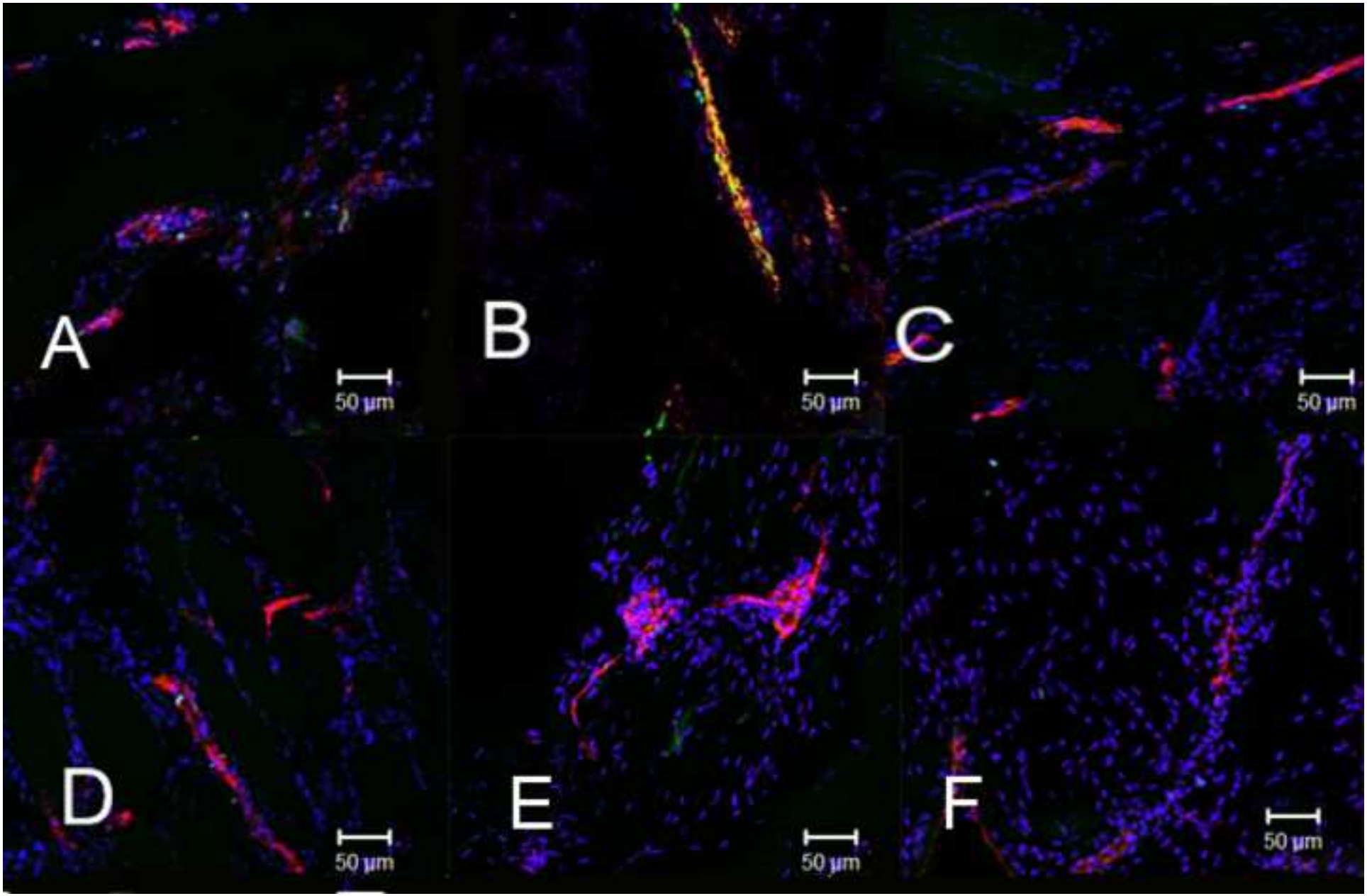

Figure 2

Click here to download high resolution image

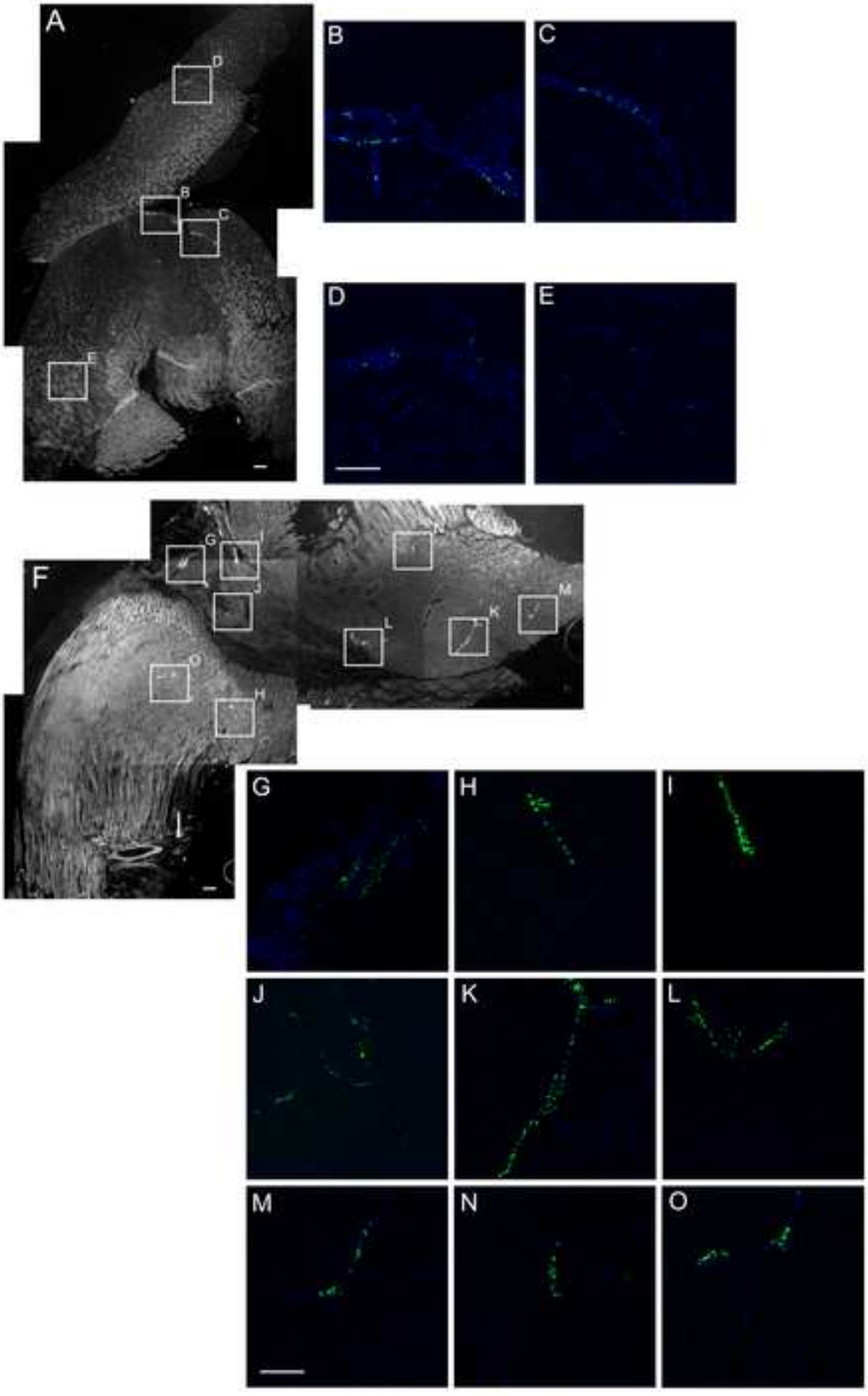

Figure 3

Click here to download high resolution image

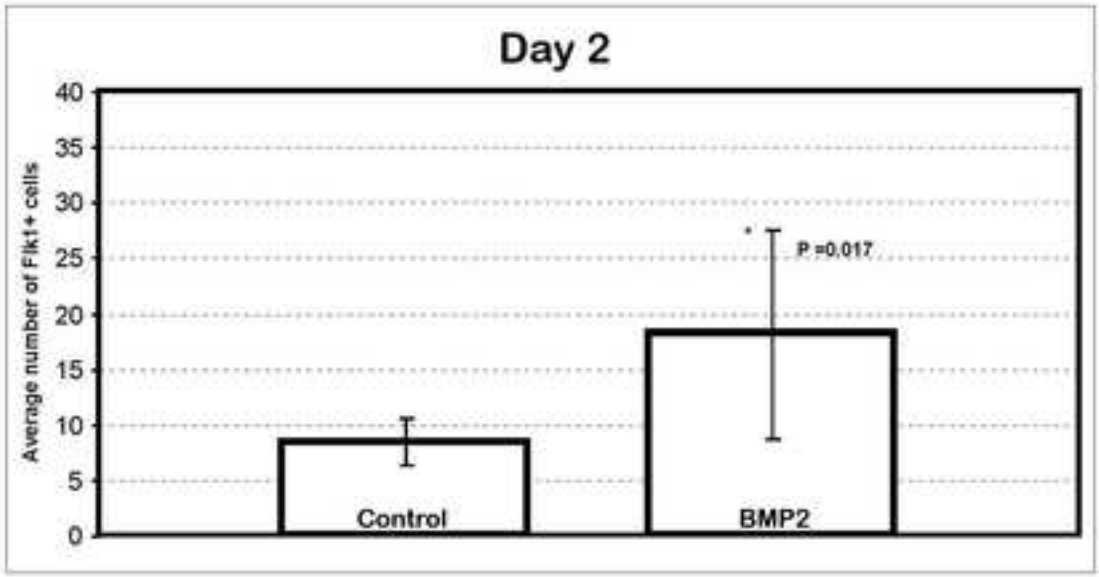

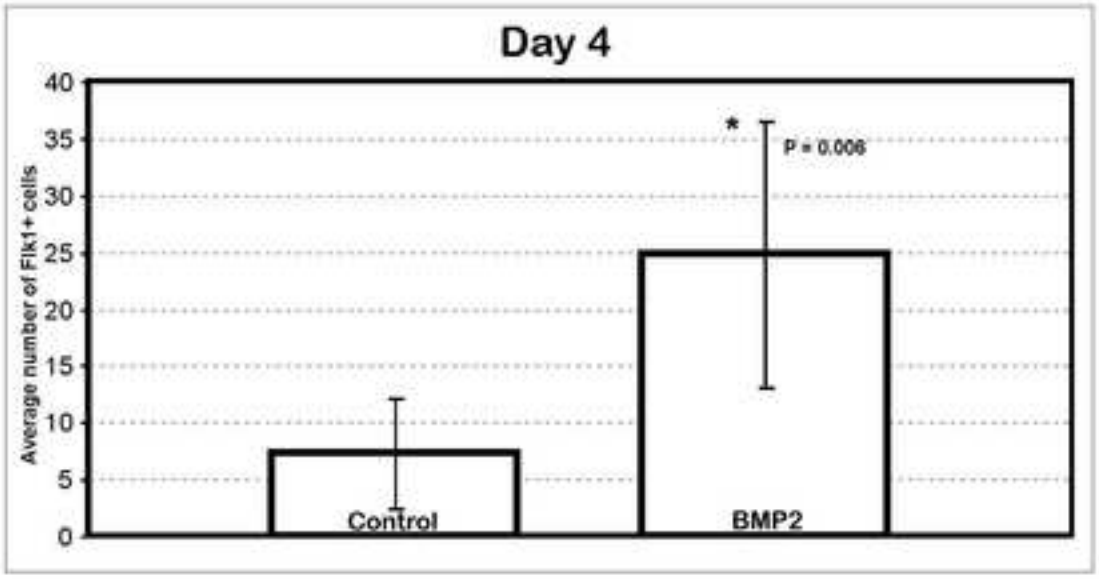

Figure 4

Click here to download high resolution image

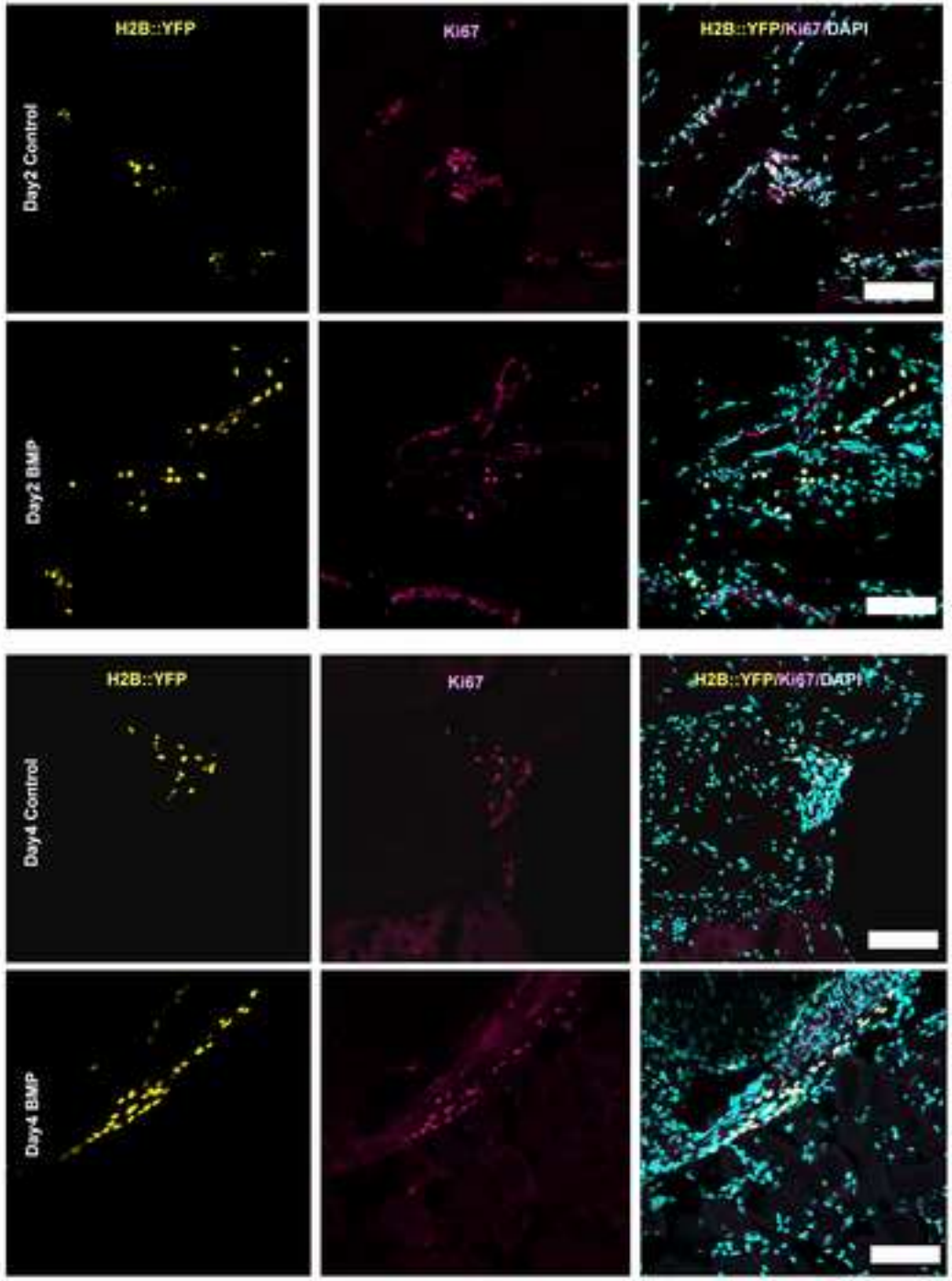

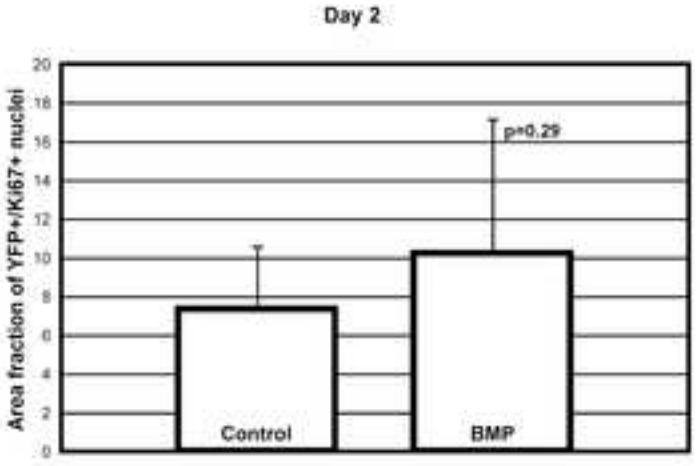

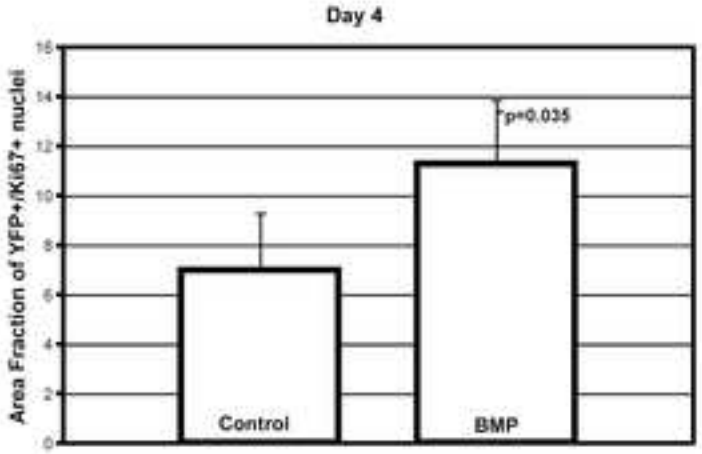

Figure 5

Click here to download high resolution image

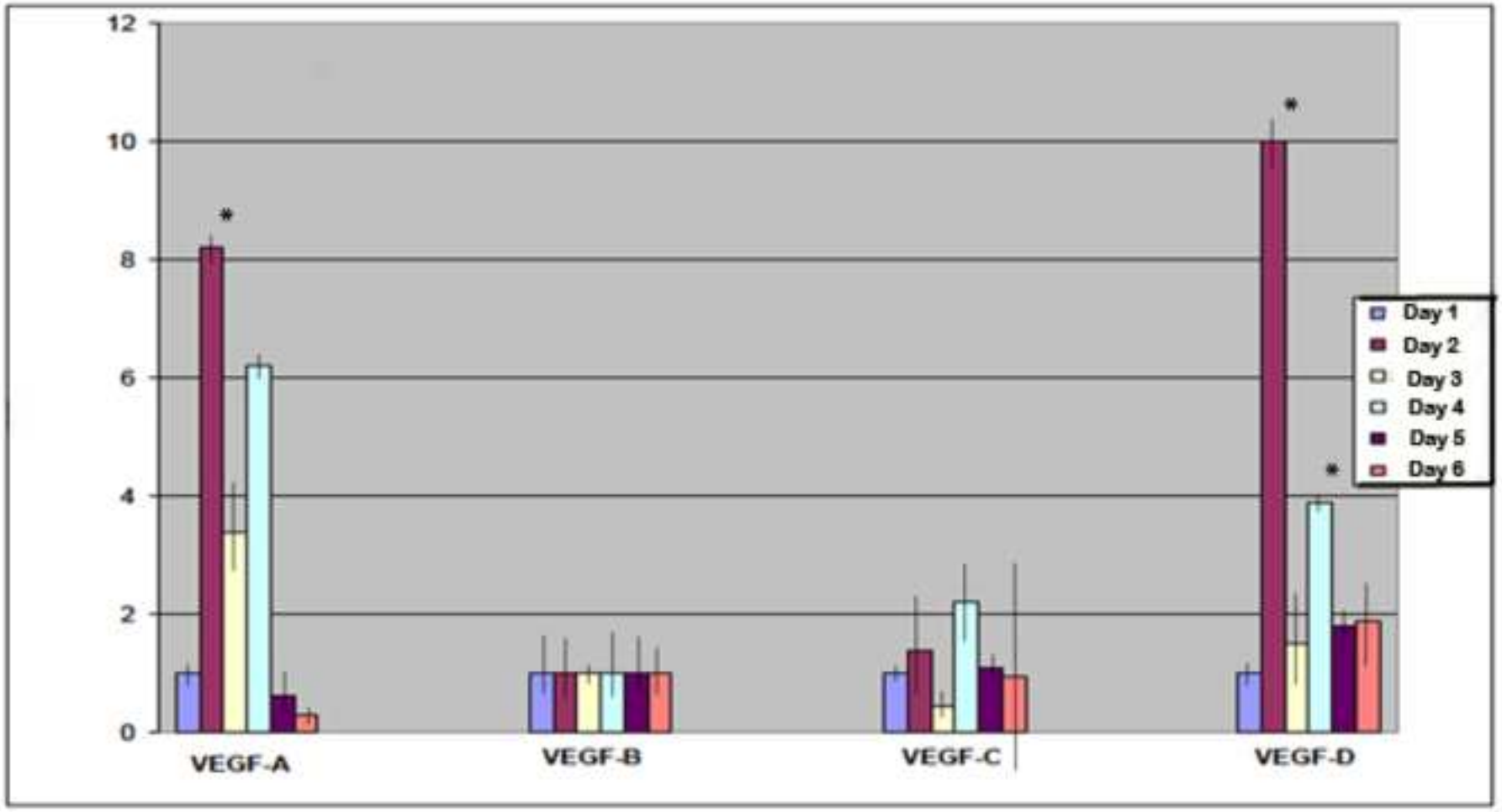

Figure 6

Click here to download high resolution image

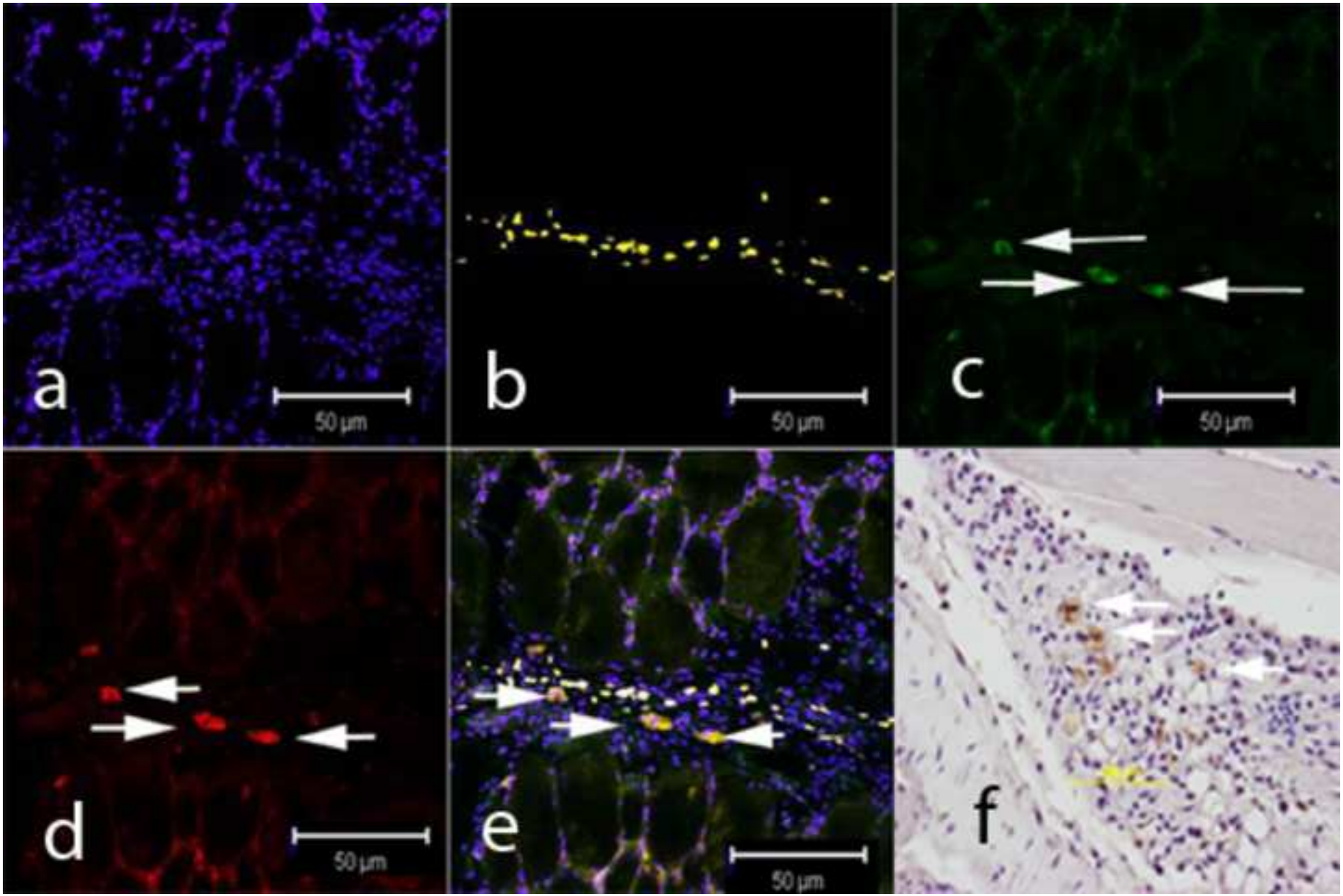

Cathepsin-K sensitive poly(ethylene Glycol) hydrogels for degradation in response to bone formation

Chih-Wei Hsu[a], Ronke M. Olabisi[a], Elizabeth A. Olmstead-Davis[b], Alan R. Davis[b], Jennifer L. West[a]

[a]*Department of Bioengineering, Rice University, 6100 Main St., MS 142, Houston, TX 77005, USA*

[b]*Center for Cell and Gene Therapy, Baylor College of Medicine, Houston, TX 77030, USA*

Abstract

The objective of this study was to develop a new class of synthetic bone graft materials that promote bone formation in response to remodeling efforts of osteocytes. We have chosen to use a poly(ethylene glycol) diacrylate (PEGDA) hydrogel as a model system to demonstrate this new strategy. A cathepsin K-sensitive peptide, GGGMGPSGPWGGK (GPSG), was incorporated into the backbone of the PEGDA polymer to produce a crosslinkable GPSG hydrogel structure. Degradation profiles of the GPSG hydrogels were obtained in the presence of enzymes including cathepsin K and proteinase K, which both resulted in degradation of 80% of the hydrogel material in a 24 hr time period compared to 40% degradation in the presence of nonspecific collagenases. No degradation was observed when the hydrogels were incubated with plasmin. Differentiated MC3T3-E1 osteoblasts and RAW264.7 osteoclasts were seeded on GPSG hydrogels to test cell-induced degradation at the surface. Observed surface features and resorption pits were analyzed by differential interference contrast (DIC) and fluorescence images by confocal microscopy. These features provide evidence of cell mediated remodeling of the synthetic hydrogel material. In summary, we have demonstrated that by incorporating a cathepsin k-sensitive GPSG hydrogel can be further integrated with surrounding tissue after implantation via bone resorption.

Key words: Bioresorption, Bone graft, Hydrogel, Osteoclast, Scaffold.

1. Introduction

Bone grafting is a common procedure in orthopedic surgery, and both autografts and allografts have been commonly used in spinal fusion, revision total hip arthroplasty, maxillofacial reconstruction, and repair of segmental skeletal defects caused by tumor resection or trauma [1-4]. Although autografts are considered the gold standard for repairs of bone defects, its usage is limited by donor-site morbidity and availability, and the procedure also requires additional surgeries for graft harvesting often resulting in persistent postoperative pain and the risk of neurovascular damage at donor sites [5, 6]. Although no additional surgeries are performed on patients for allografts, these procedures hold risks of infection, immunorejection, disease transmission, and unfavorable mechanical properties [7-10]. Due to the high demand for bone grafts, several strategies have been developed to assist bone grafts or function as substitutes, such as demineralized bone matrix (DBM), ceramic, gene therapy, graft composite, or bone morphogenetic proteins (BMPs) [11-14]. In order to mimic the properties of autografts, an ideal bone-graft

substitute has to be osteoconductive, osteoinductive, and osteogenic. Furthermore, the bone grafts must be able to integrate with the host without triggering an immunoresponse [12].

In a previous study, we demonstrated that encapsulation of adenovirus-transduced cells expressing recombinant human BMP-2 (rhBMP-2) within non-degradable poly(ethylene glycol) diacrylate (PEGDA) hydrogels can facilitate bone formation *in vivo* [14]. Human diploid fetal lung fibroblasts (MRC-5) were transduced with the adenovirus Ad5F35BMP2 and encapsulated within PEGDA hydrogels. Encapsulated cells transduced with rhBMP-2 in PEGDA hydrogels were implanted into the quadricep muscles of each of the two hind legs of female NOD/SCID mice. Endochondral bone was detected around implanted hydrogels after 3 weeks. This model demonstrated that the PEGDA scaffold provided osteoconduction, rhBMP-2 expressed by transduced cells provided osteoinduction, and the progenitor cells recruited by rhBMP-2 were osteogenic. However, because the implanted PEGDA hydrogels were non-degradable, the induced bone only formed shells around the hydrogel cores without penetrating or replacing the hydrogels. To better develop a bone graft substitute, the hydrogel needed to be modified to enable integration within the surrounding tissue.

The objective in this paper is to use design a new class of biomaterial that can be gradually integrated with new endochondral bone via the process of bone remodeling. In this study, we use PEGDA hydrogels as a model system to demonstrate that can be gradually remodeled through bone resorption by osteoclasts. The degradable hydrogel is designed by introducing a short peptide fragment Gly-Pro-Ser-Gly (GPSG) of type I collagen (α-1) (160-163), which was found to be highly cleavable by cathepsin K [17]. Cathepsin K is a protease predominantly expressed in osteoclasts during bone resorption [16, 18]. After incorporating this cathepsin K-sensitive peptide into a PEG backbone, we tested the degradation profiles of the cathepsin K sensitive GPSG hydrogel *in vitro*. We also tested the hydrogel to determine whether it could be degraded by osteoclasts or osteoblasts.

2. Materials and Methods

2.1 Synthesis and characterization of acryloyl-PEG-succinimidyl carbonate (acrylol-PEG-SMC)

All reagents were obtained from Sigma unless otherwise noted. 50 mM of PEG (3,400 Da; Fluka, Milwaukee, WI) was reacted with 75 mM silver (I) oxide and 55 mM acryloyl chloride in anhydrous dichloromethane (anDCM). Thirty mM of potassium iodine was added as catalyst, and the mixture was reacted at 0-4 ^{O}C overnight. To purify the acryloyl-PEG-OH, silver (I) oxide was first removed by filtering the mixture through a Celite 521 pad (Spectrum Chemical Manufacturing Corp, Gardena, CA). For further purification, the filtrate was dried by using a Rotovap, re-dissolved in de-ionized water, and adjusted to pH 3 with 6N HCl. After heating to 35 ^{O}C and venting to air for 1 h, activated charcoal (Fisher Scientific, Pittsburgh, PA) was added to the mixture and stirred overnight to absorb iodine. The charcoal was then

removed via filtration. Sodium chloride (25% W/V) was dissolved in the aqueous filtrate followed by DCM extraction. The organic phase was collected and extracted again with 2 M potassium bicarbonate to remove chloride ions. Acryloyl-PEG-OH was recovered by precipitation in cold ethyl ether, filtered, dried under vacuum overnight, and lyophilized until completely dry. To proceed with the succinimidyl carbonate conjugation, 25 mM acryloyl-PEG-OH was mixed with 75 mM pyridine and 100 mM N,N'-disuccinimidyl carbonate in anhydrous acetonitrile. After reacting under argon overnight, pyridine and acetonitrile were removed with a Rotovap. The mixture was then re-dissolved in anhydrous DCM and filtered to remove unreacted N,N'-disuccinimidyl carbonate. Acetate buffer (0.1 M, pH 4.5, 15% NaCl) was then used for phase extraction. The organic layer was collected and then dried by anhydrous $MgSO_4$. Acryloyl-PEG-SMC was recovered following precipitation in cold ethyl ether, filtered, and dried under vacuum overnight. The products were analyzed by ^{1}H-NMR (Advance 400, Bruker, Germany) and matrix-assisted laser desorption ionization time of flight mass spectrometry (MALDI-ToF; Bruker Daltonics, Billerica, MA) and stored at -80^{O}C under argon.

2.2 Synthesis and characterization of the cathepsin K sensitive PEG-GGGMGPSGPWGGK-PEG, PEG-RGDS, and fluorescently-labeled PEG-RGDS conjugates

The Cathepsin K-sensitive peptide sequence GGGMGPSGPWGGK was synthesized on an APEX 396 peptide synthesizer (Aapptec, Louisville, KY). A tryptophan residue was incorporated into the peptide sequence for the purpose of tracking *in vitro* degradation by monitoring UV absorbance at 280 nm. The peptide was then cleaved from the polystyrene resin (95 % trifluoroacetic acid, 2.5 % water, and 2.5 % triisopropylsilane), precipitated in ethyl ether, and purified by dialysis. Following purification, the molecular weight of the synthesized peptide was confirmed with MALDI-ToF. The crosslinkable cathepsin K sensitive acryloyl-PEG-GGGMGPSGPWGGK-PEG-acryloyl (GPSG) polymer was synthesized by reacting the peptide with acryloyl-PEG-SMC in a 2.1:1 (PEG:peptide) molar ratio in 50 mM sodium bicarbonate buffer (pH 8.5) at room temperature overnight. The product was dialyzed, lyophilized, and stored under argon at -20^{O}C until use. The cell adhesive peptide Arg-Gly-Asp-Ser (RGDS, American Peptide, Sunnyvale, CA) was also reacted with acryloyl-PEG-SMC in a 1.1:1 molar ratio to give acryloyl-PEG-RGDS. Conjugation products were analyzed by ^{1}H-NMR and gel permeation chromatography (GPC; Polymer Laboratories, Amherst, MA) with UV/Vis and evaporative light scattering detectors. Fluorescently Labeled acryloyl-PEG-RGDS was synthesized as previously described [27]. In brief, purified acryloyl-PEG-RGDS was mixed with Alexa Fluor 680 carboxylic acid (Invitrogen, Carlsbad, CA) in 50 mM sodium bicarbonate buffer in a 1:10 (acryloyl-PEG-RGDS:dye) molar ratio and allowed to react for 1 h at room temperature. The desired products were then purified by a Sephadex G-25 fine chromatography column (Amersham Bioscience, Uppsala, Sweden) followed by dialysis and then lyophilized. Recovered products were stored under argon at -20 ^{O}C until use.

2.3 In vitro degradation profiles of the GPSG hydrogel

The degradation profiles of GPSG hydrogel were measured by monitoring the release of tryptophan into solution after incubation with different enzymes. A pre-polymer solution was prepared by combining 0.1 g/ml crosslinkable GPSG polymer with 1.5 % (v/v) triethanolamine, 37 mM 1-vinyl-2-pyrrolidinone, and 1 % (v/v) of 10 mM eosin Y in tris buffered saline (TBS; pH 7.5, 10 mM $CaCl_2$, 0.1 % Tween 20, 0.2 mg/ml sodium azide). The precursor solution was sterilized by filtration using a 0.22 μm filter (Millpore Corporation Bedford, MA). For *in vitro* enzyme degradation test, 3 μL of pre-polymer solution was transferred to the bottom corner of each micro-cuvette (Brandtech, Essex, CT) and polymerized by exposing to visible light for 2 minutes. Following equilibrium swelling overnight in 250 μL TBS buffer, each hydrogel was incubated with 250 μL enzyme solution at $37^{O}C$ for 24 hours. Proteinase K (Invitrogen), plasmin, type I and type III collagenase (COL I and COL III; Worthington, Lakewood, NJ) were prepared in TBS buffer to the final concentration of 0.05 mg/ml. Procathepsin K (Enzo Life Science, Plymouth Meeting, PA) was first activated in 35 mM sodium acetate (pH 3.5) for 2 hours at room temperature. Activated cathepsin K was then adjusted to 0.05 mg/ml in 50 mM sodium acetate buffer (NaOAc; pH 5.5, 2.5 mM EDTA, 1 mM DTT, 0.01 % Triton X-100, 0.2 mg/ml sodium azide). Hydrogels were also incubated in TBS and NaOAc buffer as negative controls. Degradation was evaluated by measuring the absorbance change at 280 nm of test solutions to monitor the release of tryptophan over time with a UV/Vis spectrophotometer (Carey 50, Varian, Palo Alto, CA).

2.4 Cell maintenance of MC3T3-E1 and RAW 264.7 cells

Murine pre-osteoblast cells MC3T3-E1 subclone 4 and macrophage cells RAW 264.7 (ATCC, Manassas, VA, USA) were recovered from liquid nitrogen and cultured in alpha-MEM medium (Gibco BRL, Canada) and DMEM (ATCC), respectively. Culture media were supplemented with 10 % fetal bovine serum (FBS; Atlanta Biologicals, Lawrenceville, GA), 100 U/ml penicillin, and 100 mg/ml streptomycin (Gibco BRL, Canada). Cells were incubated at $37^{O}C$ with 5 % CO_2. The medium was refreshed every 2–3 days and confluent cells were subcultured through trypsinization for MC3T3-E1 and scraping for RAW 264.7. All experiments were conducted using cells between passages 4-10. MC3T3-E1 cells were differentiated into osteoblasts via supplied 50 ug/ml ascorbic acid and 10 mM b-glycerophosphate to the growth medium. Differentiation medium was subsequently replaced every 2-3 days. To differentiate cells to multinuclear osteoclasts, RAW 264.7 were cultured at a density of 1.5×10^5 cells/cm^2 and allowed to adhere for 4 hours. Medium was then supplied with 30 ng/ml of receptor activator of nuclear factor kappa B ligand (RANKL; R&D Systems Inc., Minneapolis, MN) and replaced every 2 days. The cells were then cultured for 4 days before further use.

2.5 Serum gradient purification of differentiated multinuclear RAW264.7

Differentiated multinuclear RAW264.7 (dRAW264.7) were purified by a serum gradient [28]. After

differentiation in culture medium supplied with 30 ng/ml RANKL for 4 days, dRAW264.7 cells were trypsinized and resuspended in 15 ml of Moscona's high carbonate (MHB; pH 7.2, 137 mM NaCl, 2.7 mM KCl, 0.4 mM NaH_2PO_4, 12 mM $NaHCO_3$, and 11 mM dextrose) solution. A serum gradient was prepared by placing a layer of 15 ml 70% FBS solution in MHB at the bottom of a 50 ml conical tube, and then slowly overlaying with a second layer of 15 ml 40% FBS solution. Fifteen ml of cell suspension was then slowly added to the top without disturbing the layers. The tube was then capped and held undisturbed at room temperature for 30 minutes to permit cells to separate based on size. The top 17 ml layer, middle 16 ml layer, and bottom 12 ml layer were collected separately. Cells in each layer were centrifuged down and seeded in tissue culture plates overnight. After attaching, cells were fixed and stained for the activity of tartrate-resistant acid phosphatase (TRAP).

2.6 Surface degradation studies of differentiated RAW 264.7 and MC3T3- E1 on GPSG hydrogels

Flat hydrogel sheets for surface degradation studies were formed by adding 10 mM acrylate-PEG-RGDS and 1 mM Alexaflour 680 labeled acrylate-PEG-RGDS to the pre-polymer mixture and polymerizing between a mica sheet (Ted Pella, Inc., Redding, CA) and glass slide separated by a 1 mm Teflon spacer. The mica sheet resulted in hydrogels with atomically smooth surfaces. Both MC3T3-E1 and RAW 264.7 cells were differentiated for 4 days in differentiation media in tissue culture plates. Differentiated MC3T3-E1 (dMC3T3-E1) were subcultured and seeded on to the atomically smooth hydrogel surfaces at a density of 5 x 10^4 cells/cm^2. Differentiated multinuclear RAW264.7 osteoclasts collected at the bottom layer of serum gradient were also seeded on smooth hydrogel surfaces at the same density. Hydrogels seeded with both osteoblasts and osteoclasts were then cultured in differentiation medium for 48 hours before further analysis.

2.7 Confocal microscopy of pit formation on cathepsin K sensitive PEG hydrogel surface

After a 48 hour incubation on smooth hydrogel surfaces, cells were either detached from the hydrogel surface by 20 mM EDTA or fixed and stained with 4',6-diamidino-2-phenylindole (DAPI; Invitrogen) and rhodamine phalloidin (Invitrogen). Differential interference contrast (DIC) or fluorescence images were taken by LSM-5 LIVE microscope systems (Carl Zeiss Inc., German). Z-stack images were acquired with a 20X objective. The z distance between each step was 0.253 μm. Images were all processed with ImageJ 142 (NIH, Bethesda, MD). Three dimensional image reconstructions were processed using OsiriX Medical Imaging software (version 3.0.2; the OsiriX Foundation, Geneva, Switzerland).

3. Results

3.1 Characterization of synthesized materials.

^{1}H-NMR analysis demonstrated that acryloyl-PEG-SCM was successfully synthesized and conjugated to GGGMGPSGPWGGK and RGDS. After purification, the acryloyl-PEG-SCM showed the methylene protons

of PEG as a triplet at 3.6–3.7 ppm, the succinimidyl carbonate protons at 2.6 ppm, as well as the acrylate protons at 5.9–6.4 ppm. After conjugation to GGGMGPSGPWGGK and RGDS, the peak for the succinimidyl carbonate protons disappeared, but peaks for the methylene protons of PEG and acrylate protons remained. The shift in molecular weight of conjugated products was also evaluated by GPC.

3.2 In vitro degradation of Cathepsin K-sensitive GPSG hydrogels

The hydrogels with the cathepsin K sensitive peptide GGGMGPSGPWGGK were designed to carry a cathepsin K sensitive cleavage site between serine and proline [25]. Proteinase K was used as a positive control. While the hydrogel degrades, the peptide that was incorporated into the hydrogel structure will be cleaved by enzymes and gradually release into solution. The degradation profiles of GPSG hydrogels were measured by monitoring the concentration change of tryptophan in solution at UV absorbance of 280 nm. Crosslinkable GPSG hydrogels were polymerized in microcuvettes and incubated with enzyme solutions. After equilibilium swelling in TBS overnight, hydrogels were treated with different enzymes to evaluate the degradation profiles (Figure 1). After incubation with different enzyme solutions for 24 hr, hydrogels in cathepsin K and proteinase K solutions had similar degradation profiles, both indicating a rapid tryptophan concentration increase within the first hour and reaching about 80% release of total tryptophan at 24 hr. No degradation was observed when hydrogels were incubated in TBS buffer, NaOAc buffer, and plasmin. Hydrogels incubated in nonspecific collagenase I and collagenase III solutions also released 40% of incorporated tryptophan after a 24 hour incubation.

3.3 Differentiation of RAW264.7

Raw 264.7 cells were differentiated in culture medium containing 30 ng/ml RANKL for 4 days. Differentiated cells were then trypsinized and separated by serum gradient based on gravity. Cells collected at the top, middle, and bottom fractions of the gradient solution were reseeded on tissue culture plate and stained for TRAP activity (Figure 2). Non-differentiated RAW264.7 cells were stained TRAP negative. Although all stained TRAP positive after differentiation, not all of the cells can fuse into multinuclear cells (Figure 2A). After separation by serum gradient, the top fraction of the gradient contained most of the mononuclear cells. The middle fraction of the gradient contained mixed groups of mononuclear and multinuclear cells. The majority of cells at the bottom fraction were multinuclear cells, which contained a very small portion of mononuclear cells (Figure 2B to D). The multinuclear cells collected at the bottom fraction were also stained TRAP positive, which indicted that they were active osteoclasts. The bottom fraction of TRAP+ dRAW 264.7 osteoclasts were then used for hydrogel degradation studies.

3.4 DIC images of cathepsin K sensitive hydrogel surfaces seeded with dMC3T3E1 and dRAW264.7

To evaluate if the GPSG hydrogels can be degraded by osteoblasts or osteoclasts, dMC3T3-E1 osteoblasts and dRAW264.7 osteoclasts were seeded on atomically smooth hydrogel surface polymerized

against a mica sheet. After 48 hours, osteoblasts and osteoclasts were detached by 20mM EDTA, and the hydrogel surfaces were examined with DIC images under confocal microscopy (Figure 3). No features were detected on the surfaces seeded with dMC3T3-E1 osteoblasts (Figure 3A). On the surfaces seeded with dRAW264.7 osteoclasts, several features were observed after cells were detached (Figure 3B). The intensity profile of the DIC image (Figure 3D) suggests that the features on the hydrogels were depressions.

3.5 Three dimensional image reconstruction of dRAW264.7 cells on the surface of cathepsin K sensitive hydrogels

To further confirm the depressed imperfections observed on hydrogel surface were actual resorption pits generated by dRAW264.7, osteoclasts on GPSG hydrogels were fixed and stained with DAPI for nuclei and rhodamine phalloidin for F-actin. Hydrogels were then examined under confocal microscopy. dRAW264.7 cells stained with DAPI and rhodamine phalloidin showed multinuclear and polarized cells on the hydrogel surface, and the GPSG hydrogel was polymerized with Alexafluor680 labeled acryloyl-PEG-RGDS (Figure 4A; Supplement A video). A sealing ring of F-actin and multiple nuclei were clearly observed (Figure 4B). On the hydrogel surface where the osteoclast was located, a decrease in the fluorescent signal was observed (Figure 4C). The z-stack images were then examined closely by three-dimensional reconstructions using a volume rendering method. Figure 4D is the side view, showing the osteoclast attached to the hydrogel. From the three-dimensional perspective of the image from the top (Figure 4E) and bottom (Figure 3F) of the hydrogel, the loss in fluorescent signal of the hydrogel reveals a hole in the hydrogel through which the cell can be seen. This signal loss is indicative of activity by the differentiated RAW264.7 osteoclasts, degrading the underlying hydrogel and creating a pit, resulting in the fluorescent intensity loss. No signal loss was observed on the gels seeded with dMC3T3-E1 cells.

4. Discussion

An ideal autologous bone graft substitute has to comprise the properties of an osteoconductive, osteoinductive, osteogenic, and bioresorbable material. We have previously demonstrated that encapsulated cells transduced with rhBMP-2 in poly(ethylene glycol) diacrylate hydrogel gels can be osteoinductive and osteogenic. But with non-degradable PEGDA hydrogel, newly induced bone could only form shells around hydrogel cores without further remodeling. Without removing the hydrogel, it highly restricts the application of this system. To better modify this system, we developed a PEGDA hydrogel system that can be remodeled specifically by the process of bone resorption, which will allow the hydrogel system to be able to support and protect transduced cells and also be gradually replaced via the process of bone remodeling.

In the current study, we have described a PEGDA hydrogel system which was designed to be specifically

degraded by bone resorption. By synthesizing a cathepsin K sensitive peptide GGGMGPSGPWGGK that is derived from collagen type I, we have developed a PEGDA hydrogel containing GPSG that is highly sensitive to cathepsin K *in vitro*. We also tested the GPSG hydrogel with non-specific collagenases type I and III, which showed minor degradation effects when compared to cathepsin K. At the same enzyme concentration, cathepsin K demonstrates much higher cleavage ability than non-specific collagenases within 24 hours incubation periods. No degradation was observed when incubated GPSG hydrogels with plasmin.

Additionally, we tested the sensitivity of GPSG hydrogel seeded with osteoblasts and osteoclasts. While the GPSG hydrogel has been shown to be highly sensitive to cathepsin K compared to non-specific collagenases, we want to further test if cell attachment and migration of osteoblasts and osteoclasts will cause any degradation of the GPSG hydrogel. Ideally, we expected to observe resorption pits on the hydrogel surface after seeding with osteoclasts, with only minor degradation on surfaces seeded with osteoblasts that is caused by collagenases. We have demonstrated that our GPSG hydrogel can be degraded by osteoclasts but not osteoblasts. When examined under DIC after cells removal, surface resorption pits were only observed on the GPSG hydrogel surfaces seeded with dRAW264.7 osteoclasts, but not with dMC3T3 osteoblasts after 48 hours of incubation. Surface resorption pits were further examined by fluorescence confocol microscopy while activated osteoclasts were still attached on the hydrogel surface, which confirmed the pits were generated by resorption of osteoclasts.

With this designed property, progenitor cells recruited by rhBMP-2 proteins will start the process of bone formation around the hydrogel. Once the shell of endochondral bone forms around the GPSG hydrogels, bone resorption will start to remodel the endochondral bone shell, along with the GPSG hydrogel core by cathepsin K. Osteoblasts will then move to the void left behind by the degraded hydrogel and replace it with bone. Controlled degradation via osteoclasts will not only allow the hydrogel to be gradually integrated with the surrounding tissue, it will also prolong the survival of the encapsulated cells and rhBMP-2 production. In the mean time, with the GPSG hydrogel being gradually removed during the process of bone remodeling, it will prevent the early rupture of the hydrogel and prevent the release of transduced cells from inducing an immunoresponse.

5. Conclusions

In summary, we have successfully used the PEG hydrogel as a model system to demonstrate a new strategy to improve biomaterial integration through the process of bone resorption. By incorporating the GPSG peptide sequence into the backbone of the polymer material, the hydrogel graft can be gradually degraded by cathepsin K secreted by osteoclasts during the process of bone resorption. We have demonstrated that this new strategy yields a material that is subject to specific degradation by

bone-forming osteoclasts. In the future, this system can be further investigated *in vivo* to match the speed of bone formation and hydrogel degradation for bone graft applications.

Acknowledgments

This research was supported by Department of Defense (W81XWH-04-1-0068).

References

1. Price CT, Connolly JF, Carantzas AC, Ilyas I. Comparison of bone grafts for posterior spinal fusion in adolescent idiopathic scoliosis. Spine (Phila Pa 1976) 2003 Apr 15;28(8):793-798.
2. Goldberg VM. Selection of bone grafts for revision total hip arthroplasty. Clin Orthop Relat Res 2000 Dec(381):68-76.
3. Nishida J, Shimamura T. Methods of reconstruction for bone defect after tumor excision: a review of alternatives. Med Sci Monit 2008 Aug;14(8):RA107-113.
4. Malizos KN, Zalavras CG, Soucacos PN, Beris AE, Urbaniak JR. Free vascularized fibular grafts for reconstruction of skeletal defects. J Am Acad Orthop Surg 2004 Sep-Oct;12(5):360-369.
5. Kim DH, Rhim R, Li L, Martha J, Swaim B, Banco RJ, et al. Prospective study of iliac crest bone graft harvest site pain and morbidity. Spine J 2009 Jun 17.
6. Ebraheim NA, Elgafy H, Xu R. Bone-graft harvesting from iliac and fibular donor sites: techniques and complications. J Am Acad Orthop Surg 2001 May-Jun;9(3):210-218.
7. Khan SN, Cammisa FP, Jr., Sandhu HS, Diwan AD, Girardi FP, Lane JM. The biology of bone grafting. J Am Acad Orthop Surg 2005 Jan-Feb;13(1):77-86.
8. Sutherland AG, Raafat A, Yates P, Hutchison JD. Infection associated with the use of allograft bone from the north east Scotland Bone Bank. J Hosp Infect 1997 Mar;35(3):215-222.
9. Tomford WW. Transmission of disease through transplantation of musculoskeletal allografts. J Bone Joint Surg Am 1995 Nov;77(11):1742-1754.
10. Wheeler DL, Enneking WF. Allograft bone decreases in strength in vivo over time. Clin Orthop Relat Res 2005 Jun(435):36-42.
11. Keating JF, McQueen MM. Substitutes for autologous bone graft in orthopaedic trauma. J Bone Joint Surg Br 2001 Jan;83(1):3-8.
12. Cornell CN. Osteobiologics. Bull Hosp Jt Dis 2004;62(1-2):13-17.
13. Mulconrey DS, Bridwell KH, Flynn J, Cronen GA, Rose PS. Bone morphogenetic protein (RhBMP-2) as a substitute for iliac crest bone graft in multilevel adult spinal deformity surgery: minimum two-year evaluation of fusion. Spine 2008 Sep 15;33(20):2153-2159.
14. Bikram M, Fouletier-Dilling C, Hipp JA, Gannon F, Davis AR, Olmsted-Davis EA, et al. Endochondral bone formation from hydrogel carriers loaded with BMP2-transduced cells. Ann Biomed Eng 2007 May;35(5):796-807.

15. Hahn MS, McHale MK, Wang E, Schmedlen RH, West JL. Physiologic pulsatile flow bioreactor conditioning of poly(ethylene glycol)-based tissue engineered vascular grafts. Ann Biomed Eng 2007 Feb;35(2):190-200.
16. Hill RS, Cruise GM, Hager SR, Lamberti FV, Yu X, Garufis CL, et al. Immunoisolation of adult porcine islets for the treatment of diabetes mellitus. The use of photopolymerizable polyethylene glycol in the conformal coating of mass-isolated porcine islets. Ann N Y Acad Sci 1997 Dec 31;831:332-343.
17. Buxton AN, Zhu J, Marchant R, West JL, Yoo JU, Johnstone B. Design and characterization of poly(ethylene glycol) photopolymerizable semi-interpenetrating networks for chondrogenesis of human mesenchymal stem cells. Tissue Eng 2007 Oct;13(10):2549-2560.
18. Cruise GM, Scharp DS, Hubbell JA. Characterization of permeability and network structure of interfacially photopolymerized poly(ethylene glycol) diacrylate hydrogels. Biomaterials 1998 Jul;19(14):1287-1294.
19. Mann BK, Schmedlen RH, West JL. Tethered-TGF-beta increases extracellular matrix production of vascular smooth muscle cells. Biomaterials 2001 Mar;22(5):439-444.
20. Sawhney AS, Pathak CP, Hubbell JA. Modification of islet of langerhans surfaces with immunoprotective poly(ethylene glycol) coatings via interfacial photopolymerization. Biotechnol Bioeng 1994 Jul;44(3):383-386.
21. Gobin AS, West JL. Cell migration through defined, synthetic ECM analogs. FASEB J 2002 May;16(7):751-753.
22. Lee SH, Miller JS, Moon JJ, West JL. Proteolytically degradable hydrogels with a fluorogenic substrate for studies of cellular proteolytic activity and migration. Biotechnol Prog 2005 Nov-Dec;21(6):1736-1741.
23. Hill PA. Bone remodelling. Br J Orthod 1998 May;25(2):101-107.
24. Vaananen HK, Zhao H, Mulari M, Halleen JM. The cell biology of osteoclast function. J Cell Sci 2000 Feb;113 (Pt 3):377-381.
25. Nosaka AY, Kanaori K, Teno N, Togame H, Inaoka T, Takai M, et al. Conformational studies on the specific cleavage site of Type I collagen (alpha-1) fragment (157-192) by cathepsins K and L by proton NMR spectroscopy. Bioorg Med Chem 1999 Feb;7(2):375-379.
26. Lecaille F, Bromme D, Lalmanach G. Biochemical properties and regulation of cathepsin K activity. Biochimie 2008 Feb;90(2):208-226.
27. Hahn MS, Taite LJ, Moon JJ, Rowland MC, Ruffino KA, West JL. Photolithographic patterning of polyethylene glycol hydrogels. Biomaterials 2006 Apr;27(12):2519-2524.
28. Collin-Osdoby P, Yu X, Zheng H, Osdoby P. RANKL-mediated osteoclast formation from murine RAW 264.7 cells. Methods Mol Med 2003;80:153-166.

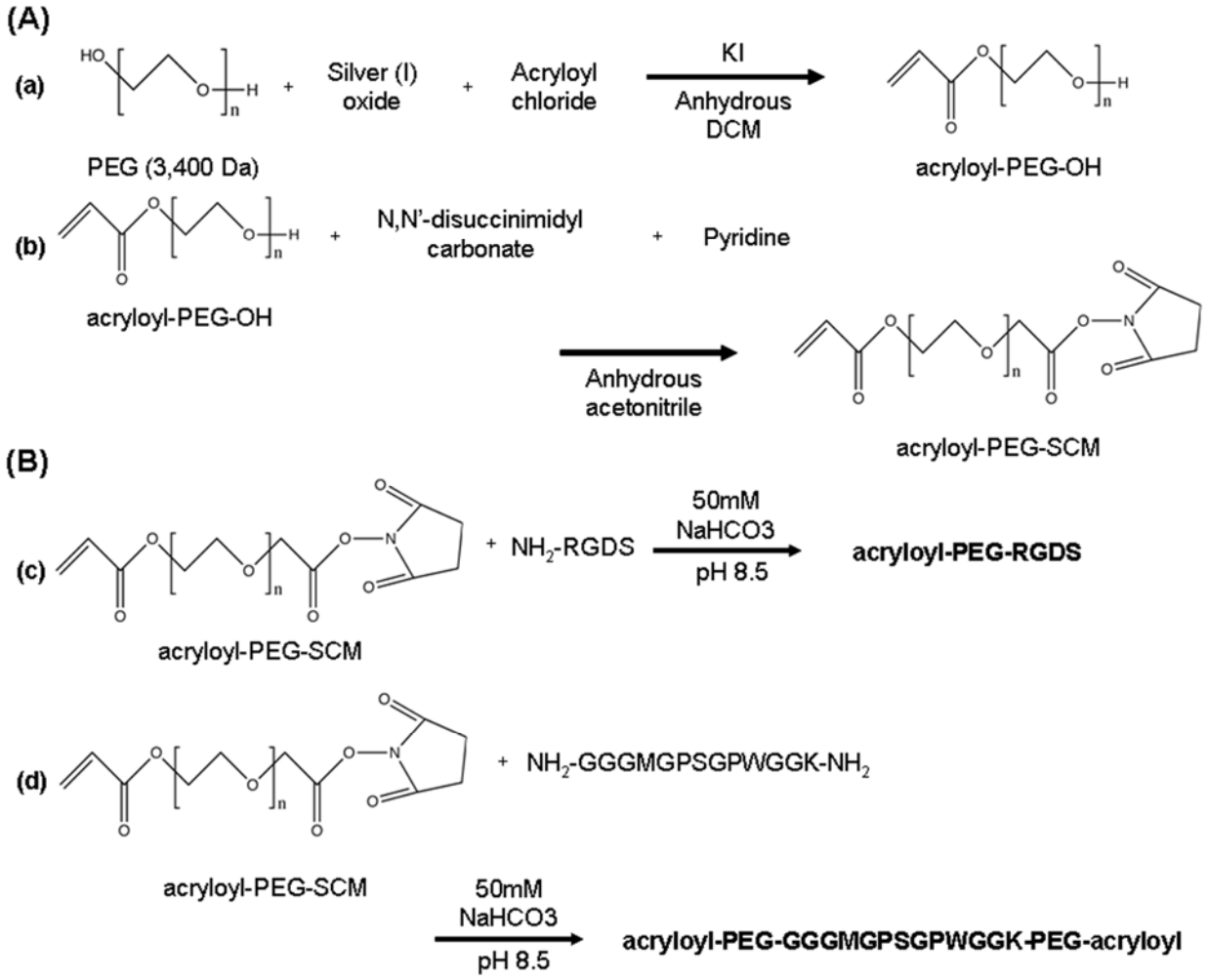

Scheme 1. (A) Synthesis of acryloyl-PEG-succinimidyl carbonate (acryloyl-PEG-SCM) and (B) modification of PEG derivatives. 3,400 Da PEG was first proceeded with (a) monoacrylation to produce acryloyl-PEG-OH. Monoacrylated PEG was then reacted with N,N'-disuccinimidyl carbonate to produce acryloyl-PEG-SCM (b). Acryloyl-PEG-SCM was then reacted with adhesive ligand RGDS to form acryloyl-PEG-RGDS (c) or reacted with cathepsin K-sensitive peptide GGGMGPSGPWGGK to form crosslinkable cathepsin K sensitive GPSG polymer (d).

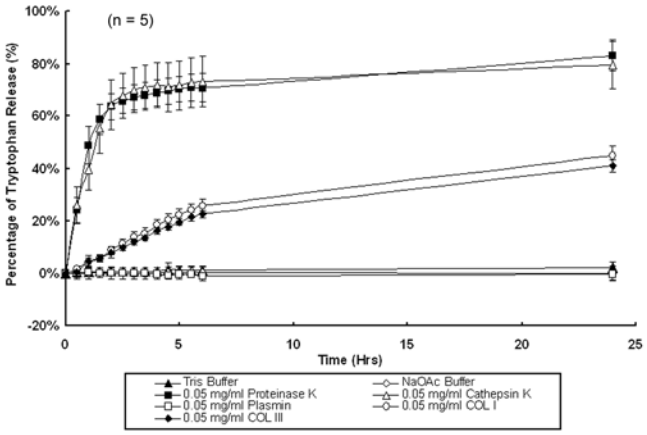

Figure 1. Degradation profiles of cathepsin K-sensitive GPSG hydrogels. Hydrogel droplets (3 μl) were polymerized in each micro-cuvette and swelled overnight with 250 μl of TBS buffer. Each hydrogel was incubated in buffer or enzyme solution at 0.05 mg/ml at 37^{O}C. UV absorbance at 280 nm was measured over 24 hours to monitor tryptophan release corresponding to the degradation of the GPSP hydrogels.

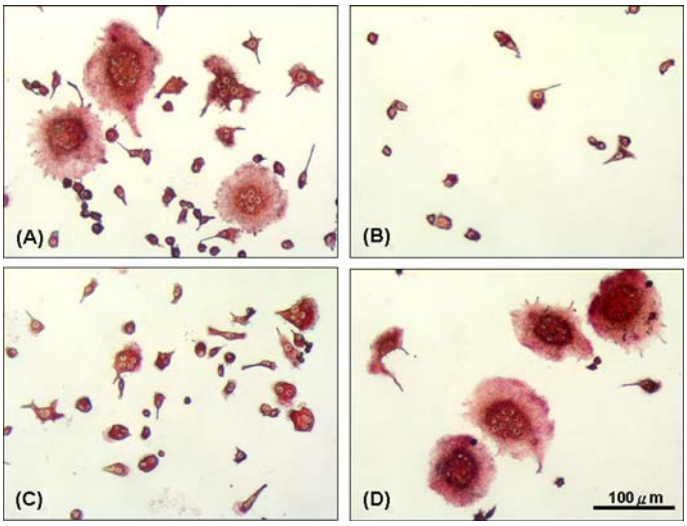

Figure 2. Isolated TRAP-positive dRAW264.7 osteoclasts by serum gradient. After differentiation in medium containing 30 ng/ml RANKL for 4 days, dRAW264.7 cells were combined with mono- and multi-nuclear cells (Figure 2A). After separation by serum gradient, the top fraction contained most of the mononuclear cells. The middle fraction of the gradient contained mixed groups of mononuclear and multinuclear cells. The majority of cells at the bottom fraction were multinuclear cells, which contained a very small portion of mononuclear cells (Figure 2B to D). The multinuclear cells collected at the bottom fraction were also stained TRAP positive, which indicted that they were activated osteoclasts. The bottom fraction of TRAP+ dRAW 264.7 osteoclasts were then used for hydrogel degradation studies.

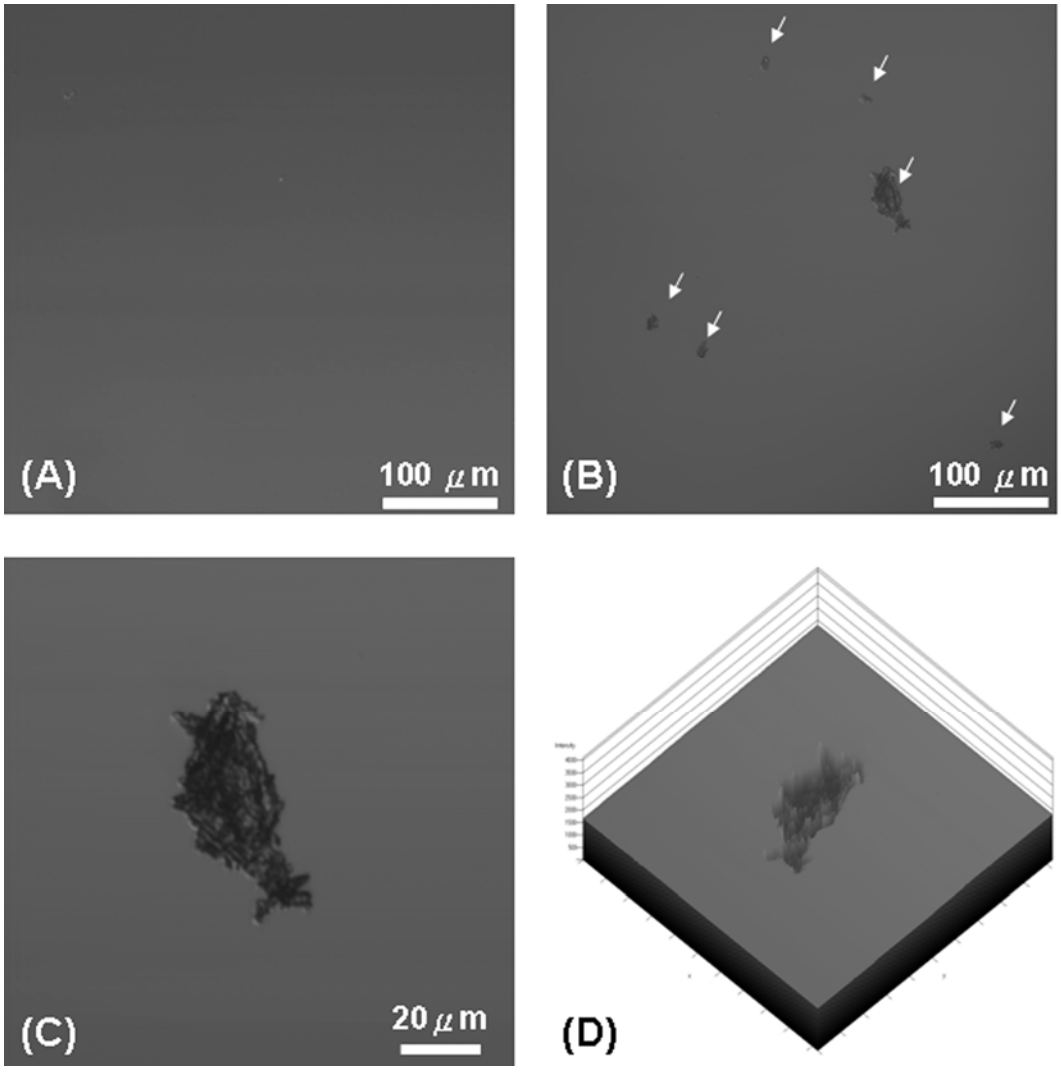

Figure 3. Differential interference contrast (DIC) images of GPSG hydrogel surfaces seeded with (A) dMC3T3-E1 osteoblasts and (B) dRAW264.7 osteoclasts. Cells were seeded on the hydrogels and cultured for 48 hours. Cells were detached with 20 mM EDTA and DIC images were obtained on a LSM LIVE 5 confocal microscope. No features were observed on gel surfaces seeded with osteoblasts (A). On the gel surface seeded with osteoclasts (B), several features can be identified after cells were detached. (C) and (D) show an enlarged image and an intensity profile of the feature, which suggests that the features on the surface were depressions.

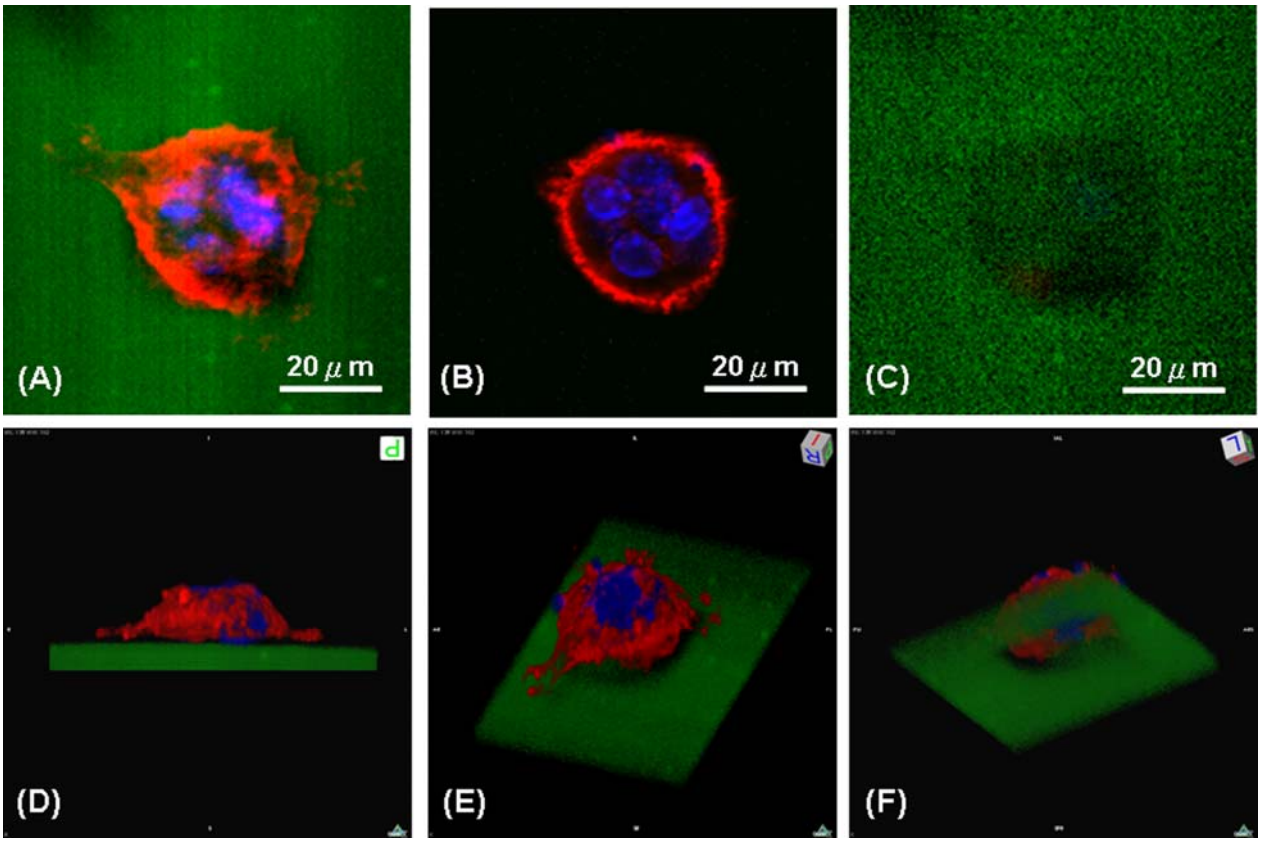

Figure 4. Three-dimensional fluorescent image reconstruction of an active osteoclast on the GPSG hydrogel surface. The GPSG hydrogel was labeled with Alexafluor 680 fluorophore (green), which is conjugated with the acryloyl-PEG-RGDS and incorporated into the hydrogel by photo-polymerization. The cells were fixed and permeabilized before staining the nuclei with DAPI (blue) and F-actin by rhodamine phalloidin (red) 48 hours after seeding. (A) Composed z-stack images of the osteoclast and hydrogel. (B) Sealing ring and multiple nuclei of the osteoclast. (C) GPSG hydrogel with fluorescent signal lost at middle. Z-stack Images were reconstructed using the volume renderings algorithm and presented from (D) side view, (E) orthogonal view from above, and (F) from bottom. The resorption site is located underneath the osteoclast, which was can be observed in the loss of the fluorescent intensity of Alexafluor 680. The resorption pit on the hydrogel surface can be clearly seen from different angles, suggesting that the GPSG hydrogel has been degraded by cathepsin K secreted by osteoclasts.

Hydrogel microsphere encapuslation of a cell based gene therapy system, increases cell survival, transgene expression, and bone volume in a model of heterotopic ossification.

Ronke M. Olabisi[1], Zawaunyka Lazard[2], Mary Hall[3], Eva Sevick[3], John A Hipp[4], Alan R. Davis[2,4,5], Elizabeth A. Olmsted-Davis[2,4,5] and Jennifer L. West[1]

[1]Department of Bioengineering, Rice University, 6500 Main St. MS 144, Houston, TX 77030, USA;

[2]Center for Cell and Gene Therapy, Baylor College of Medicine, Houston, TX 77030, USA;

[3]Center for Molecular Imaging, The University of Texas Health Science Center, Houston, TX, 77030, USA

[4]Department of Orthopaedic Surgery, Baylor College of Medicine, Houston, TX 77030, USA;

and the [5]Department of Pediatrics, Baylor College of Medicine, Houston, TX 77030, USA

Abstract

Bone morphogenetic proteins are widely known for their osteoinductive activity; however, harnessing this capacity is still a high-priority research focus. Here we present a novel technology for the delivery of high levels of BMP-2, at a targeted location, for rapid endochondral bone formation. This system enhances our previously described cell based gene therapy system by micro-encapsulating adenovirus transduced cells in non-degradable poly(ethylene glycol) diacrylate (PEGDA) hydrogels prior to intramuscular delivery. *In vitro* studies to measure BMP-2 secretion, specific- activity, and cell viability showed that AdBMP2-transduced cells in monolayer culture were similar to those derived from the same number of these transduced-cells encapsulated into a microsphere structure, suggesting that the polymer did not adversely affect the gene therapy system. Furthermore, *in vivo* studies showed a significant increase in the length of transgene expression after microencapsulation when compared to the un-encapsulated cells. In addition, when comparable numbers of transduced cells were intramuscularly injected into mice, the resultant heterotopic bone formation showed an approximate two-fold greater volume than the un-encapsulated cells. The data suggests that microencapsulation prolongs BMP-2 expression and appears to spread the delivery of the protein over a greater area of tissue, resulting in a significant increase in the region of heterotopic ossification. Histological analysis of the resultant bone formation shows new bone forming directly around the encapsulated cells, compared to a very dense and significantly smaller region for the directly injected cells, suggesting that the material can be used to form bone of a specific size and shape. Thus, incorporation of the PEG-DA hydrogel microspheres significantly advances current gene therapy

approaches for bone repair, particularly in scenarios of substantial traumatic injury.

Introduction

Although bone possesses the capacity to repair major insults due to traumatic injury, degeneration or disease often requires surgical intervention and bone grafting[1-3]. In the United States, approximately 550,000 million fractures annually require bone grafting[4]. This number does not include the millions of total joint arthroplasties, spinal arthrodeses, maxillofacial surgeries and implant fixations that require bone replacement or repair[5]. In an effort to circumvent the obstacles associated with grafts, researchers have used osteoinductive growth factors, such as BMPs[6, 7]. BMP2 possesses the ability to induce heterotopic ossification or *de novo* bone formation at targeted locations and was recently approved by the FDA for use in spinal arthrodesis.

However, many clinicians have found recombinant BMP-2 to have inconsistent efficacy, especially in complex clinical scenarios such as traumatic injury[8-11]. These findings have led to a renewed emphasis to develop better methods of delivering BMP-2[12]. BMPs are rapidly cleared when administered in solution, reducing their efficacy and requiring large doses to attain a therapeutic effect[7]. This BMP clearance necessitates a carrier that can retain and sequester BMPs, such as collagen[6, 7]. There is some degree of natural binding affinity that BMPs have for collagen, which has led to the use of collagen sponges as the BMP carrier of choice in the clinical setting[4, 7, 12]. Unfortunately, collagen poses problems of its own. As a natural substance, it can elicit an immune response[7, 13]. Furthermore, collagen presents handling difficulties, does not maintain a stable form, and use of a collagen sponge reduces the bioavailability of BMP to such a degree that large amounts are necessary for a therapeutic response[6, 7, 13, 14]. Given these drawbacks, the search for alternative carrier materials that are biocompatible, biodegradable, osteoinductive and osteoconductive are of the utmost importance. [7, 15].

Here we present a novel system in which poly(ethylene glycol) diacrylate (PEGDA) hydrogels encapsulate cells that produce and secrete high levels of BMP-2. Hydrogels are insoluble networks of polymer chains that swell in aqueous solutions. PEGDA hydrogels are widely used in tissue engineering applications because they are bioinert and mimic many physical properties of the extra-cellular matrix of soft tissues[6, 16]. Physical characteristics of hydrogels such as stiffness and permeability can be designed to better approximate a tissue of interest, to regulate nutrient/waste diffusion, or to prevent interaction with immune cells[6, 16]. Because of the immunoprotection they provide, hydrogels are also widely used for cell encapsulation[6, 16, 17]. Previous attempts to encapsulate our cell based gene therapy system into a single large structure resulted in a significant decrease in BMP-2 expression as compared to that obtained from the un-encapsulated cells[6]. Concommitent with that was a decrease in the resulting bone formation. The current system retains high-level BMP-2 expression from AdBMP2 transduced cells after their encapsulation in PEGDA hydrogel microspheres. The encapsulation of this cell therapy

system into these structures actually provides enhanced BMP-2 expression in the aggregate *in vivo* when compared to direct injection of cells. Further, gene expression is spatially controlled by encapsulating the cells in PEGDA hydrogel microspheres, and restricts rapid immune clearance of these delivery cells. Thus, per cell number injected, more host tissue was actually involved in heterotopic ossification, suggesting that inclusion of the hydrogel enhanced the efficacy of our cell therapy system. The resultant osteogenesis showed a pattern of heterotopic bone formation surrounding the microspheres in an integrated structure, suggesting that inclusion of the biomaterial would enable patterning and specified placement of the new bone formation when compared to directly injected cells, without reducing the efficacy of the BMP-2. The data shows the potential of enhancing the osteoinductive capacity of current BMP-2 therapy approaches by encapsulation within a PEGDA hydrogel: both in regenerating large volumes of tissues and in shaping the size and structure the bone produced, essential for cranial facial reconstruction.

Methods

Cell Culture

Human diploid fetal lung fibroblasts (MRC-5) were obtained from the American Type Culture Collection (ATCC; Manassas, VA) and propagated in a humidified incubator at 37°C and 5% CO_2 in Dulbecco's Modified Eagle's Medium (DMEM; Sigma, St. Louis, MO) supplemented with 10% fetal bovine serum (FBS; HyClone, Logan, UT), 1000 U/L penicillin, 100 mg/L streptomycin, and 0.25 μg/ml amphotericin B (Invitrogen Life Technologies, Gaithersburg, MD), as previously described[18]. Murine bone marrow stromal cells (W20-17; a gift from Genetics Institute, Cambridge, MA) were propagated and maintained as described by Thies et al.[19].

Adenoviruses and cell transduction

Adenoviruses: Replication defective E1-E3 deleted first generation human type 5 adenovirus (Ad5) were constructed to contain cDNAs for BMP2 in the E1 region of the virus[18]. Replication defective human adenovirus type 35 fiber (Ad5F35) were constructed to contain cDNAs for BMP2 in the E1 region of the virus[20]. For the viruses Ad5BMP2, Ad5dsRED, and Ad5empty cassette the viral particle (VP)-to-plaque-forming unit (PFU) ratios were 1:83, 2, and 111 respectively, and all viruses were confirmed to be negative for replication-competent adenovirus. MRC-5 cells were transduced as previously described with Ad5BMP2, Ad5dsRED or Ad5empty cassette at a viral concentration of 2500 VP/cell[18,21]. Briefly, virus was added to fresh supplemented DMEM and incubated with cells at 37°C overnight.

Microencapsulation

Hydrogel precursor solutions were formed by combining by 0.1 g/ml 10 kDa PEGDA (10% w/v) with 1.5% (v/v) triethanolamine/HEPES buffered saline (HBS, pH 7.4), 37 mM 1-vinyl-2-pyrrolidinone, 0.1 mM eosin Y, and transuduced MRC-5 cells for a final concentration of 6×10^4 cells/µl. Acetophenone was combined in 1-vinyl-2-pyrrolidinone at a concentration of 300 mg/ml. The acetephenone was then added to mineral oil at 3 µl/ml and mixed well. The microspheres were formed after adding the hydrogel precursor solution into the mineral oil, emulsifying by vortex for 2 s while continuously exposing to white light for an additional 20 s. Microspheres were isolated by two series of media washes and centrifugation at 1350 rpm. Cells and microspheres were quantified by measuring the amount of soluble formazan produced by cellular reduction of the tetrazolium compound [3-(4,5-dimethylthiazol-2-yl)-5-(3-carboxymethoxyphenyl)-2-(4-sulfophenyl)-2H-tetrazolium, inner salt; MTS]. Briefly, cells were counted with a coulter counter and a serial dilution was used as a standard curve. Microsphere and cell samples were plated in a 24-well plate with 1 ml of culture medium and 200 µl of CellTiter 96® AQueous One Solution Reagent was added into each well of the plate. The plate was incubated for 1 hour at 37°C in a humidified, 5% CO_2 atmosphere and then the absorbance was recorded at 490 nm in a plate reader. These microspheres were stable following intramuscular injection, as determined by retrieval of the microspheres post-injection to confirm that the majority of the microspheres remained intact. Further, to ensure proper comparisons between the microspheres and the monolayer cells we measured the loss of cells following the encapsulation procedure and loss in the injection needle. Approximately 80 % cell loss occurs during encapsulation and injection (Figure 1A), which is accounted for and equalized between groups prior to injection.

Preparation of cells for intramuscular injection

Cells transduced with Ad5BMP2, Ad5dsRED, Ad5empty cassette were removed with trypsin, and separated into two groups: one for direct injection and one for injection following microencapsulation. Cells directly injected were suspended at a concentration of 5×10^6 cells per 100 µl of PBS and aspirated into a syringe with a 22 gauge needle. Microencapsulated cells were encapsulated at a concentration of 5×10^6 cells per 300 µl of microspheres, which were in turn suspended in 1 ml of PBS and aspirated into a syringe with an 18 gauge needle. The greater volume of PBS and lower needle gauge enables the aspiration and injection of the microspheres, which would otherwise clog the needles.

Viability assays

Cells were evaluated for their viability following microencapsulation. MRC-5 cells were transduced with Ad5F35BMP2, harvested and encapsulated in microspheres as described. One week after microencapsulation, microspheres were incubated with media and 2 μM calcein acetoxymethyl ester (calcein AM, Invitrogen, Inc.) for 20 min in a 37°C in a humidified, 5% CO_2 incubator. Microspheres were imaged under a confocal microscope (ex/em ~495 nm/~515 nm).

BMP-2 Quantification

BMP-2 expression was evaluated for MRC-5 cells transduced with Ad5F35BMP2 or Ad5F35HM4 using ELISA and alkaline phosphatase (AP) assays. ELISA assays were performed with a BMP-2 Quantikine ELISA kit from R&D Sys-tems (Minneapolis, MN) using culture supernatant collected 72 hours after adenovirus transduction. Transduced cells were microencapsulated or plated directly in 0.4 μm pore polycarbonate membrane transwell inserts (Corning Inc., Lowell, MA) and W20-17 cells were cultured in the wells of 6 well plates. After 72 hours W20-17 cells were assayed for AP activity using a chemiluminescence procedure[20]. Cellular AP was extracted by conducting three freeze-thaw cycles on the W20-17 cells in a 100-μM/cm^2 concentration of 25 mM Tris-HCl (pH 8.0) and 0.5% Triton X-100. Then a ready to use chemiluminescent substrate disodium 3-(4-methoxyspiro{1,2-dioxetane-3,2-(5-chloro)tricyclo[3.3.1.$1^{3,7}$]decan}-4-yl) phenyl phosphate (CSPD) substrate with Sapphire-II enhancer (Tropix; Applied Biosystems, Foster City, CA) was added to the samples for enhanced AP sensitivity. The light output after a 2 sec delay was integrated from each sample for 10 sec with a luminometer (TD-20/20; Turner BioSystems, Sunnyvale, CA). AP levels were recorded in relative luminescence units (RLU). These AP levels were then normalized to protein content with the bicinchoninic acid (BCA) assay with bovine serum albumin as the standard curve. Data are presented as percent AP induction relative to that of basal control cells not exposed to BMP-2. Statistical analysis was performed as described previously[18]. Briefly, all data were taken in triplicate and reported as mean and standard deviation. A Student t test with 95% confidence interval ($p < 0.05$) was done between the untreated control and each experimental condition.

Live animal optical fluorescence imaging.

Mice were imaged longitudinally for approximately one month post-injection of microencapsulated or un-encapsulated fibroblasts transduced with AddsRED (2500 vp/cell).

Fluorescent imaging was performed at excitation and emission wavelengths of 568 nm and 590 ±10 nm, respectively. The excitation light was supplied by a 200 W Argon/Krypton laser and the emission light was collected by passing through holographic and bandpass filters and focused onto an electron-modulated charge-coupled device (EMCCD) camera using a Nikkon camera lens. Exposure times were approximately 200 ms. Image analysis was performed using ImageJ software. Fluorescence intensity (FI) was measured and recorded for a region of interest (ROI) for each site of the animal injected with cells. The ROI dimensions were kept constant for every site imaged and each ROI was chosen to include the optimal fluorescent signal for the given site. A target to background ratio (TBR) of FI was calculated for each site by subtracting a background (B) ROI from the target (T) ROI, and then dividing the result by the background (B) ROI; TBR = (T-B)/B. The TBR value was plotted versus time (i.e., day post-injection of cells). Results represent the mean TBR of FI for unencapsulated and/or encapsulated AddsRed or Adempty cassette transduced cells (n=4 per group). Statistical analyses were performed using the Student's t-Test, unpaired.

Heterotopic bone assay

Microencapsulated or unencapsulated cells were collected in syringes then delivered by intramuscular injection into the hind limb quadriceps muscle of nonobese diabetic/severely compromised immunodeficient (NOD/SCID) female mice (8–12 weeks old; Charles River Laboratories; Wilmington, MA) (n = 6). Animals were euthanized two weeks after injection of the transduced cells. Hind limbs were harvested and placed in formalin. All animal studies performed were in accordance with an Institutional Animal Care and Use Committee (IACUC) approved protocol.

Histological analysis

Harvested mouse hind limbs were fixed in formalin and decalcified. Hind limbs were then divided longitudinally and sectioned from the inner surface outward. Serial sections (5 μm) encompassing the entire hind limb reactive site were prepared (approximately 15-30 sections per tissue specimen). Every fifth slide was stained with hematoxylin and eosin to locate the region of interest. All tissue images presented in this report are representative of the other tissues isolated within the groups. All sections were analyzed by light microscopy.

Microcomputed tomography

Micro-CT exams were obtained of the left and right legs at 15 μmresolution (eXplore Locus SP; GE Healthcare, London, ON, Canada). A hydroxyapatite phantom was scanned alongside each specimen and was used to convert the scan data from arbitrary units to units of equivalent bone

density. A 3D region-of-interest was defined for each specimen to isolate the new mineralized tissue from the normal skeletal structures (femur, tibia, patella). The scans were thresholded to exclude any tissue with a density less than 100 mg/cc, and the tissue volume within the region of interest was calculated as a measure of the total amount of mineralized tissue. The tissue mineral content was measured as an estimate of the total mineral in the region and the tissue density was calculated to quantify the density of the mineralized tissue. The resulting data were analyzed by one-way analysis of variance to identify any differences between the un-encapsulated and microencapsulated cells.

Results

Validation of the microsphere's containing AdBMP2 transduced cells.

High levels of BMP-2 can lead to rapid heterotopic ossification in both animal models and humans[8, 18, 22]. We previously demonstrated the rapid clearance of our AdBMP2 transduced cells within the murine models[18, 23], thus limiting both the levels of BMP-2 that can be achieved locally as well as length of time the tissues receive an inductive signal. To circumvent this limitation, we encapsulated the transduced cells within PEGDA hydrogel microspheres. In order to ensure that the cells tolerated encapsulation and that BMP-2 could freely diffuse out of the material; cells were microencapsulated and then stained using a Live/Dead cytotoxicity assay to determine the number and extent of viable cells within the PEGDA hydrogel microspheres. With this method, live cells enzymatically convert non-fluorescent calcein acetoxymethyl (calcein AM) into fluorescent calcein, while an ethidium homodimer compound enters dead cells through damaged membranes and binds DNA to emit red fluoresence (Figure 1). As seen in Figure 1, cells that had been encapsulated within PEGDA microspheres and placed in culture for seven days, showed high viability, 95.08% ± 0.47%, suggesting that microencapsulation process was not leading to cell death.

The level of BMP-2 in the culture supernatant was then measured to determine if the protein could adequately diffuse from the microspheres. Equivalent numbers of cells were transduced with AdBMP2 or AdEmpty cassette (2500 vp/cell) and either placed in culture directly, or after microencapsulation in PEGDA microspheres. Culture supernatant was removed 72 hours later, and BMP-2 and its activity within the supernatants were quantified (Figure 2). BMP-2 levels were quantified by ELISA and found to be approximately 17,500 pg/ml and 15,000 pg/ml of culture supernatant for directly plated and microencapsulated cells, respectively. No BMP-2 was detected in either culture supernatant from Adempty cassette transduced cells, or control cells which had no additions. In larger bead structures, we observed a significant drop in the

level of BMP-2 as compared to equivalent numbers of cells either directly plated or in microspheres (data not shown). The data suggests that optimal BMP-2 production and secretion is achieved when cells are encapsulated into the smaller microsphere structures. Further, the data shows that the PEG-DA hydrogel material is not affecting the production, secretion or diffusion of BMP-2 within the microspheres (figure 2A).

We next assayed BMP-2 activity in the culture supernatant to confirm that the protein that diffused through the PEGDA hydrogel possessed similar specific activity as BMP-2 in culture supernatant from cells directly plated. The release of proteins from hydrogels is related both to diffusion distances and the hydrogel mesh size, both of which change with swelling[24]. The hydrogels in the current study were formed with 10% 10 kDa PEGDA, which has been estimated to have a mesh size of 280 Å. Proteins having radii smaller than the hydrogel mesh size enjoy relatively free diffusion through the polymer[25]. Mature BMP-2 is a small protein (approximately 16 kDa) and it has been suggested that it dimerizes immediately after synthesis. The biologically active form of BMP-2 is a homodimer whose dimensions are 70 Å × 35 Å × 30 Å[26]. Thus, BMP should pass freely through the microshperes. To confirm this result and ensure that the PEG-DA hydrogel microspheres were not selecting for a less active form of BMP-2, culture supernatants were tested in a cell based functional assay. Culture supernatants were tested, using the murine bone marrow stromal cell line, W20-17 cells, which have previously been shown to respond to functional BMP-2 by undergoing osteogenesis with a rapid increase in alkaline phosphatase (AP)[19]. W20-17 cells were exposed for 72 hours to a portion of the culture supernatants used for BMP-2 quantification and then cells were lysed for quantification of alkaline phosphatase (AP) activity (figure 2B). Both the culture supernatants from cells directly plated and encapsulated in microspheres led to significant elevation in alkaline phosphatase over the cells with no additions, suggesting the BMP-2 is functionally active. Further, culture supernatant from cells which had been transduced with Adempty cassette did not elevate alkaline phosphatase significantly above the W20-17 cells with no additions (figure 2B). The data collectively suggest that microencapsulation of the cells in PEG-DA hydrogel does not significantly reduce the level of functional BMP-2 produced after transduction of the cells with AdBMP2.

In vivo comparison of transgene expression with and without encapsulation in PEG-DA hydrogel. To determine if the microencapsulation would prevent rapid clearance of the transduced cells and ultimately extend transgene expression, cells were transduced with an adenovirus possessing the reporter gene dsRED or an empty cassette control virus. This adenovirus was similar to the AdBMP2 virus; accept that it possessed a dsRED cassette in place of the BMP-2, and cells were transduced in a similar manner. Cells (5×10^7) were transduced

with AddsRED (5000 vp/cell) and remained as a monolayer, or microencapsulated into microspheres, and 24 hours later directly injected into the muscle of the mouse hindlimb. As a control, 5 x 10^7 cells were transduced with Adempty cassette virus (5000 vp/cell) and the encapsulated into microspheres and similarly injected into mouse hindlimbs (n=4). Reporter expression within the tissues was then followed by live animal imaging for 2 to 34 days Fluorescent imaging was performed at excitation and emission wavelengths of 568 nm and 590 +10 nm, respectively (figure 3). The excitation light was supplied by a 200 W Argon/Krypton laser and data were quantified and reported as a target to background ratio, where the specific signal was normalized to any background or autofluorescence.

Two days after the initial injection of cells, dsRED expression was readily detected whether cells were encapsulated or not and in no cases were cells or microspheres detected migrating from the injection site. Because solution spread is a function of injection volume[27, 28], dsRED expression in the tissues receiving the microspheres encompasses a larger volume than the encapsulated counterpart (Figure 3A). However, the magnitude of expression should not be affected by injection volume and dsRED expression was significantly elevated in microencapsulated cells compared to directly injected cells (Figure 3B), suggesting that the directly injected cells may already be starting to be cleared from the tissues. Reporter expression in animals receiving AdBMP2 transduced cells directly injected was substantially reduced after seven days and was indistinguishable from control (Figure 3B). This result was similar to our previous findings where the delivery cells are rapidly cleared[18]. In contrast, the microencapsulated cells continued to be significantly elevated over background (Figure 3B). This was not due to autofluorescence of PEGDA indicated by the absence of signal at 590 $\pm$10 nm in microencapsulated control cells. This 590 $\pm$10 nm dsRED fluorescent signal was significantly elevated over that of microencapsulated cells transduced with Adempty cassette for 15 days (Figure 3B). After 15 days, these levels dropped; however, signal was still detectable (Figure 3A, arrows) in some animals, suggesting that the microencapsulated cells remained viable to express the dsRED transgene. Collectively, the data suggest that microencapsulation prolongs transgene expression within the tissues.

In vivo bone formation with and without microencapsulation in PEGDA hydrogels.

PEGDA microspheres encapsulating AdBMP2 transduced cells were next tested *in vivo* to determine whether prolonged BMP-2 expression could enhance heterotopic bone formation. As with the live animal imaging, similar numbers of AdBMP2 transduced cells were either directly or following microencapsulation injected into the muscle in mouse hindlimb and the resulting

heterotopic ossification was analyzed. MicroCT analysis of the resulting bone showed a significantly greater region or volume of heterotopic ossification in tissues receiving microspheres (Figure 4A, C) than those receiving directly injected cells (Figure 4B, D). Quantification of the groups (n=6) enabled direct comparison. Cross sectional microCT analysis of the newly formed bone revealed a similar architecture between the two samples. Heterotopic bone formed by both the microspheres, and the directly injected cells had a pattern of dense bone surrounding a hollow interior (Figures 4C and D); however the circumference of bone within the directly injected cells was significantly smaller.

Microencapsulated AdBMP2 transduced cells resulted in approximately twice the bone volume produced when these cells were directly injected (Figure 5B). However, the bone tissue mineral content or mass of the new bone although trending towards an elevation in samples that received the microspheres, was statistically similar between these groups (Figure 5A). Most likely the lack of statistical significance results from the change in tissue mineral density of the new bone (figure 5C). It appears to be slightly less dense, leading to the overall similarity in mass. Interestingly, the less dense bone obtained from the microspheres, may in part be related to the fact that the microspheres have spread out the area of BMP2 release over a greater volume, and thus effectively diluted the concentration of BMP2 in any given area.

To further analyze the newly formed bone, tissues were processed, paraffin embedded and the new bone was visualized by hematoxylin and eosin staining. Both groups had significant new bone formation within the muscle (Figure 6). In tissues that had received the direct injection of AdBMP2 transduced cells there was a small compact piece of bone forming a ring-like structure encircling what appears to be blood and tentative stroma, and just exterior to this structure was significant adipose (Figure 6A). A similar structure was observed in tissues that had received microspheres (Figure 6B). Since the microspheres do not degrade over time, they appear histologically as gaps or holes within the matrix (Figure 6B). Thus, despite the presence of nondegradable microspheres, both structures were patterned to have a denser bone structure with a bone marrow like cavity on the interior.

Discusson

Here we present a novel system for the sustained production and release of BMP2 in a targeted manner. This approach expands on our previously reported cell based gene therapy system, which successfully employs adenovirus transduction of fibroblasts to express high levels of BMP-2 at a targeted location[6, 18, 23]. Because the transduced cells are rapidly cleared within 7 days after injection, PEGDA was utilized as a carrier that would prolong the expression of the BMP-2 within the tissues. We previously implanted AdBMP2 transduced cells in macroencapsulated in

larger hydrogel beads to demonstrate that cells entrapped within PEGDA hydrogels could continue to produce bone[6]. In this study, we demonstrate that microencapsulated cells survive the process, continue to express BMP-2 and produce more bone volume than nonencapsulated cells. Microencapsulation permits delivery via injection, avoiding surgery. Furthermore, PEGDA hydrogels are unique as carriers for bone regeneration.

PEGDA is a synthetic polymer that is highly hydrophilic, hence resistant to protein adsorption and cell adhesion and is therefore non-immunogenic and highly biocompatible[6, 29]. Due to these properties, PEGDA hydrogels are widely used in tissue engineering applications because they are FDA approved for oral, dermal and intravenous applications, they are bioinert and they can be tuned to mimic many physical properties of the extra-cellular matrix of soft tissues, such as stiffness and permeability[6, 30, 31]. Careful manipulation of these physical characteristics enable PEGDA hydrogels to better approximate a tissue of interest, to regulate nutrient/waste diffusion, or to prevent interaction with immune cells[6, 16]. Current carriers in clinical use, such as collagen sponges, do not retain BMP-2 efficiently, require large amounts of recombinant BMP-2 for a therapeutic effect, and are often plagued with variability, such as differences in handling, material properties and in some cases triggering immunogenic responses[6, 7, 13, 14]. Furthermore, because collagen can bind BMP2, our previous studies (Gugala et al Biomaterials 28(2007) 4469-4479) suggest that it reduced the efficacy of BMP2 in general. Additionally the inflammation associated with the collagen sponge can also reduce the ability to produce targeted bone formation.

Our approach avoids these issues because we use a synthetic polymer for microencapsulation, which minimizes immune reponse to the polymer and does not bind BMP2. In addition our approach is independent of cell line, permitting the transduction of any type of cell[32], and with efficient transduction can deliver functional BMP2 continually to the target site, over several days. Furthermore, we are able to get high transduction efficiencies, requiring a modest quantity of cells and microspheres for a therapeutic effect; for instance, in our current system we injected 300 µl of microspheres containing 2 million cells.

The millimeter scale beads employed in our previous study were a proof of concept and exceeded the 250 µm diffusion limit beyond which cell death is inevitable[6]. As a result BMP-2 culture supernatant levels were significantly reduced in the beads compared to monolayer[6]. The radii of the microspheres in this study were roughly in the 50 - 150 µm range, well under the diffusion limit. Given the same volume of PEGDA carrier, when cells were: 1) encapsulated in a single hydrogel; 2) equally divided into four hydrogels or 3) microencapsulated, the greatest amount of detectable BMP-2 in the culture supernatant came from the microspheres, which released identical levels as the monolayer (data not shown). In addition, encapsulated cells fared as well as cells in monolayer with a 95 % viability after seven days within the microspheres.

While *in vitro* cell survival between encapsulated and unencapsulated cells was comparable, *in vivo* cells protected within microspheres fared better than the directly injected counterparts. The duration of the dsRED fluorescence emitted from the microencapsulated cells demonstrates that microspheres are resistant to clearance and migration. Furthermore, microencapsulation does not interfere with the expression of the BMP2 transgene. Cells in both monolayer and microspheres were able to make identical levels of functional protein. Since bone formation occurred immediately surrounding the microspheres, the area of new bone formation could easily be defined by the volume of material delivered. This is not true for the directly injected cells that stay tightly clustered, and will reside in adipose regions that can easily be compressed to hold the additional volume. Thus exact spatial placement of the transduced cells, and resultant bone formation, is far less sensitive, and subject to other variables that may influence it, whereas, delivery of the microspheres, because of their structure, can fill large regions of the tissue, and produce bone of in a desired location and size. This is a critical parameter for implementation of the therapy to traumatic bone injury.

Interestingly, spreading out the region in which BMP2 is expressed through microsphere delivery resulted in a significant increase in the volume of bone, and decrease in bone density. We hypothesize that the decrease in density, is because the bone formation process overall was reduced, due to the lower concentration of BMP2 over the greater volume. In comparsion, the cells directly injected which sit as a cluster within the tissues would produce the same amount of BMP2 but in a much smaller volume, and resultant bone formation shows a small dense compact bone. Surprisingly, marrow-like structures formed in both the directly injected cells and the microencapsulated cells which were intriguing because in both cases the new structures possessed similar patterning to the normal skeleton. This indicates that despite the hydrogel's capacity to dictate the shape of the newly forming bone, it does not interfere with the structural patterning that is part of the biology of bone formation. However, any interference of the hydrogel in the final bone density can be overcome by using hydrogels that are degradable by enzymes produced during bone formation.

Conclusions

We present a system for targeted bone formation, in which our previously described ex vivo gene therapy system is encapsulated into PEGDA microspheres, t, allows for prolonged expression of the BMP2. Further the microspheres are moldable, and take up a specific volume, that allows for bone to form immediately adjacent to there location in the tissues. Thus, the combination of the BMP2 cell based gene therapy, and PEGDA microencapsulation provides a novel method for forming bone of specific shape and size. Further, it prevents an immune reaction, against the

material, and thus can provide a much longer window for expression of the BMP within the target site. Our system is the first of its kind to induce bone formation, and may impact gene therapy approaches to come.

Figure Legends

Figure 1. Viability of AdBMP2 transduced cells (2500 vp/cell) within microspheres was assessed at day 7 using a LIVE/DEAD® Viability/Cytotoxicity Kit for mammalian cells (Invitrogen, Molecular Probes, Eugene, OR). **A.** Live cells appear green, **B.** dead show red. **C.** Overlay of panels A and B. Living cells accounted for 95.08% ± 0.47% of total cells encapsulated.

Figure 2. Comparison of BMP2 expression, secretion and activity after PEGDA encapsulation. **A.** BMP2 protein in culture supernatant, taken from AdBMP2 or Adempty cassette transduced cells (25000 vp/cell) (monolayer) or those encapsulated in PEGDA microspheres was quantified daily over one week using an ELISA. **B.** Alkaline phosphatase activity in W20-17 cells after addition of conditioned media from AdBMP2 or Adempty cassette transduced cells (25000 vp/cell) (monolayer) or those encapsulated in PEGDA microspheres. As a negative control, we also included culture supernatant from untransduced cells. Alkaline phosphatase activity is depicted as the average relative chemiluminescences units (RLU) where n=3. Error bars represent means ± SD for n=3. A student t-test was applied to demonstrate significance and all the samples demonstrated significance at the confidence interval $p < 0.05$.

Figure 3. A. Optical fluorescence imaging of mice injected with cells expressing dsRed. Top panels (a through c) are images of a representative mouse (n=4) injected with dsRed-expressing cells encapsulated in microspheres and bottom panels (d through f) are of a mouse injected with dsRed-expressing cells directly, without microspheres. The images were taken at day 4, 12 and 29 post-injection of cells. By day 29, the fluorescent signal is at background levels or was undetectable for the mouse given dsRed-expressing cells without microspheres (f). Whereas, the signal remains detectable in the mouse given dsRed-expressing cells encapsulated in microspheres (c).

B. Mean Target-to-Background Ratio (TBR) of Fluorescence Intensity (FI) in mice given unencapsulated dsRed Cells, microencapsulated dsRed cells or microencapsulated control cells. * $p \leq 0.05$ for microencapsulated dsRed cells versus microencapsulated contol cells; † $p \leq 0.05$ for microencapsulated dsRed cells versus unencapsulated dsRed cells; ‡ $p \leq 0.05$ for unencapsulated

dsRed cells versus microencapsulated control cells.

Figure 4. Micro computational analysis of the resultant heterotopic bone formation. Top images (**A, B**) are 3D surface renderings of the resultant heterotopic bone, while bottom images (**C, D**) are cross-sectional slices through the new bone. Panels A, C show the resultant mineralization of the muscle tissues after injection of AdBMP2 transduced cells (2500 vp/cell) and encapsulation into PEGDA microspheres (**A, C**) and/or direct injection (**B, D**). Both have a denser rim of bone, with a hollow interior structure, suggesting that the biomaterial did not alter bone patterning.

Figure 5. Quantification of the heterotopic ossification using micro computational analysis. Cells were transduced with AdBMP2 and either directly injected or encapsulated into microspheres prior to injection, and the resultant heterotopic bone was analyzed two weeks later. Tissue parameters, **A.** Bone tissue mineral content; **B.** bone volume of mineralized tissue and ; **C.** Bone tissue mineral density were calculated for the newly formed bone (n=6 per group) and the means and standard deviations for each group calculated and compared to one using a one-way analysis of variance. Results indicate that mineral content is statistically equivalent ($p=0.2$) between the groups, whereas the microspheres had a significantly greater volume ($p=0.038$) than the AdBMP2 transduced cells directly injected. Alternatively, the bone tissue mineral density was significantly denser for the group receiving the cells directly as compared to the microspheres ($p=0.029$). Panel **D.** shows a 3D volume rendering of new bone formed in cell only and microencapsulated cells, respectively.

Figure 6. Photomicrographs of heterotopic ossificationHematoxylin and eosin stains of new bone formation. **A.** direct injection. **B.** Microsphere encapsulated cells. Both groups show small compact pieces of bone forming ring-like structures, encircling what appears to be blood and tentative stroma in the inner region, with significant adipose just exterior to the new bone. Scale bars are 500 μm.

1. Murugan, R. & Ramakrishna, S. Development of nanocomposites for bone grafting. *Composites Science and Technology* **65**, 2385-2406 (2005).
2. Srouji, S., Blumenfeld, I., Rachmiel, A. & Livne, E. Bone defect repair in rat tibia by TGF- 1 and IGF-1 released from hydrogel scaffold. *Cell and tissue banking* **5**, 223-230 (2004).
3. Yoneda, M. et al. Repair of an intercalated long bone defect with a synthetic biodegradable bone-inducing implant. *Biomaterials* **26**, 5145-5152 (2005).
4. Mussano, F., Ciccone, G., Ceccarelli, M., Baldi, I. & Bassi, F. Bone Morphogenetic Proteins and Bone Defects: A Systematic Review. *Spine* **32**, 824 (2007).
5. Mistry, A. & Mikos, A. Tissue engineering strategies for bone regeneration. *Advances in Biochemical Engineering Biotechnology* **94**, 1-22 (2005).
6. Bikram, M. et al. Endochondral Bone Formation from Hydrogel Carriers Loaded with BMP2-transduced Cells. *Annals of Biomedical Engineering* **35**, 796-807 (2007).
7. Lutolf, M. et al. Repair of bone defects using synthetic mimetics of collagenous extracellular matrices. *Nature Biotechnology* **21**, 513-518 (2003).
8. Bishop, G.B. & Einhorn, T.A. Current and future clinical applications of bone morphogenetic proteins in orthopaedic trauma surgery. *Int Orthop* **31**, 721-727 (2007).
9. Cahill, K.S., Chi, J.H., Day, A. & Claus, E.B. Prevalence, complications, and hospital charges associated with use of bone-morphogenetic proteins in spinal fusion procedures. *JAMA* **302**, 58-66 (2009).
10. Gautschi, O.P., Frey, S.P. & Zellweger, R. Bone morphogenetic proteins in clinical applications. *ANZ Journal of Surgery* **77**, 626-631 (2007).
11. Jung, R.E. et al. A randomized-controlled clinical trial evaluating clinical and radiological outcomes after 3 and 5 years of dental implants placed in bone regenerated by means of GBR techniques with or without the addition of BMP-2. *Clinical Oral Implants Research* **20**, 660-666 (2009).
12. Liu, Y., Hunziker, E., Vaal, C. & Groot, K. Biomimetic Coatings vs. Collagen Sponges as a Carrier for BMP-2: A Comparison of the Osteogenic Responses Triggered in vivo Using an Ectopic Rat Model. *Key Engineering Materials* **254**, 619-622 (2004).
13. Schmoekel, H. et al. Bone repair with a form of BMP-2 engineered for incorporation into fibrin cell ingrowth matrices. *Biotechnology and Bioengineering* **89**, 253-262 (2005).
14. Weber, F., Eyrich, G., Grätz, K., Maly, F. & Sailer, H. Slow and continuous application of human recombinant bone morphogenetic protein via biodegradable poly

(lactide-co-glycolide) foamspheres. *International Journal of Oral & Maxillofacial Surgery* **31**, 60-65 (2002).

15. Halstenberg, S., Panitch, A., Rizzi, S., Hall, H. & Hubbell, J. Biologically engineered protein-graft-poly (ethylene glycol) hydrogels: a cell adhesive and plasmin-degradable biosynthetic material for tissue repair. *Biomacromolecules* **3**, 710-723 (2002).
16. Peppas, N.A. in Biomaterials Science: An Introduction to Materials in Medicine. (ed. A.S.H. B. D. Ratner, F. J. Schoen and J. E. Lemons) 100-107 (Elsevier Academic Press, San Diego; 2004).
17. Tsang, V. et al. Fabrication of 3D hepatic tissues by additive photopatterning of cellular hydrogels. *The FASEB Journal* **21**, 790 (2007).
18. Fouletier-Dilling, C. et al. Efficient and Rapid Osteoinduction in an Immune-Competent Host. *Human Gene Therapy* **18**, 733-745 (2007).
19. Thies, R. Recombinant human bone morphogenetic protein-2 induces osteoblastic differentiation in W-20-17 stromal cells. *Endocrinology* **130**, 1318-1324 (1992).
20. Olmsted, E. et al. Adenovirus-Mediated BMP2 Expression in Human Bone Marrow Stromal Cells. *Journal of Cellular Biochemistry* **82**, 11-21 (2001).
21. Davis, A., Wivel, N., Palladino, J., Tao, L. & Wilson, J. Construction of adenoviral vectors. *Molecular biotechnology* **18**, 63-70 (2001).
22. Kimelman, N. et al. Review: gene- and stem cell-based therapeutics for bone regeneration and repair. *Tissue Eng* **13**, 1135-1150 (2007).
23. Fouletier-Dilling, C. et al. Novel compound enables high-level adenovirus transduction in the absence of an adenovirus-specific receptor. *Human Gene Therapy* **16**, 1287-1297 (2005).
24. van Dijk-Wolthuis, W.N.E., Hoogeboom, J.A.M., Van Steenbergen, M.J., Tsang, S.K.Y. & Hennink, W.E. Degradation and release behavior of dextran-based hydrogels. *Macromolecules* **30**, 4639-4645 (1997).
25. Elbert, D.L., Pratt, A.B., Lutolf, M.P., Halstenberg, S. & Hubbell, J.A. Protein delivery from materials formed by self-selective conjugate addition reactions. *Journal of Controlled Release* **76**, 11-25 (2001).
26. Scheufler, C., Sebald, W. & Hulsmeyer, M. Crystal structure of human bone morphogenetic protein-2 at 2.7 A resolution. *Journal of Molecular Biology* **287**, 103-115 (1999).
27. Myers, R.D. Injection of solutions into cerebral tissue: relation between volume and diffusion. *Physiology & Behavior* **1**, 171 (1966).
28. Tehovnik, E.J. & Sommer, M.A. Effective spread and timecourse of neural inactivation caused by lidocaine injection in monkey cerebral cortex. *J Neurosci Methods* **74**, 17-26

(1997).
29. Gao, J.X. et al. UV embossing of sub-micrometer patterns on biocompatible polymeric films using a focused ion beam fabricated TiN mold. *Chem. Mater* **16**, 956-958 (2004).
30. Fu, J., Fiegel, J., Krauland, E. & Hanes, J. New polymeric carriers for controlled drug delivery following inhalation or injection. *Biomaterials* **23**, 4425-4433 (2002).
31. Greenwald, R.B., Choe, Y.H., McGuire, J. & Conover, C.D. Effective drug delivery by PEGylated drug conjugates. *Advanced drug delivery reviews* **55**, 217-250 (2003).
32. Gugala, Z., Olmsted-Davis, E., Gannon, F., Lindsey, R. & Davis, A. Osteoinduction by ex vivo adenovirus-mediated BMP2 delivery is independent of cell type. *Gene Therapy* **10**, 1289-1296 (2003).

Figure 1:

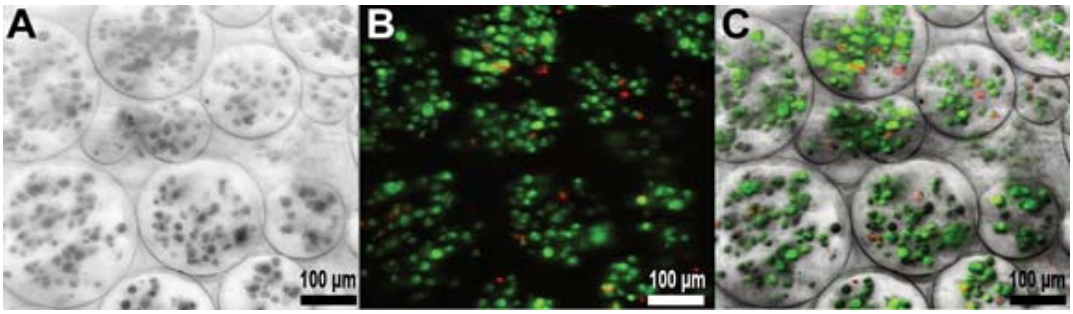

Figure

2A:

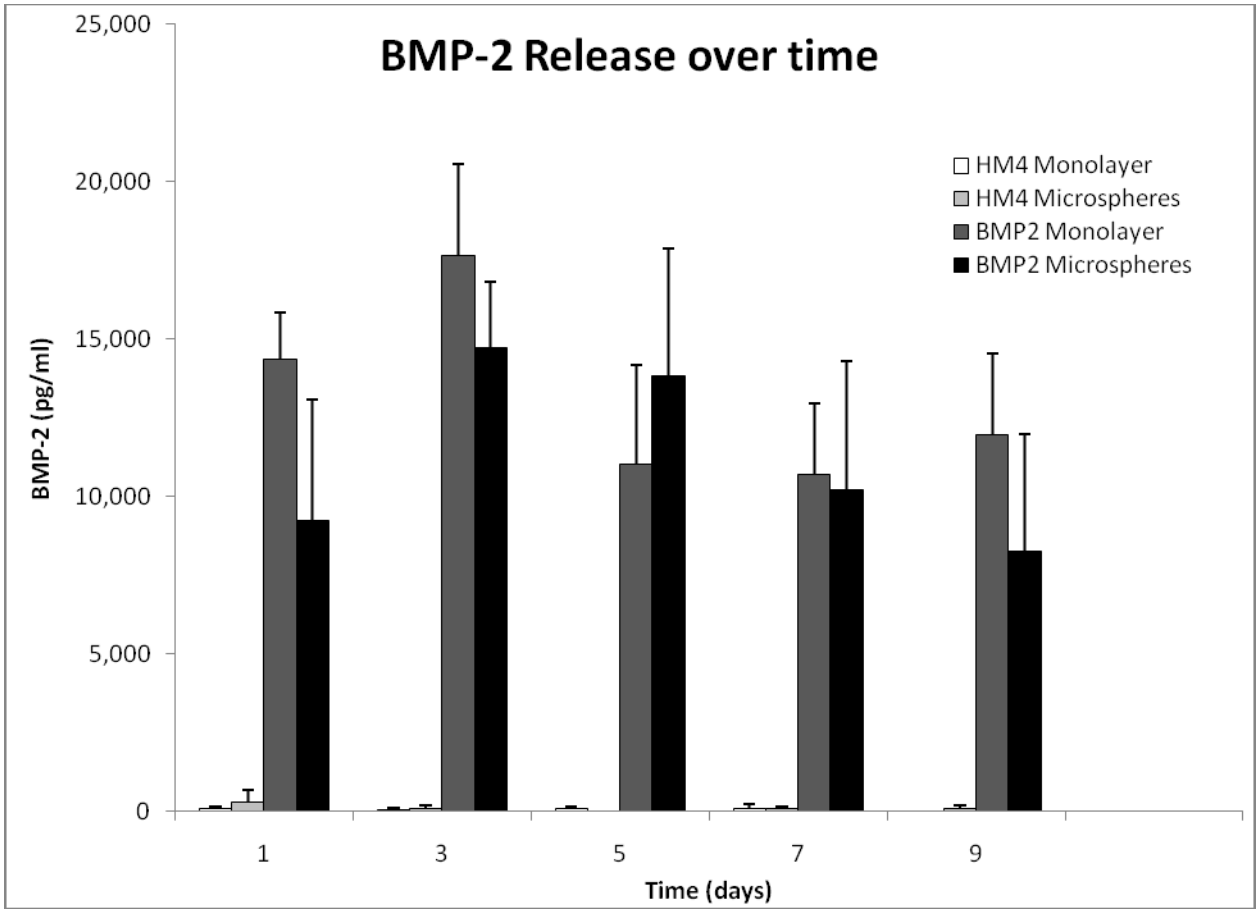
BMP-2 Release over time
25,000
20,000
15,000
10,000
5,000
0
BMP-2 (pg/ml)
1
3
5
7
9
Time (days)
HM4 Monolayer
HM4 Microspheres
BMP2 Monolayer
BMP2 Microspheres

Figure 2B:

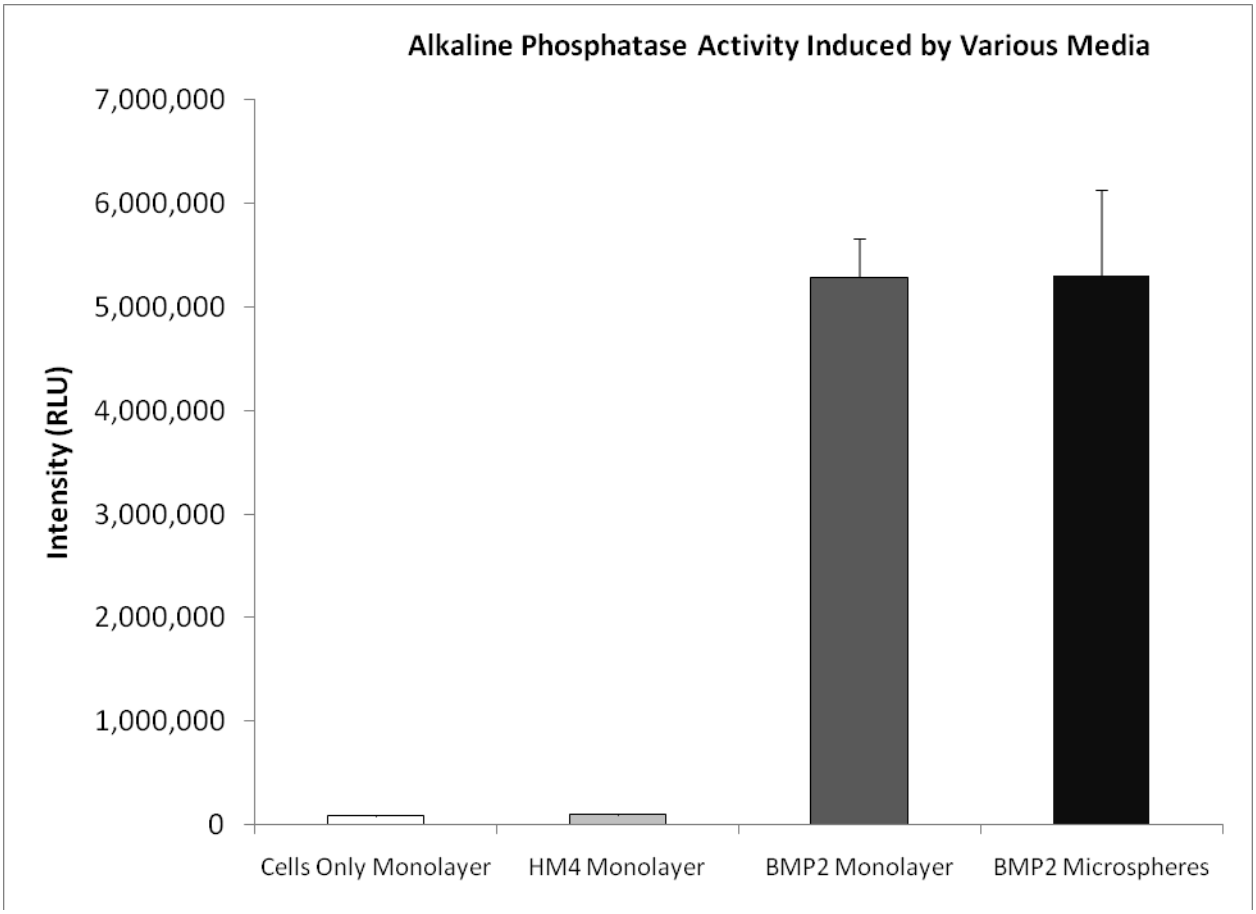
Alkaline Phosphatase Activity Induced by Various Media
Intensity (RLU)
7,000,000
6,000,000
5,000,000
4,000,000
3,000,000
2,000,000
1,000,000
0
Cells Only Monolayer
HM4 Monolayer
BMP2 Monolayer
BMP2 Microspheres

Figure 3:

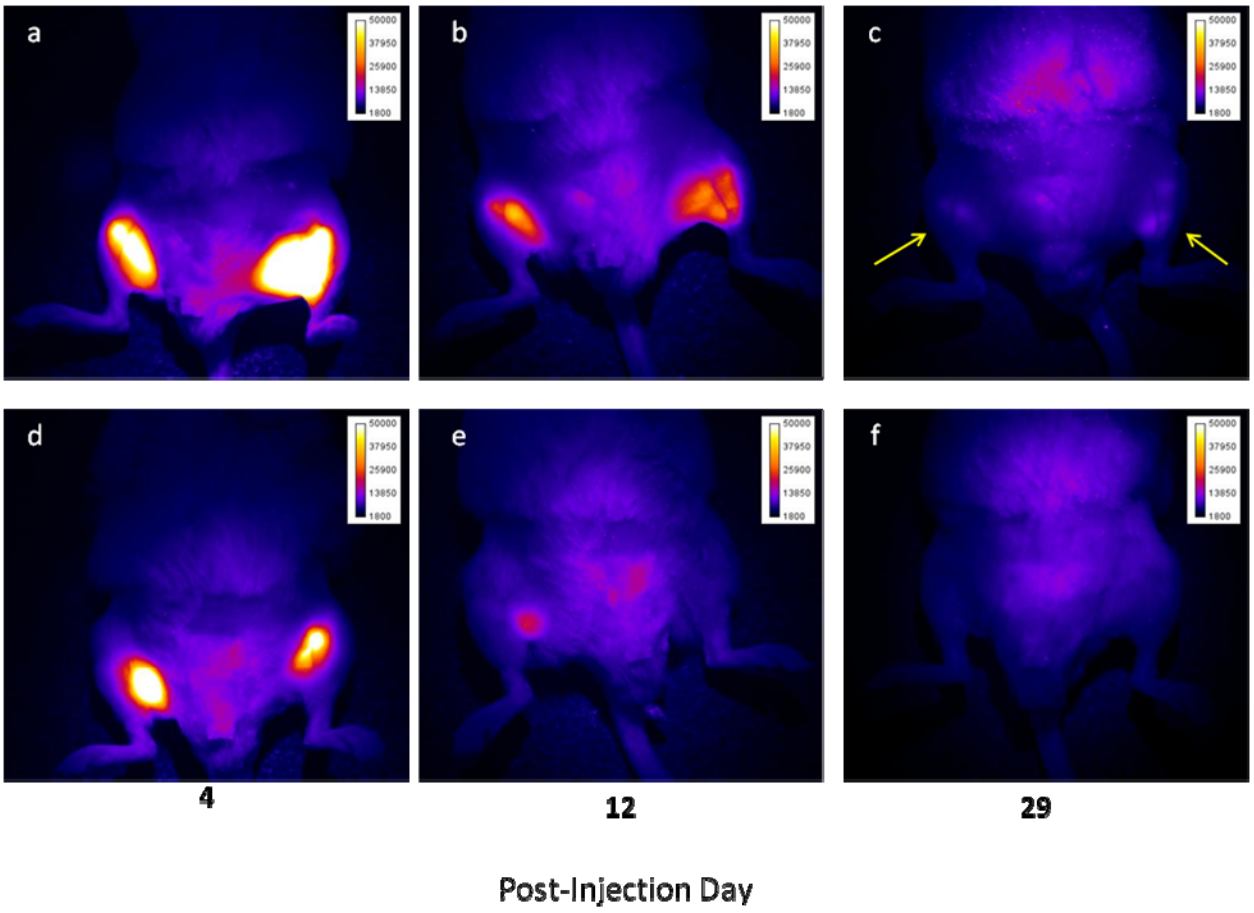
a
b
c
d
e
f
50000
37950
25900
13850
1800
4
12
29
Post-Injection Day

G

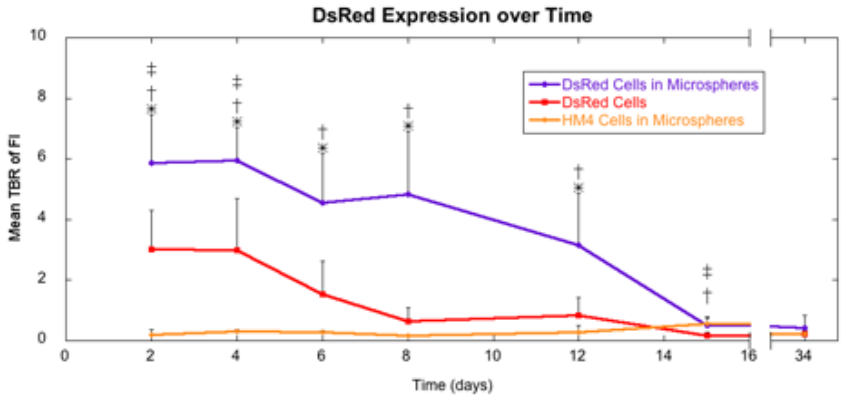
DsRed Expression over Time
DsRed Cells in Microspheres
DsRed Cells
HM4 Cells in Microspheres
Mean TBR of FI
Time (days)
0
2
4
6
8
10
12
14
16
34

Figure 4:

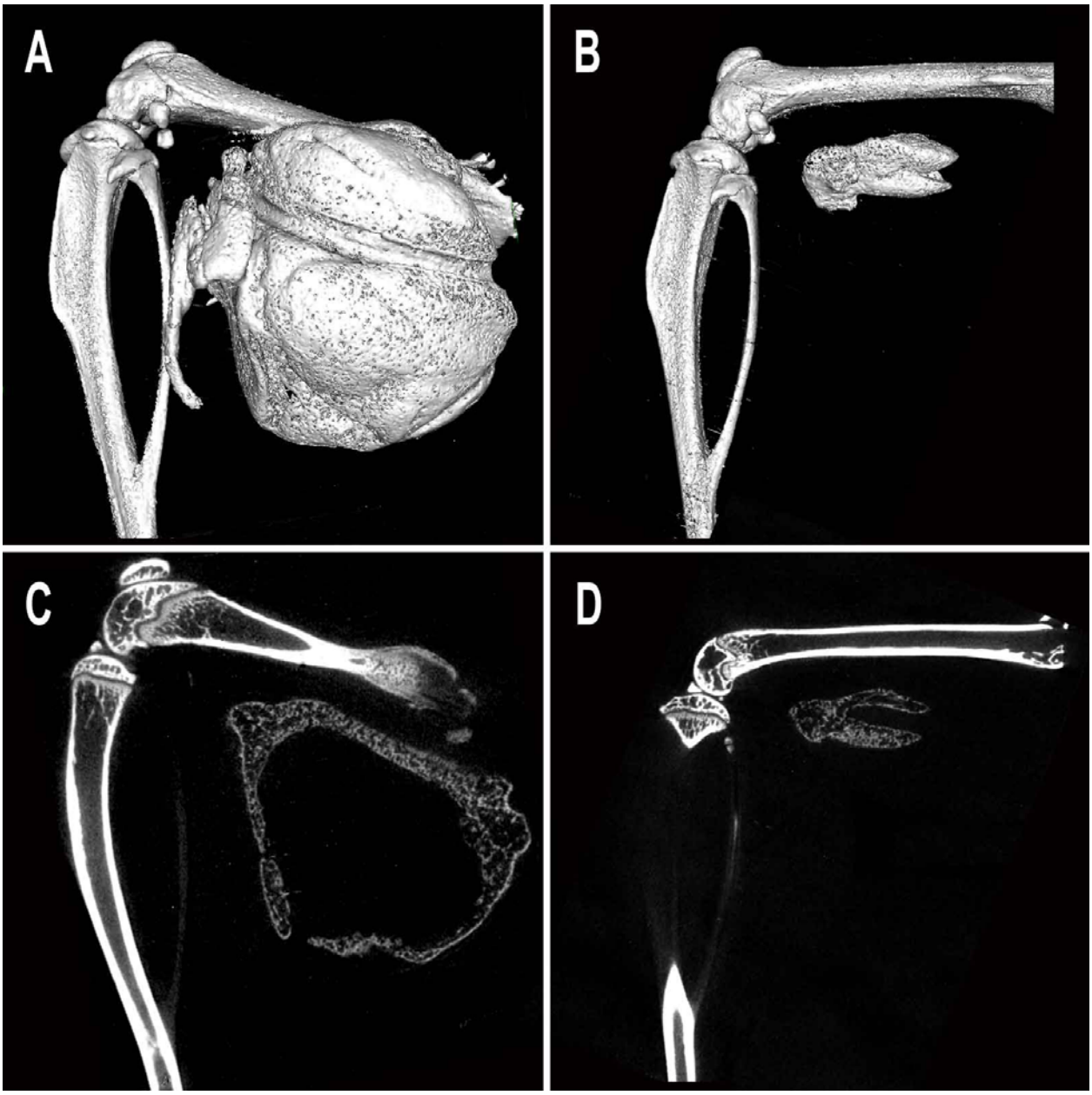

Figure 5:

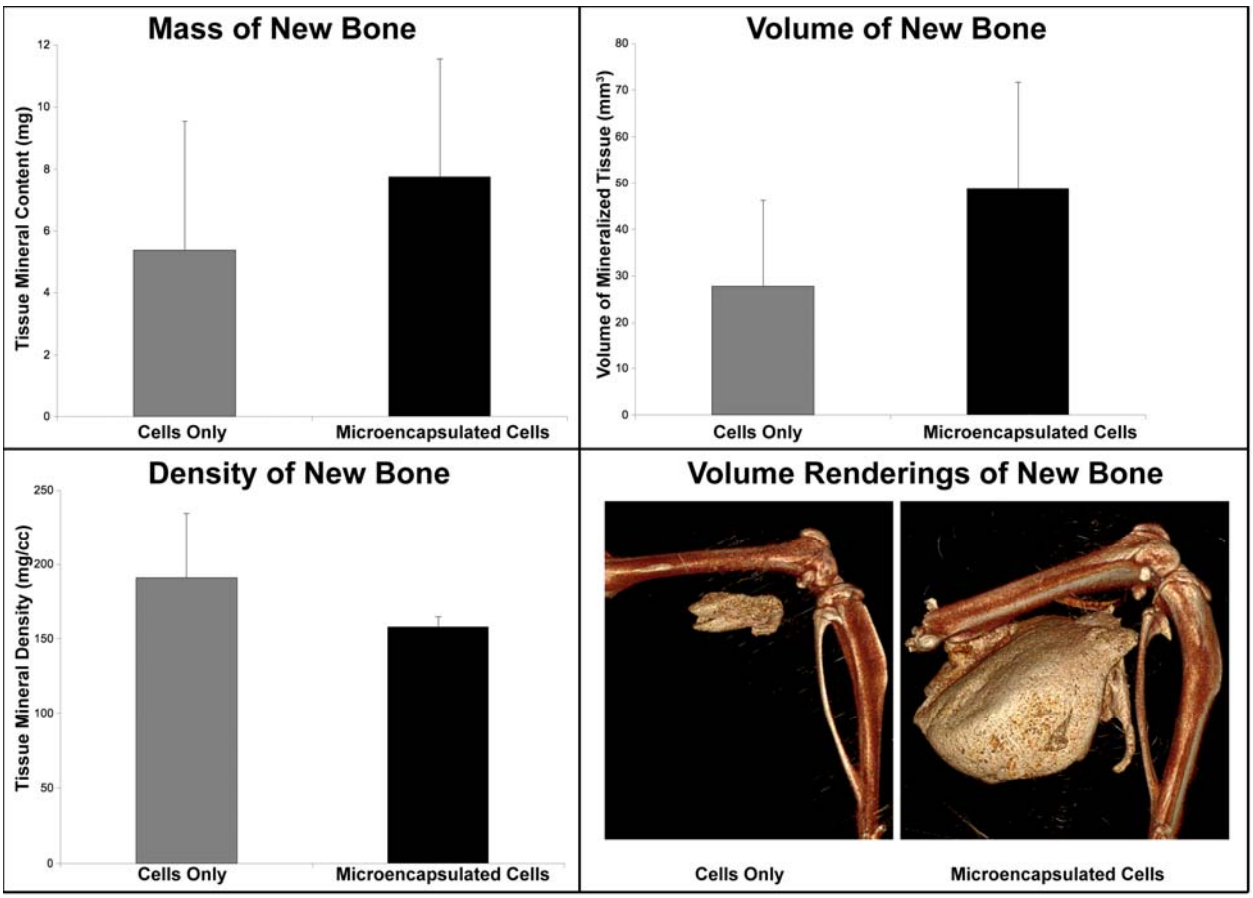
Mass of New Bone
Tissue Mineral Content (mg)
0
2
4
6
8
10
12
Cells Only
Microencapsulated Cells
Volume of New Bone
Volume of Mineralized Tissue (mm³)
0
10
20
30
40
50
60
70
80
Cells Only
Microencapsulated Cells
Density of New Bone
Tissue Mineral Density (mg/cc)
0
50
100
150
200
250
Cells Only
Microencapsulated Cells
Volume Renderings of New Bone
Cells Only
Microencapsulated Cells

Figure 6:

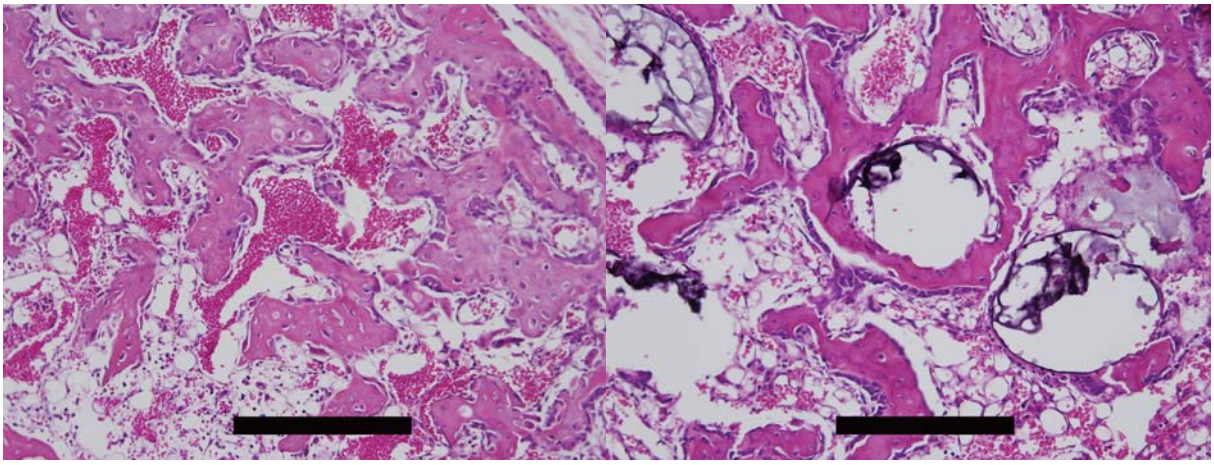

An Injectable Method for Non-Invasive Spine Fusion.

Ronke M Olabisi[1], Zawaunyka Lazard[2], Michael Heggeness[3], Kevin M Moran [3], John A Hipp[3], Ashvin Dewan[3], Alan R. Davis[2-4], Jennifer L. West[1] and Elizabeth A. Olmsted-Davis[2-4]

[1]Department of Bioengineering, Rice University, 6100 Main St. MS 144, Houston, TX 77005, USA

[2]Center for Cell and Gene Therapy, Baylor College of Medicine, Houston, TX 77030, USA;

[3]Department of Orthopaedic Surgery, Baylor College of Medicine, Houston, TX 77030, USA;

[4]Department of Pediatrics and Center for Cell and Gene Therapy, Baylor College of Medicine, One Baylor Plaza, Houston, TX 77030, USA;

Spine fusion has been achieved by a single injection of a cell-based gene therapy system, along the paraspinous musculature, which rapidly induces heterotopic ossification, and ultimately spinal arthrodesis. The system does not require additional hardware or invasive surgery to decorticate the vertebral bone, but rather harnesses the body's capacity to rapidly produce heterotopic bone. By targeting the location of the heterotopic ossification, new bridging bone between the vertebrae and fusion to adjacent skeletal bone was obtained as early as two weeks. Reduction in spine flexion-extension also occurred as early as two weeks after injection of the gene therapy system in 40% of the mice, with greater than 90% fusion by four weeks. These studies are the first to harness heterotopic ossification, and use it as a safe and efficacious injectable, system for the spinal arthrodesis.

INTRODUCTION

Of the over 1 million bone grafts performed annually worldwide, 50% involve spinal fusions and 25% of these patients complain of donor site pain from the autograft harvest site for up to 2 years post-operatively(Deyo et al. 2004). These complications have driven the search for and subsequent use of alternatives. This has led to the growing use of bone morphogenetic proteins (BMPs), which have long been demonstrated to induce bone formation (Kimelman et al. 2007, Lutolf et al. 2003, Mussano et al. 2007).

Recombinant human BMP2 (rhBMP-2) is FDA approved for use on collagen sponges for the treatment of open long bone fractures and in metal cages for spinal fusion[2]. Without the sponge or the cage, the BMP2 cannot be localized and tends to diffuse from the desired site, reducing its efficacy and leading to adverse effects such as edema, ectopic bone formation and bone resorption in the graft area(Garrison et al. 2007, Lutolf et al. 2003). Because BMPs are so rapidly diffused, large quantities of the protein are required, making the procedure very expensive (Lutolf et al. 2003). Furthermore, although the use of rhBMP-2 for spinal fusion may negate the need for an additional surgical procedure to harvest autograft bone, the method still necessitates an operation that introduces a permanent foreign object into the body(Mussano et al. 2007). Spinal fusion also requires decortication of the transverse processes of the vertebrae targeted for fusion, stripping of the paraspinous musculature from bone and a fairly long operative time(Deyo et al. 2004) (Hecht et al. 1999). Beyond the pain associated with decortication and stripping this leads to other complications. S tripping the musculature compromises the stability afforded by these

muscles, disrupts the blood supply to both bone and muscle and promotes scar formation. Even with addition of this powerful morphogen, there is still a considerable failure rate (Garrison et al. 2007) causing researchers to search for better methods for delivering higher doses of BMP2.

Recently Shore et al, (Shore et al. 2006) demonstrated that a mutation in the BMP2 receptor was responsible for the observed heterotopic ossification (HO) in the genetic disease fibrous dysplasia ossificans progressiva (FOP). Soft tissues in individuals with this genetic disorder are replaced with heterotopic bone. The HO can rapidly form within a few days, and even replace skeletal bone if it becomes weight bearing. It readily fuses to the skeletal bone, and often leads to ankylosis of the joints. Harnessing this capacity in a targeted, controlled manner, would potentially allow for the regeneration of skeletal bones.

Gene therapy approaches hold much promise in achieving locally high levels of BMP2 for production of robust heterotopic ossification. However, the efficient transduction of cells posed a problem for many of the currently tested systems resulting in low BMP expression (Olmsted-Davis et al. 2002). In many cases, this problem is then exacerbated by inclusion of a collagen sponge or other biomaterial that rapidly binds the BMP, again reducing its effectiveness[13]. Finally inclusion of the biomaterial and invasive decortication procedures cause undesired inflammation, which weakens bone healing (Garrison et al. 2007)

Here we demonstrate the ability of cells expressing high levels of BMP2 to launch heterotopic ossification, at a targeted location, and ultimately fuse two or more vertebrae within the lumbar spine. Fusion of both the heterotopic bone to the skeletal bone, and the resultant bridging of two vertebrae are rapidly achieved, through simple injection. Within two weeks 40-100% of the spines in two different murine models were considered fused by all criteria, radiological, histological, and biomechanical. In samples tested 4-6 weeks after induction, greater than 90% of the mice had achieved spine fusion in both models, and noticeable scoliosis was observed radiologically in the animal's spines suggesting that the fusion could restrain the spine, even during continued growth.

RESULTS

To determine if our cell based gene therapy system induces spine fusion through intramuscular injection without invasive surgery or additional carriers, we established two different murine models for testing. We have previously characterized these models and found that the formation of bone in each, by injection of BMP2-producing cells, is similar (12). Here we apply the cell based gene therapy system to the paraspinous musculature in the region of the vertebral laminae, to determine whether heterotopic bone formation can:1) be targeted to this location; 2.) form bridging bone between two or more skeletal vertebra and 3) ultimately fuse the spine. Figure 1 shows a schematic depiction of this approach, in which either adenovirus transduced cells expressing functional BMP2, or cells transduced with a similar adenovirus vector lacking BMP2 (Adempty cassette), are delivered to the paraspinous musculature of a mouse through a simple injection at points adjacent to the levels of desired fusion. With this system, heterotopic ossification is generated rapidly, fused and remodeled into two or more of the adjacent vertebra, reducing spine motion.

Radiological Analysis of Bone Formation:

Accordinglyheterotopic bone formation was allowed to progress for 2, 4 and 6 weeks, after initial

injection of the AdBMP2 or empty cassette transduced cells. Spines were removed and analyzed for the presence of heterotopic bone, and spinal arthrodesis. In all AdBMP2 injections, heterotopic bone formation occurred along the injection site, adjacent to the spine, with greater than 90% bridging and fusing to the skeletal bone. (Figure 2, three dimensional reconstructions E-L). Two dimensional radiographs (figure 2, panels A-D and M-P) show the cross sections through the tentative fusion. The radiographs and three dimensional reconstructions demonstrate that both the immune incompetent system, NOD/Scid mice receiving human cells transduced with AdBMP2 (panels I-P), and immune competent system, C57BL/6, receiving AdBMP2 transduced allogeneic murine cells (panels A-H), appear to produce similar bone within 4 to 6 weeks. This new bone appears to be remodeled with a contiguous cortical bone exterior. Although we did observe 40% of the samples in the NOD/Scid animals with potential points of fusion, panel N shows a scenario in which the heterotopic bone, although extensive, has not yet fused into the vertebrae. It appears in panel J, that the heterotopic bone occurred slightly distal to the vertebral bodies. Interestingly, we did not see similar findings in wild type mouse models, as seen in panel B even at two weeks the substantial bone has fused to the adjacent vertebra.

In the cross-sectional radiographs, vertebral cortical bone appears to be integrated with the heterotopic bone (figure 2, panel B-D, O-P). The points of fusion appear to be in the laminae region of the vertebra, with the majority of cases encompassing the entire spinous and transverse processes, suggesting significant fusion. In this case although the location of the fusion is unchanged, only limited portions of the spinous and transverse process are actually integrated. In no case did we observe bone formation or bridging in the samples receiving the Adempty cassette transduced cells. The apparent fusion appeared to be rapid, within two weeks, and limited in size and scale, to region of muscle which received the cells. Further, at no time did we observe bone formation within the spinal canal.

Histological Analysis of the Spine Fusion:

To confirm that the apparent mineralized bone observed on the radiographs is true osteoid, and that it has integrated at these tentative points of fusion, we isolated the spine and adjacent tissues for histological analysis using techniques previously described (Fouletier-Dilling et al. 2007). The spines were embedded in paraffin blocks, five micron sections cut, and every fifth section was stained with hematoxylin and eosin to identify the tentative point of fusions. Representative photomicrographs (2X and 4X) of samples from either model, taken 2, 4 and 6 weeks after induction of heterotopic ossification are shown in figure 3. In all cases we observed structures of mature bone, such as osteoclasts, osteocytes and tentative bone marrow elements in the heterotopic bone, as well as cartilage, analogous to the growth plate structures in the normal long bone. However the heterotopic bone appeared to grow in a direction towards the skeletal bone, with the most mature bone being distal to the skeletal bone in the 2 week samples. Figure 3, panel A-B, shows that there is substantial new bone, adjacent and fused with the more mature vertebral bone, along the transverse process, and laminae region of the vertebra. Although mature bone with tentative marrow elements was observed at 2 weeks; this structure was always distal to the vertebral bone (data not shown), suggesting that the original heterotopic ossification started *de novo*, in the muscle and grew towards the vertebrae to encompass the bone. By four weeks, (figure 3, panel C-D), the heterotopic bone is much more mature, and at the point of fusion, a very cellular reaction, that appears to be rapidly removing the mature cortex of the skeletal bone was noted. It is unclear whether the large number of cells is recruited to this

boundary or is expanding from the vertebral periosteum, but as noted in panel G, the mature cortical bone of the vertebra appears to be heavily resorbed (moth-eaten) and undergoing removal by the maturing heterotopic bone. By 6 weeks, this boundary is completely remodeled (figure 3; panel E-F) with the two bones now contiguous as one integrated structure with a well defined cortex and trabecular interior, which houses the bone marrow. Interestingly, the only evidence remaining of the newly formed heterotopic ossification is the presence of substantial amounts of adipose tissue, which is found within heterotopic regions, in contrast to the mature marrow within the vertebra (panel F). Figure 3, all cases show what appears to be fusion with the transverse process within the laminae region of the vertebra, which was the target region for fusion. Depending on the depth of the section, more or less of this region was involved in the fusion site. In many cases the fusion actually encompassed both the spinous process through the laminae to the transverse process. In all tissues analyzed, the vertebral body did not appear to undergo growth, and there was no evidence of new bone formation within the spinal canal, similar to our observed radiological findings.

Biomechanical Analysis to Confirm Reduced Motion of the Spine:

The clinical goal of spine fusion is to reduce motion within the vertebral column; therefore, we developed a method for measuring flexion-extension of the spine. In this analysis spines were x-rayed before and after bending, and intervertebral motion was quantified using KIMAX QMA software (Medical Metrics, Inc.). This software has been validated to measure intervertebral motion with an accuracy of better than 0.5° of rotation and 0.5 mm of translation (Hipp et al. 2005, Zhao et al. 2005). Results of this analysis are shown in Table 1. In no cases did tissues receiving the Adempty cassette transduced cells, show a reduction in motion or spine stiffening. Whereas in NOD/Scid animals that received the human cells transduced with AdBMP2, approximately 40% of the spines at 2 weeks and 90% of those at 4 and 6 weeks had reduced movement, consistent with fusion of at least one level. Interestingly, the C57BL/6 group receiving AdBMP2 transduced cells, at all time points, consistently showed a reduction in motion within the lumbar spine correlating with fusion (Table 1).

Table 1: Spinal fusion in injected animals

Group	N	Strain	Time	Spines with 2 or more vertebrae fused (%)
Adempty cassette transduced cells	9	NOD/Scid	6 weeks	0 %
AdBMP2 transduced cells	9	NOD/Scid	2 weeks	44 %
AdBMP2 transduced cells	9	NOD/Scid	4 weeks	90 %
AdBMP2 transduced cells	9	NOD/Scid	6 weeks	90 %
Adempty cassette transduced cells	8	C57BL/6	6 weeks	0%
AdBMP2 transduced cells	8	C57BL/6	2 weeks	100%

AdBMP2 transduced cells	4	C57BL/6	4 weeks	100%
AdBMP2 transduced cells	8	C57BL/6	6 weeks	100%

Functional Demonstration of Fusion:

To further confirm spine fusion, the isolated spines used for mechanical testing were bleached to remove soft tissues, and analyzed on a gross level to see if the bone was contiguous. Figure 5, panel A, a representative 6 week spine shows that in this fusion, 5 vertebrae of the lumbar spine are actually remodeled into a single structure. In all cases with biomechanical constraint of the spine after the induction of bone formation, there was also integration of the vertebra with heterotopic bone, which was observed after removal of the soft tissues. In cases that did not meet our criteria for fusion (several NOD/Scid animals at 2 weeks) in that they did not appear to be constrained after induction of bone formation, there was heterotopic bone that was not integrated with the vertebrae but rather individual bones, confirming our biomechanical findings.

Further, in both immune copentent and incompetent models the radiomicrographs show a distinct scoliosis in 6 month old growing mice, which received the Ad5BMP2 transduced cells injected into one side of the paraspinous musculature that parallels the spine. Figure 5, panel C, representative radiographs show a distinct curvature of the spine towards the area of new bone formation and tentative fusion. This was observed in a large number of animals with heterotopic bone and tentative fusion, but absent in animals that received the control cells (panel B).

DISCUSSION

Our system is the first approach reported in the literature to achieve rapid and clinically relevant spinal fusion in an animal model, through a single intramuscular injection. Reported time scales for spinal fusion using cell and gene therapy approaches range between 6 weeks and 3 months; using gene therapy approaches, spinal fusion typically proceeds between 4 and 12 weeks (Gottfried and Dailey 2008, Kimelman et al. 2007). Nevertheless, despite the reported successes using these approaches, the results were tempered with difficulties, in isolating stem cell populations to use as delivery cells, and low gene transduction efficiencies(Gottfried and Dailey 2008, Kimelman et al. 2007) (Aslan et al. 2009). The work presented here circumvents these issues. We looked at two different models which we have previously characterized(Deyo et al. 2004), and found that we could achieve fusion in both systems in as little as two weeks after initial intramuscular injection. Surprisingly, we observed 100% fusion in the immune competent wild type mice within two weeks of induction, yet only 40% fusion at two weeks in the system that used human cells transduced with AdBMP2. Upon analysis of the three dimensional reconstructions, it appeared that the new bone was slightly distal to the vertebra in the NOD/Scid immune incompetent mice, whereas it was more closely associated with the vertebra in the wild type. Previous comparisons of these two systems show that they function almost identically in production of heterotopic bone(Deyo et al. 2004).Therefore it is unlikely that this difference is linked to the immunodeficiency, but rather that as we progressed, we improved our ability to place the cells proximal to the vertebra within the paraspinous musculature, indicating that placement may be critical to the eventual fusion.

These results suggest that heterotopic bone can be rapidly induced by delivering locally high

levels of BMP2. This is not surprising since recombinant BMP2 is current used clinically; however, the rapid one week time frame has not previously been reported(see ref. (Mussano et al. 2007) for review). This may be a direct result of our ability to produce high levels of BMP2 for a prolonged period of time.This process may be explained by taking cues again from the human genetic disease FOP,Thus, physiological doses of BMP2 normally released after trauma effectively become high doses, leading to rapid heterotopic ossification at the local injury site. During adenovirus transduction, multiple virus particles enter the cell with large amounts of vector DNA being effectively delivered to the nucleus. Because of its episomal nature, the vector DNA is present at high copy number, driving high-level expression of BMP2. Therefore, one of the things separating adenovirus from other gene therapy vectors is the high level of transgene expression that can be achieved after efficient transduction.(Berkner 1988) As long as the virus can efficiently infect the specific cell types (Fouletier-Dilling et al. 2005) this system can be used to produce these high doses of BMP. Thus we have developed this as a cell based gene therapy system rather than a direct approach, to circumvent potential problems with inefficient uptake of the adenovirus, problems that prohibit production of the BMP2 levels necessary for achieving rapid fusion(Olmsted-Davis et al. 2002). This is perhaps why our approach is so extremely effective at making rapid targeted bone. Further, by prior transduction of the cells with the virus, no free adenovirus is delivered to the animal, minimizing adverse effects of the virus on other tissues. In addition to forming bone rapidly, this study is the first to demonstrate the ability of heterotopic ossification to form bridging bone and fuse adjacent vertebral bone without contribution from the skeletal bones. Both current clinical approaches using recombinant BMP2 and other gene therapy approaches(Deyo et al. 2004) require exposure of the vertebra and decortication to induce bone growth and ultimately fusion of the skeletal bone to heterotopic bone. Often autologous bone graft is harvested to use in place of ectopic bone, which requires an additional extensive surgical procedure. Here through both histological analysis and biomechanical analysis we demonstrate the ability of the heterotopic bone to fuse into skeletal bone without exposure and decortication.

In addition, all spines receiving the AdBMP2 transduced cells appeared to have extensive heterotopic bone formation upon radiological analysis. In no cases did we observe any ossification in the spinal canal. In the animals receiving Adempty cassette transduced cells, there was no ossification whatsoever. The results suggest that the heterotopic bone formation is targetable to a discrete location. Upon radiological analysis of samples taken 2,4, and 6 weeks after initial injection of the AdBMP2 transduced cells, heterotopic bone was found between the transverse process adjacent to the paraspinous musculature receiving the cells and laminae. This heterotopic bone eventually encompassed these structures, fusing the spine. In many cases we observed significant fusion of the entire laminae, from the tip of the spinous process through the entire transverse process. There was some variation in the amount of vertebral bone involved in each fusion, but this did not seem to affect the overall arthrodesis itself. Further, since the material can target the location of bone formation, perhaps the variation observed could also be a result of placement of the materials within the spinous musculature of the mice. Regions of soft tissue adjacent to corresponding distal structures of the same vertebra were not involved in any bone formation and appeared normal in these radiographs.

Histological analysis of this model suggests that the heterotopic bone grows into the skeletal bone with a somewhat organized growth plate, cortex, and tentative periosteum, similar to the vertebral bone. Initially less mature bone is observed at the junction of fusion, and depending on the model, these results in reduction of motion in approximately 40-90 % of the animals tested. Interestingly, as the two bones fuse there appears to be a cellular reaction, which is destructive

to the vertebral cortex. This process allows for the replacement of the cortical boundary with mature trabecular bone and bone marrow over time. It is not surprising from these results that in all cases the latter 4 and 6 week structures are well fused both histologically and biomechanically. Interesting to note, by 6 weeks, the old vertebral structure is gone, with the only remnants of the newer heterotopic bone being found in the marrow cavity. This observation suggests that adipose may form in the bone marrow cavity prior to the housing of true bone marrow, since in all less mature heterotopic bone, we observed extensive white fat, while in the vertebral bone marrow there was very little if any present. Whether this tissue plays a key role in establishment of the marrow is yet to be determined.

Ideally, upon successful fusion, the newly fused heterotopic bone should restrict mobility within the spine. Therefore biomechanical testing was performed to measure the changes in angle of the spine under force. In spines with a significant reduction in mobility, we observed well integrated collagen fibers running contiguously through the bone, suggesting that it was a remodeled single structure, whereas those that appear as two separate structures under polarized light were not capable of reducing flexion-extension. . In animals with reduced spinal mobility, we also observed scoliosis due to the arthrodesis. Since the epiphyseal growth plates of rodents do not close until two years of age (the approximate life span of laboratory mice), their skeletons essentially do not stop growing(Windahl et al. 2002). The fusion of the vertebrae in essence mechanically fixed the right side of the spine, causing imbalanced growth, resulting in scoliosis.The ability to fuse the spine without surgical intervention would be a significant advancement in healthcare. The creation of a bony fusion by means of the percutaneous injection of a biologically active material, without extensive surgical dissection and bony decortication, would have many clear clinical advantages. This system is quite versatile, in that any cell can be used as a delivery cell, as long as adequate transduction with adenovirus is achieved(Gugala et al. 2003). Thus qualified cell lines used in current clinical trials, such as mesenchymal stem cells, can be readily adapted for use in this cell based gene therapy system, making it very feasible to introduce clinically. The rapid onset of bone in addition to the rapid clearance of the transduced cells bodes well for the future therapeutic application of this system in humans.The system presented herein could potentially markedly decrease the pain, blood loss, and recovery time for patients undergoing these procedures, thus significantly reducing healthcare and associated costs. Further, this system could potentially improve success rates of this procedure, thus improving the quality of healthcare in this arena overall.

MATERIALS and METHODS

Cell Culture

Human diploid fetal lung fibroblasts (MRC-5) and murine osteoblasts (MC3T3-E1) were obtained from the American Type Culture Collection (ATCC; Manassas, VA) and propagated in a humidified incubator at 37°C and 5% CO_2 in α-minimum essential medium (α-MEM; Sigma, St. Louis, MO) and Dulbecco's Modified Eagle's Medium (DMEM; Sigma, St. Louis, MO) supplemented with 10% fetal bovine serum (FBS; HyClone, Logan, UT), 1000 U/L penicillin, 100 mg/L streptomycin, and 0.25 μg/ml amphotericin B (Invitrogen Life Technologies, Gaithersburg, MD), as previously described (Fouletier-Dilling et al. 2007)[12]. Murine stromal cells (W20-17; a gift from Genetics Institute, Cambridge, MA) were propagated and maintained as described by Thies *et al*(Thies et al. 1992).

Adenoviruses

Replication defective E1-E3 deleted first generation human type 5 adenovirus (Ad5) or a human type 5/35 adenovirus (Ad5F35) in which the normal fiber protein has been substituted for the human adenovirus type 35 fiber (Ad5F35) were constructed to contain cDNAs for human BMP2 in the E1 region of the viruses(Davis et al. 2001). Two independent viruses were used based on their efficiency for transducing either human or mouse cells as described previously(Fouletier-Dilling et al. 2005). For the viruses Ad5BMP2, Ad5F35BMP2, Ad5-empty cassette, and Ad5F35empty cassette the viral particle (VP)-to-plaque-forming unit (PFU) ratios were 55, 76, 200, and 111, respectively, and all viruses were confirmed to be negative for replication-competent adenovirus. Ad5 viruses were used for the murine MC3T3-E1 cells and Ad5F35 viruses were used for the human MRC-5 cells (Fouletier-Dilling et al. 2005).

Cell transduction

MC3T3-E1 cells (1×10^6) were transduced with Ad5BMP2 or Ad5-empty at a viral concentration of 5000 VP/cell with 1.2% GeneJammer®, as previously described(Fouletier-Dilling et al. 2005). Briefly, GeneJammer® was added at 3% to α-MEM without supplements to and incubated for 10 min at room temperature. Ad5BMP2 or Ad5-empty was then added at the aforementioned concentrations and the mixture was further incubated for 10 min at room temperature. This virus solution was then diluted with supplemented α-MEM to achieve 1.2% GeneJammer® per volume. The resulting solution was next incubated 37°C for 4 hr with cells at an amount that just coated them, and then the mixture was diluted with supplemented medium at an amount appropriate for cell culture and incubated at 37°C overnight. MRC-5 cells were transduced as previously described with Ad5F35BMP2 or Ad5F35HM4 at a viral concentration of 2500 VP/cell(Davis et al. 2001). Briefly, virus was added to fresh supplemented DMEM and incubated with cells at 37°C overnight.

BMP-2 Quantification

BMP-2 expression was evaluated for MC3T3 and MRC-5 cells transduced with Ad5BMP2, Ad5-empty, Ad5F35BMP2 or Ad5F35HM4 using ELISA and alkaline phosphatase assays. Culture supernatant from transduced cells were collected 72 hours after adenovirus transduction and assayed with a BMP-2 Quantikine ELISA kit from R&D Systems (Minneapolis, MN) to measure BMP-2 expression. Transduced cells were cultured in 0.4 μm pore polycarbonate membrane transwell inserts (Corning Inc., Lowell, MA) and W20-17 cells were cultured in the wells of 6 well plates. After 72 hours W20-17 cells were assayed for alkaline phosphatase activity using a chemiluminescence procedure[18]. Three freeze-thaw cycles were performed in a 100-μM/cm^{2}concentration of 25mM Tris-HCl (pH 8.0) and 0.5% Triton X-100 in order to extract cellular alkaline phosphatase and this activity was then measured by adding a ready to use CSPD substrate with Sapphire-II enhancer (Tropix; Applied Biosystems, Foster City, CA) to the samples. After a 2 sec delay, the light output from each sample was integrated for 10 sec with a luminometer (TD-20/20; Turner BioSystems, Sunnyvale, CA). Alkaline phosphatase levels were recorded in relative luminescence units (RLU) and normalized to protein content with the bicinchoninic acid (BCA) assay, using bovine serum albumin to derive a standard curve. BMP2 protein levels and functional activity were found to be similar to previously published results per cell number and virus dose (Olmsted-Davis et al. 2002)

Spinal Fusion

Female NOD/SCID and C57BL/6 mice (8–12 weeks old; Charles River Laboratories; Wilmington, MA) and maintained in accordance to Baylor College of Medicine Institutional Animal Care and

Use Committee (IACUC) protocols. Prior to paraspinous injections, the back of each mouse was prepared and a limited skin incision was made to reveal the paraspinous muscles. Although the injection could have been done without opening the skin, to insure appropriate placement of the material we opened the skin, prior to intramuscular injection. Transduced cells were removed with trypsin, resuspended at a concentration of 5×10^6 cells per 100 µl of PBS, and then delivered by intramuscular injection into the right paraspinous muscles along the length of the spine (Figure 1). After 2, 4 and 6 weeks, mice were sacrificed and the spines with attendant musculature were removed and fixed in formaldehyde solution (VWR; Sugar Land; TX).

MicroCT analysis

The intact spines were scanned at 14 µm resolution with a commercial micro-CT system (GE Locus SP, GE Heathcare, London, Ontario). Three-dimensional reconstructions of the spine and any mineralized tissue in the surrounding muscle were created at 29 µm resolution to visualize endochondral mineralized tissues. A volume of interest was defined for each specimen, and a threshold was chosen to exclude any non-mineralized tissue. The total volume of endochondral bone was then measured (eXplore MicroView, v. 2.0, GE Healthcare, London, Ontario) and spines of the animals were not taken into account for the measurements of mineralized tissue in the muscles of the animals.

Histological analysis

Fixed spines were decalcified in hydrochloric acid, processed and embedded into a single paraffin block, where serial sections were then cut at a thickness of 5-7 µm. The sections were stained with hematoxylin and eosin and observed under light microscopy. To further confirm the vertebral fusion, a subset of spines (n=9) were immersed in bleach for approximately one hour which removed all soft tissues. Midway through this process, nylon wire was threaded up the spinal canal in order to maintain the relative position of the vertebrae.

Biomechanical Testing

Prior to sectioning, formaldehyde fixed spines were encased in alginate in order to obtain flexion and extension radiographs. Spines were suspended in an in-house mold. Alginate powder was combined in an equal volume to water (30 ml of each) and mixed until smooth. The alginate was poured into the mold and allowed to solidify. Solidified molds were placed in an in-house spring-loaded clamp with rigid 100° arcs (Figure 4). Radiographs were taken of molds in flexion and extension orientations for each spine. These digitized radiographs were used to quantify intervertebral motion with Food and Drug Administration (FDA)-approved software (KIMAX QMA, Medical Metrics, Inc.) that has been validated to measure intervertebral motion with an accuracy of better than 0.5° of rotation and 0.5 mm of translation (Hipp et al. 2005, Zhao et al. 2005)[20, 21]. Intervertebral motion was measured at each level. Preliminary data (unpublished) demonstrated that the normal mouse spine undergoes an average of 5° of intervertebral motion using this test. Spines were considered fused when adjacent vertebrae did not exhibit rotation beyond 1.5°.

Statistical Analysis

Statistical analysis was performed as described previously(Fouletier-Dilling et al. 2007)[12]. Briefly, all data were taken in triplicate and reported as mean and standard deviation. A Student t test with 95% confidence interval ($p < 0.05$) was done between the untreated control and each experimental condition.

Figure Legends:

Figure 1: Schematic depiction of spine fusion using the cell based gene therapy system. AdBMP2 transduced cells injected into the muscle, rapidly recruit host cells to undergo all stages of endochondral ossification (Fouletier-Dilling et al. 2007). Within one week mineralized osteoid can be detected in photomicrographs and radiographs.

Figure 2: Radiographs of C57BL/6 (panels A-H) and NOD/Scid (panels I-P) spines imaged after intramuscular injection into the paraspinous musculature of cells transduced with Adempty cassette control virus (panels A, E, I, and M) or AdBMP2 (panels B-D, F-H, J-L, and N-P). Control animals injected with Ad5HM4 were scanned 6 weeks after delivery of the transduced cells (panels A, E, I and M). Mice receiving the AdBMP2 transduced cells, were scanned 2 weeks (panels B, F, J, N); 4 weeks (panels C, G, K, O); and 6 weeks (D, H, L, P) after the initial induction of heterotopic ossification. Two dimensional x-rays (panels A-D; C57BL/6 and panels M-P; NOD/Scid) show a cross section through the three dimensional reconstructions (panels E-H; C57BL/6 and I-L; NOD/Scid) of tentative fusions between the heterotopic ossification and the vertebral bone.

Figure 3: Representative photomicrographs of tentative vertebral fusion with the heterotopic bone, taken 2 (panels A-B; 2X and 4X respectively), 4 (panels C-D; 2X and 4X respectively), and 6 (panels E-F; 2X and 4X respectively) weeks after initial injection of the AdBMP2 transduced cells. The slides were stained with hematoxylin and eosin for viewing. Panel E is a representative photomicrograph (10X) of a sample taken 4 weeks after the initial injection of AdBMP2 transduced cells. As can be seen in this sample, there are a significant number of cells associated with the boundary between the new heterotopic and old vertebral bone.

Figure 4: **Left:** Schematic of the in-house flexion device. After 2, 4 or 6 weeks, spines were harvested, placed in the device to induce flexion or extension at 110º and radiographed. **Right:** Representative images used to evaluate biomechanical function of spinal fusion. Top panel shows spine in extension, bottom in flexion. Such images were evaluated with KIMAX QMA software (Medical Metrics, Inc.) to determine whether adjacent vertebrae moved past a predetermined threshold.

Figure 5: Spine fusion was observed in bones isolated from the mouse after induction of targeted heterotopic ossification (panel A). Associated soft tissues were removed by bleaching, leaving only the bone. A wire was threaded through the spinal column, to preserve the orientation of the vertebra. Unfused vertebrae hang free; fused vertebrae remain joined and rigid. Ruler is in millimeters. Radiographs of mouse spines 6 weeks after induction of spine fusion Adempty cassette (panel B) or AdBMP2 (panel C) transduced cells. Panel C, shows obvious curvature of the spine suggesting a significant scoliosis, as compared to the normal mouse spine, shown in panel B.

Refereneces

Aslan H, Sheyn D, Gazit D. 2009. Genetically engineered mesenchymal stem cells: applications in spine therapy. Regen Med 4: 99-108.

Berkner KL. 1988. Development of adenovirus vectors for the expression of heterologous genes. Biotechniques 6: 616-629.

Davis AR, Wivel NA, Palladino JL, Tao L, Wilson JM. 2001. Construction of adenoviral vectors. Mol Biotechnol 18: 63-70.

Deyo RA, Nachemson A, Mirza SK. 2004. Spinal-fusion surgery - the case for restraint. N Engl J Med 350: 722-726.

Fouletier-Dilling CM, Bosch P, Davis AR, Shafer JA, Stice SL, Gugala Z, Gannon FH, Olmsted-Davis EA. 2005. Novel compound enables high-level adenovirus transduction in the absence of an adenovirus-specific receptor. Hum Gene Ther 16: 1287-1297.

Fouletier-Dilling CM, Gannon FH, Olmsted-Davis EA, Lazard Z, Heggeness MH, Shafer JA, Hipp JA, Davis AR. 2007. Efficient and rapid osteoinduction in an immune-competent host. Hum Gene Ther 18: 733-745.

Garrison KR, Donell S, Ryder J, Shemilt I, Mugford M, Harvey I, Song F. 2007. Clinical effectiveness and cost-effectiveness of bone morphogenetic proteins in the non-healing of fractures and spinal fusion: a systematic review. Health Technol Assess 11: 1-150, iii-iv.

Gottfried ON, Dailey AT. 2008. Mesenchymal stem cell and gene therapies for spinal fusion. Neurosurgery 63: 380-391; discussion 391-382.

Gugala Z, Olmsted-Davis EA, Gannon FH, Lindsey RW, Davis AR. 2003. Osteoinduction by ex vivo adenovirus-mediated BMP2 delivery is independent of cell type. Gene Ther 10: 1289-1296.

Hecht BP, Fischgrund JS, Herkowitz HN, Penman L, Toth JM, Shirkhoda A. 1999. The use of recombinant human bone morphogenetic protein 2 (rhBMP-2) to promote spinal fusion in a nonhuman primate anterior interbody fusion model. Spine (Phila Pa 1976) 24: 629-636.

Hipp JA, Reitman CA, Wharton N. 2005. Defining pseudoarthrosis in the cervical spine with differing motion thresholds. Spine (Phila Pa 1976) 30: 209-210.

Kimelman N, Pelled G, Helm GA, Huard J, Schwarz EM, Gazit D. 2007. Review: gene- and stem cell-based therapeutics for bone regeneration and repair. Tissue Eng 13: 1135-1150.

Lutolf MP, Weber FE, Schmoekel HG, Schense JC, Kohler T, Muller R, Hubbell JA. 2003. Repair of bone defects using synthetic mimetics of collagenous extracellular matrices. Nat Biotechnol 21: 513-518.

Mussano F, Ciccone G, Ceccarelli M, Baldi I, Bassi F. 2007. Bone morphogenetic proteins and bone defects: a systematic review. Spine (Phila Pa 1976) 32: 824-830.

Olmsted-Davis EA, Gugala Z, Gannon FH, Yotnda P, McAlhany RE, Lindsey RW, Davis AR. 2002. Use of a chimeric adenovirus vector enhances BMP2 production and bone formation. Hum Gene Ther 13: 1337-1347.

Shore EM, et al. 2006. A recurrent mutation in the BMP type I receptor ACVR1 causes inherited and sporadic fibrodysplasia ossificans progressiva. Nat Genet 38: 525-527.

Thies RS, Bauduy M, Ashton BA, Kurtzberg L, Wozney JM, Rosen V. 1992. Recombinant human bone morphogenetic protein-2 induces osteoblastic differentiation in W-20-17 stromal cells. Endocrinology 130: 1318-1324.

Windahl SH, Andersson G, Gustafsson JA. 2002. Elucidation of estrogen receptor function in bone with the use of mouse models. Trends Endocrinol Metab 13: 195-200.
Zhao K, Yang C, Zhao C, An KN. 2005. Assessment of non-invasive intervertebral motion measurements in the lumbar spine. J Biomech 38: 1943-1946.

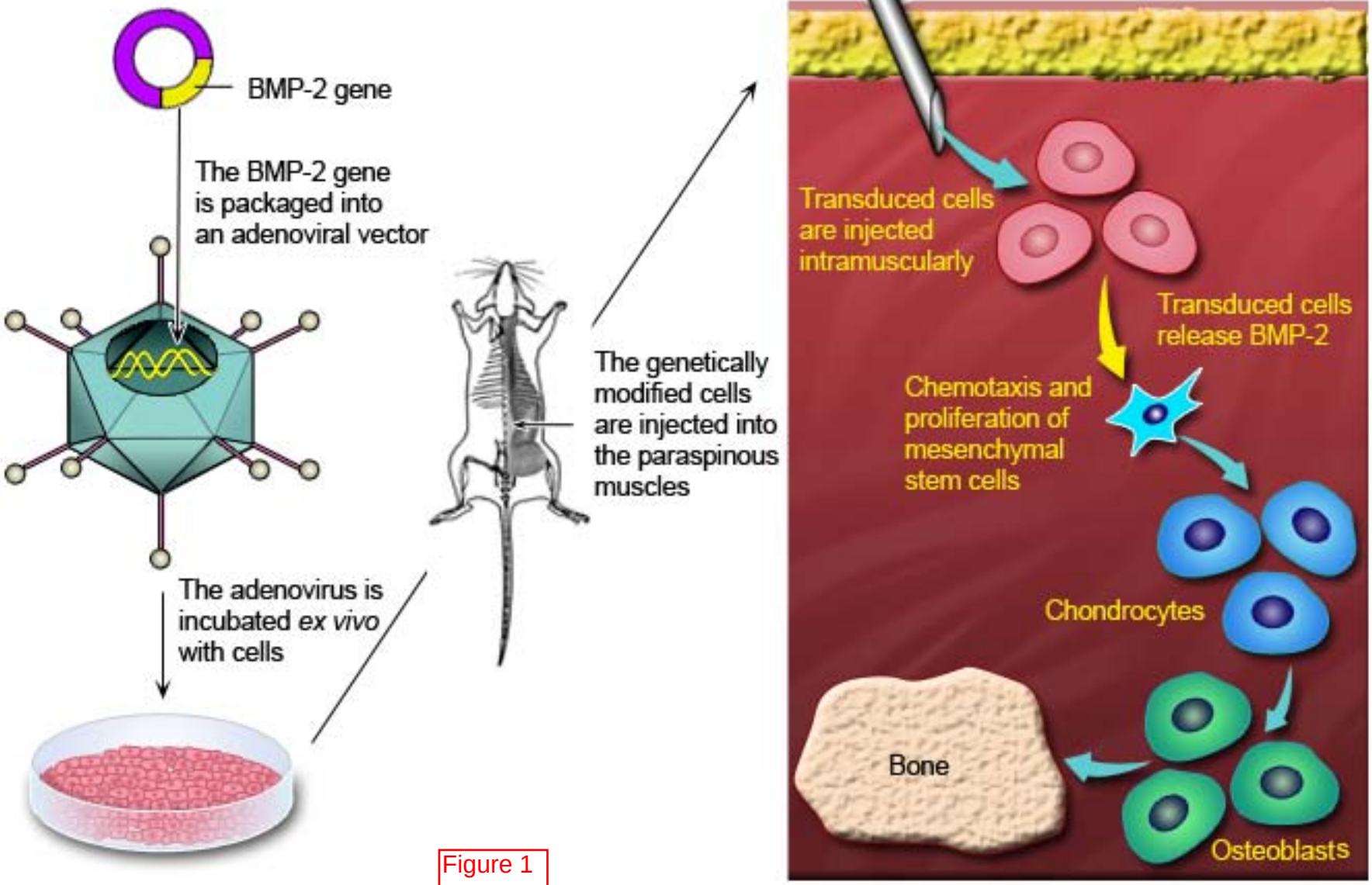
BMP-2 gene
The BMP-2 gene is packaged into an adenoviral vector
The adenovirus is incubated *ex vivo* with cells
The genetically modified cells are injected into the paraspinous muscles
Transduced cells are injected intramuscularly
Transduced cells release BMP-2
Chemotaxis and proliferation of mesenchymal stem cells
Chondrocytes
Bone
Osteoblasts

Figure 1

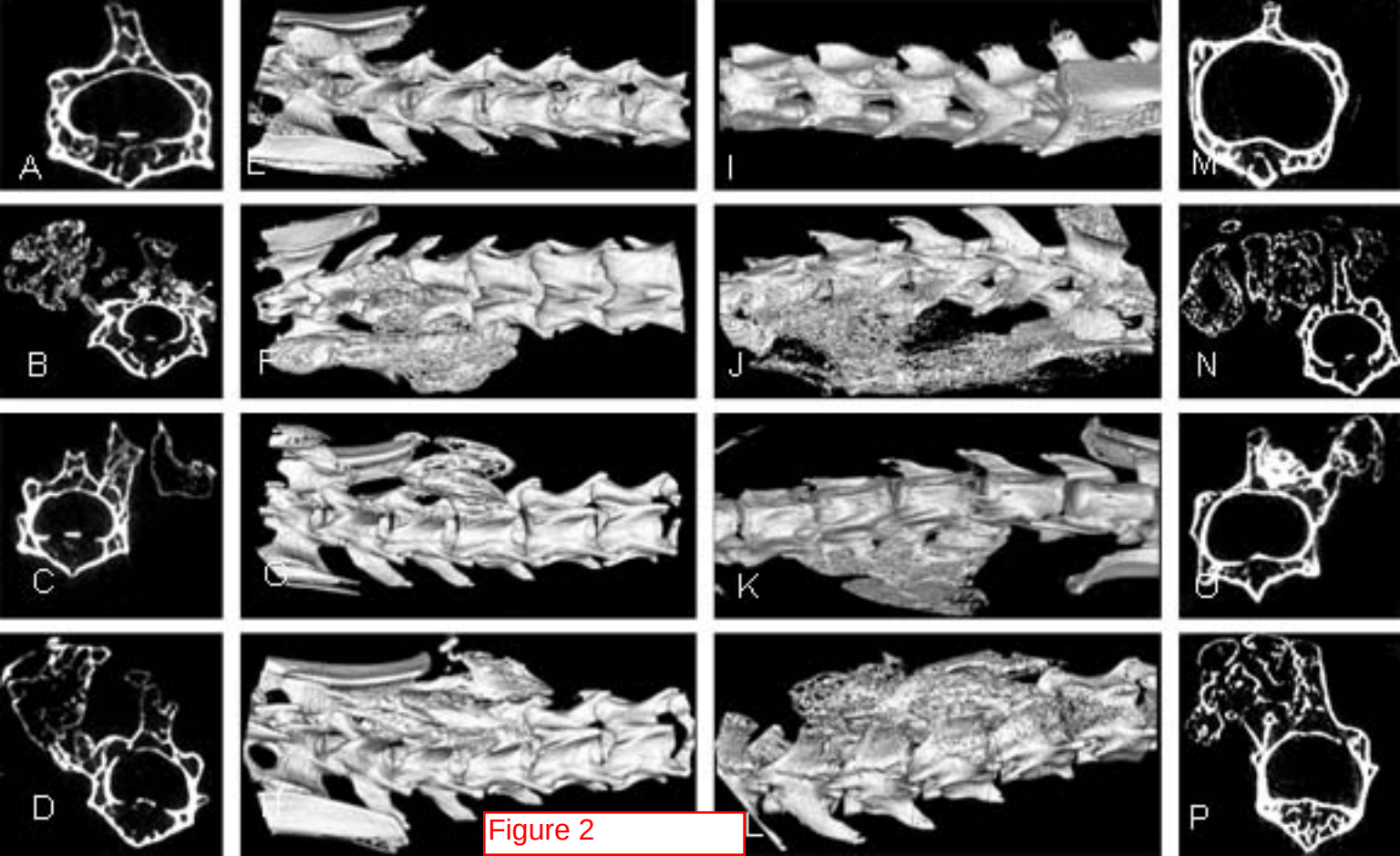

Figure 2

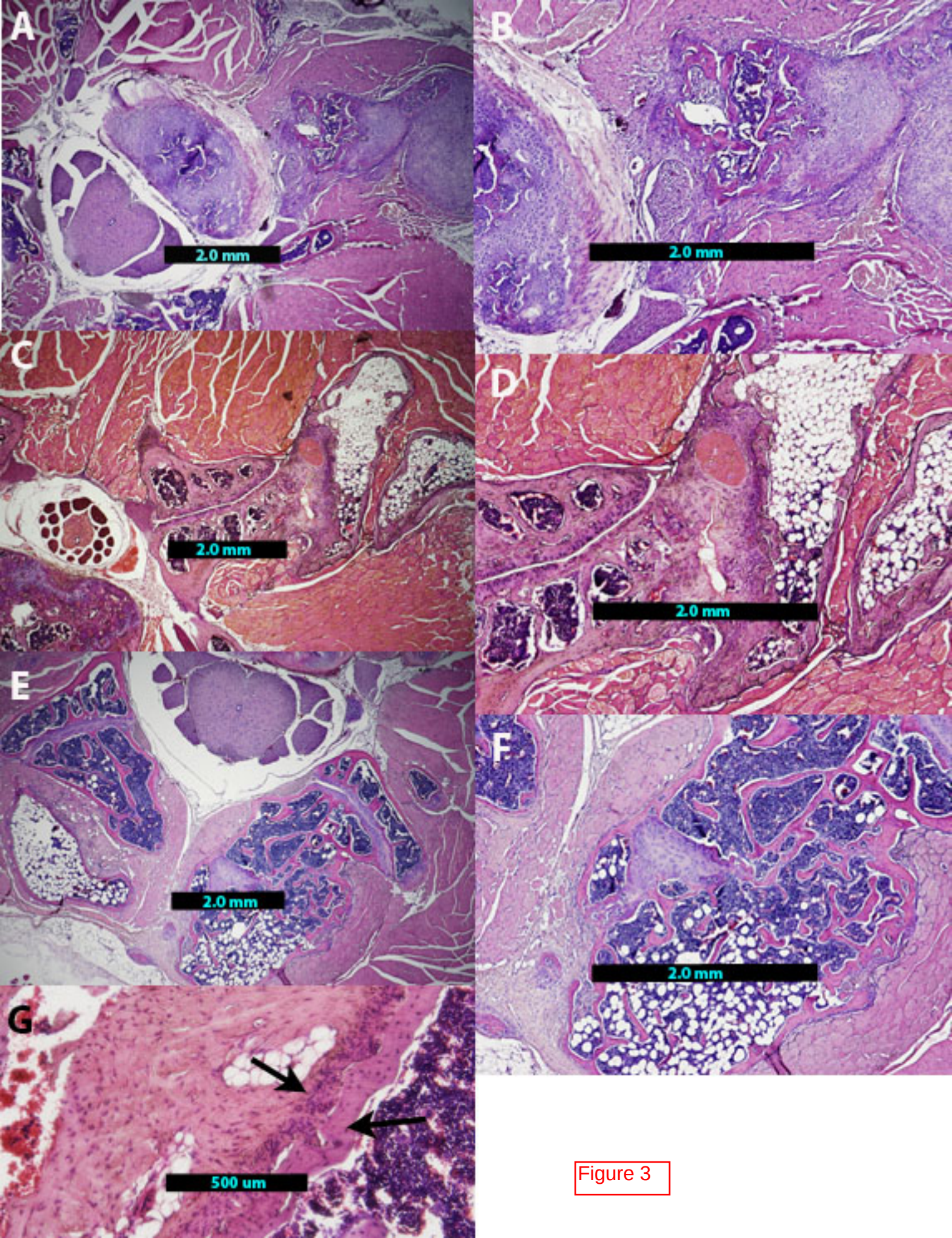

Figure 3

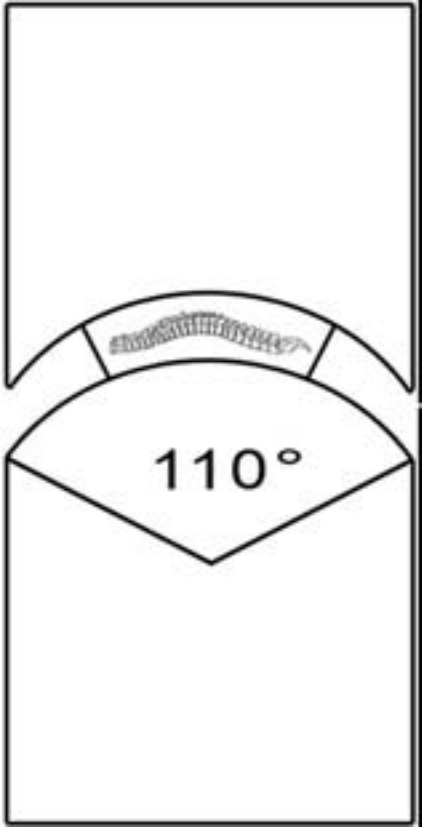

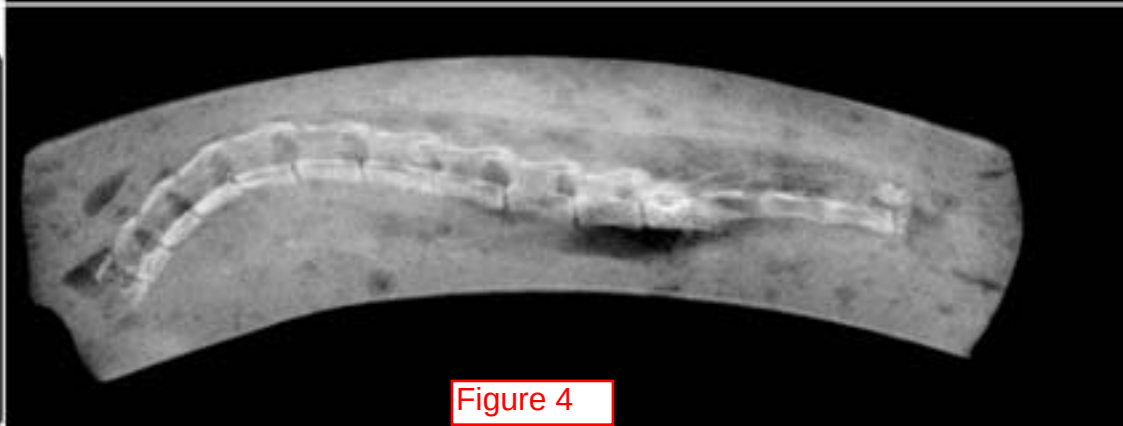

Figure 4

Figure 5